FINAL REPORT

MODELING FOR ANAEROBIC FIXED-BED BIOFILM REACTORS

by

Bill Y.M. Liu

and

John T. Pfeffer

DEPARTMENT OF CIVIL ENGINEERING
UNIVERSITY OF ILLINOIS
URBANA, ILLINOIS 61801

Technical Monitor : Barbara Goodman

prepared for
SOLAR ENERGY RESEARCH INSTITUTE
Subcontract No. XL-8-18036-4

JUNE 1989

TABLE OF CONTENTS

LIST OF TABLES

LIST OF FIGURES

LIST OF SYMBOLS AND ABBREVIATIONS

A	total surface area of biofilm, L^2
[alk]	alkalinity expressed as *mole* H^+ / L , ML^{-3}
a	interfacial contact area of gas and liquid over the liquid volume, L^{-1}
$\tilde{a}$	specific surface area of attachment medium, L^{-1}
b'	the sum of specific decay coefficient and shear loss, T^{-1}
COD	Chemical Oxygen Demand
C_A	total concentration of volatile fatty acid, ML^{-3}
C_{CH_4}	the CH_4 concentration, ML^{-3}
$C^B_{CH_4}$	the CH_4 concentration in the bulk liquid, ML^{-3}
$C_{CH_4,rear}$	CH_4 concentration at the rear of biofilm, ML^{-3}
c_{CH_4}	$C_{CH_4}/C^B_{CH_4}$
$c_{CH_4,rear}$	dimensionless CH_4 concentration at the rear of biofilm
C_{CO_2}	dissolved CO_2 concentration, ML^{-3}
$C^B_{CO_2}$	dissolved CO_2 concentration in the bulk solution, ML^{-3}
$C_{HCO_3^-}$	dissolved HCO_3^- concentration, ML^{-3}
$C^B_{HCO_3^-}$	dissolved HCO_3^- concentration in the bulk solution, ML^{-3}
$C_{CO_3^{-2}}$	dissolved CO_3^{-2} concentration, ML^{-3}
$C^B_{CO_3^{-2}}$	dissolved CO_3^{-2} concentration in the bulk solution, ML^{-3}
C^B_0	$C^B_{CO_2}/C^B_S$
C^B_1	$C^B_{HCO_3^-}/C^B_S$
C_N	total ammonia concentration, ML^{-3}
C_P	total phosphate concentration, ML^{-3}
C_S	the substrate concentration, ML^{-3}
C^B_S	the substrate concentration in the bulk liquid, ML^{-3}
C_{sul}	total sulfide concentration, ML^{-3}
$C_{T,in}$	total inorganic carbon concentration in influent, ML^{-3}
$C_{T,out}$	total inorganic carbon concentration in effluent, ML^{-3}
c_s	C_S / C^B_S
$(CH_4)_T$	total rate of CH_4 production, MT^{-1}
$(CO_2)_T$	total rate of CO_2 production, MT^{-1}
D_{CH_4}	the CH_4 diffusivity in biofilm, L^2T^{-1}
D_{CO_2}	the CO_2 diffusivity in biofilm, L^2T^{-1}

$D_{HCO_3^-}$	the HCO_3^- diffusivity in biofilm, L^2T^{-1}
$D_{CO_3^{-2}}$	the CO_3^{-2} diffusivity in biofilm, L^2T^{-1}
D_f	diffusivity of substrate in biofilm, L^2T^{-1}
D_L	diffusivity of solute in liquid, L^2T^{-1}
D_w	molecular diffusivity of the substrate in the liquid, L^2T^{-1}
d_0	D_{CO_2}/D_S
d_1	$D_{HCO_3^-}/D_S$
d_s	diameter of a sphere having the same area as a piece of packing, L
f_a	$100/Re$
f_c	mole CO_2/ mole substrate
f_e	portion of electron used for energy
f_s	portion of electron used for cell synthesis
f_m	mole CH_4/ mole substrate
g	conversion factor between volume and mole, $M^{-1}L^3$
J	substrate flux, $ML^{-2}T^{-1}$
J_{CH_4}	CH_4 flux, $ML^{-2}T^{-1}$
J_S	substrate flux (in diffusional model), $ML^{-2}T^{-1}$
$J_{S,T}$	total substrate flux, MT^{-1}
k	maximum specific rate of substrate utilization, T^{-1}
k_{0f}	the zero–order rate of substrate removal per unit volume of the biofilm
K_a	dissociation constant of acetic acid at operating temperature
K_{a1}, K_{a2}	dissociation constants of H_2CO_3 at the operating temperature
K_H	Henry's constant of CO_2 at the operating temperature, $L^{-2}T^2$
K'_H	Henry's constant of CH_4 at the operating temperature, $L^{-2}T^2$
K_L	overall liquid layer mass transfer coefficient of CO_2, LT^{-1}
K'_L	overall liquid layer mass transfer coefficient of CH_4, LT^{-1}
K_N	dissociation constant of ammonium at operating temperature
K_{P1}, K_{P2}, K_{P3}	dissociation constants of phosphate at operating temperature
K_s	Monod half–velocity coefficient, ML^{-3}
K_{S1}, K_{S2}	dissociation constants of sulfide at operating temperature
K_W	equilibrium constant of water at operating temperature
L	thickness of the stagnant liquid layer, L
L_f	biofilm thickness, L
MW_S	substrate molecular weight, M

M_{Bio}	the total attached biomass, M
M_T	total biomass, ML^{-3}
P_{CH_4}	CH_4 partial pressure inside reactor, $ML^{-1}T^{-2}$
P_{CO_2}	CO_2 partial pressure inside reactor, $ML^{-1}T^{-2}$
P_T	total pressure inside reactor, $ML^{-1}T^{-2}$
P_w	vapor pressure inside reactor, $ML^{-1}T^{-2}$
pH_f	titration end point (4.3)
Q	wastewater flow rate, L^3T^{-1}
Q_i	flow rate of stock feed solution, L^3T^{-1}
Q_g	total gas flow rate, L^3T^{-1}
R	$R_d - f_g R_a - f_s R_c$ overall stoichiometric equation
Re	Reynold's number
R_a	oxidation half reaction for electron acceptor
R_c	oxidation half reaction for bacterial cell
R_d	oxidation half reaction for electron donor
R_L	superficial liquid rate, $ML^{-2}T^{-1}$
R_s	rate of biomass loss due to shear stress, $ML^{-2}T^{-1}$
$R_{T,S}$	overall rate of biofilm loss due to shear stress, MT^{-1}
r_{sub}	the substrate utilization rate, MT^{-1}
$(r_s)_u$	substrate utilization rate within the biofilm, $ML^{-3}T^{-1}$
$(r_s)_{diff}$	molecular diffusion rate, $ML^{-3}T^{-1}$
S	rate–limiting substrate concentration, ML^{-3}
SS	suspended solids
Sc	Schmidt number
S_b	bulk substrate concentration, ML^{-3}
S_f	substrate concentration within biofilm, ML^{-3}
S_i	substrate concentration in stock feed solution, ML^{-3}
S_0	substrate concentration in influent, ML^{-3}
S_s	liquid–biofilm interface substrate concentration, ML^{-3}
S_w	substrate concentration at media surface, ML^{-3}
TSS	the total suspended solids in effluent, ML^{-3}
V	the reactor volume occupied by packing media, L^3
V_T	the total reactor volume, L^3
VSS	the volatile suspended solids in effluent, ML^{-3}

VFA	volatile fatty acid
X_f	biofilm density, ML^{-3}
Y	the true yield of bacterial mass per unit of substrate mass utilized
z	depth of biofilm, L
β_S	$\sqrt{2D_S C_S^B / k_{0f} L_f^2}$
γ	$C_S^B D_S / C_{CH_4}^B D_{CH_4}$
ϵ	porosity
η	$z\sqrt{k_{of}/2D_S C_S^B} = \quad z/\beta_S L_f$
μ	viscosity, $ML^{-1}T^{-1}$
μ_L	liquid viscosity, $ML^{-1}T^{-1}$
ξ	z/L_f
ξ'	dimensionless depth of substrate penetration
ϱ_L	liquid density, ML^{-3}
σ	shear stress over the biofilm surface, $ML^{-1}T^{-2}$
τ	empty-bed retention time in biofilm reactor , T
τ^*	dimensionless empty-bed retention time in biofilm reactor
v	flow velocity, LT^{-1}
ϕ_s	sphericity ratio of the surface area of the equivalent-volume to the actual surface area

Superscript

B	concentration in the bulk liquid
*	dimensionless form

Subscript

ALK	alkalinity
C	inorganic carbon

ABSTRACT

Modeling for Anaerobic Fixed-Bed Biofilm Reactors

Bill Y.M. Liu
and
John T. Pfeffer

Department of Civil Engineering
University of Illinois at Urbana-Champaign, 1989

Biofilm models, developed by previous researchers, were incorporated with an equilibrium model to study the physical and chemical aspects of the anaerobic fixed-bed biofilm reactors. In order to investigate the mechanism of equilibrium in an anaerobic biofilm reactor, a non-equilibrium model was derived from the equilibrium model to simulate the gas transfer process involved in biogas production. The equilibrium model well described the behavior of anaerobic fixed-bed biofilm reactors, which was verified in the experimental results. The non-equilibrium model showed that the contact area between the gas and the liquid phases is the pivotal factor controlling the state of equilibrium. This condition can only exist where there is sufficient contact area.

Operation of three different anaerobic fixed-bed biofilm reactors has substantiated that a packing material with higher specific surface area can immobilize more microorganisms, thus resulting in better treatment efficiency. However, the shear stress caused by different material might reduce the amount of biofilm retained in the reactor. In addition, the characteristics of the material also affect the effectiveness of the reactor. For example, granular activated carbon is so light and dense that the abrasion between these particles offsets the advantage of its large surface area. Experimental results also show that all biofilms are close to fully-penetrated, which simplifies the biofilm model by disregarding the resistances of the liquid layer and biofilm. Anaerobic fixed-bed biofilm reactors, in reality, behave like suspended-growth reactors.

The out-diffusion of end products in anaerobic biofilms was simulated by a diffusional model. Prediction of this model suggests that the methane concentration at the rear of biofilms is a function of the substrate concentration in the bulk liquid. As a result, a high substrate concentration in the reactor causes the biogas build-up at the back of biofilms and, eventually, sloughing. It is therefore concluded that the effective way to restore an unbalanced biofilm reactor is to decrease the feed until the bulk substrate concentration has been reduced to a level that will not cause sloughing.

I. INTRODUCTION

Anaerobic biological processes are becoming more widely used in the field of wastewater engineering. Beneficial aspects include: no power required for oxygen transfer, low biomass production which reduces the amount of residual solids for disposal, and production of a useful fuel gas. Historically, this process has been employed to stabilize sludges from wastewater treatment processes. However, research (Metcalf and Eddy, Inc., 1979) has demonstrated that industrial organic wastes can also be treated by anaerobic processes. In addition to concentrated organic wastes, Young and McCarty (1967) found that low strength soluble organic wastes can also be efficiently treated anaerobically.

The loading capacities of an anaerobic reactor are dictated by the amount of active biomass retained, provided a sufficient contact between active biomass and substrate can be assured (Lettinga *et al.*, 1983). Conventional anaerobic processes using a suspended-growth reactor require sludge recycle to obtain the required solids retention time (SRT) for effective treatment of dilute wastewaters. Efficient solids separation and recycle has been a major problem for the dispersed growth system. The development of the attached-growth system, by Young and McCarty (1967), revolutionized anaerobic treatment. The fixed-bed biofilm reactor, sometimes termed an anaerobic filter, immobilizes the biomass onto the surface of packing medium, hence dramatically reducing biomass loss in effluent. A significant increase in the SRT above the hydraulic retention time (HRT) can be obtained. Although many dynamic or steady-state models have been developed to describe the behavior of anaerobic reactors, the effects of the biomass associated with the biofilm reactors are still poorly defined. In addition, the loading limits of an upflow anaerobic fixed-bed reactor are still not well known.

The specific objectives of this research were as follows :

1. To develop an equilibrium model for chemical aspects of anaerobic reactors.
2. To modify the equilibrium model for non-equilibrium conditions.
3. To incorporate the existing biofilm models into the models above to study the biological and chemical behavior of the fixed-film anaerobic reactors.
4. To experimentally verify the validity of these models.
5. To investigate the biomass-holding ability of different packing materials for establishing reactor design criteria.

II. LITERATURE REVIEW

Many articles concerning anaerobic digestion have been published over the past years, among which some are of special significance. McCarty (1964a,b,c,d) presented a detailed discussion of the anaerobic waste treatment process in a four-part series. In 1981, a review paper by McCarty, *One Hundred Years of Anaerobic Treatment*, marked a century of use of this technique. The most recent publication, by Parkin and Owen (1986), thoroughly reviewed the fundamentals of anaerobic digestion of waste sludges. While most papers simply examined the general characteristics of the process, an article by Henze and Harremoës (1983) focused mainly on the fixed-film reactors. These publications are of a general nature and are a good source of general information on the anaerobic digestion process.

This chapter reviews literature pertinent to this research starting with a section of basic microbiology of anaerobic digestion, followed by sections on attached growth, anaerobic reactors and CH_4 enrichment.

2.1 Microbiology

Gottschalk (1985) defined fermentations as those biological processes that occur in the dark and that do not involve respiratory chains with oxygen or nitrate as electron acceptors. In fermentation, electrons released from the oxidation of the organic substrate are either accepted by organic compounds, forming the so-called organic electron sink products, or by protons, forming molecular hydrogen (Cohen, 1983). The electron sink products include alcohols and many volatile fatty acids (VFA) , such as acetate, propionate, butyrate, succinate and lactate.

2.1.1 Three-Stage Scheme for Methane Fermentation

McInerney and Bryant (1981) described the methane fermentation process as a three-stage scheme. Three major metabolic groups of bacteria are (1) hydrolytic and fermentative bacteria, (2) obligate H_2-producing, *i.e.* proton reducing, acetogenic bacteria, and (3) methanogenic bacteria. Methane is the most reduced organic compound and its formation is the terminal step of the anaerobic fermentation. Since methanogens can only utilize C_1 compounds (CO_2, CO, $HCOOH$ and CH_3OH) and one C_2 compound : acetate, all three groups of bacteria must coexist in a coordinated relationship to convert complex organics into CH_4 and CO_2.

The bacteria responsible for the process of polymer hydrolysis and the initial fermentation are a very complex mixture of many bacterial species (McInerney and Bryant, 1981). Most of these bacteria are obligate anaerobes (Toerien and Hattingh, 1969: Bryant, 1979), but some facultative anaerobes may be present. Stryer (1981) showed these bacteria can hydrolyze or liquify complex organic polymers into smaller soluble units which then can be assimilated by the bacterial cell. The long-chain fatty acids are not further degraded by fermentative bacteria, but unsaturated fatty acids are hydrogenated to their saturated forms. Carbohydrates are fermented to alcohol and short-chain fatty acids.

Hungate (1966) was the first to show that hydrogen production and utilization can influence the fermentation. Bryant (1979) pointed out that the products of the first-stage fermentation other than acetate, H_2 and CO_2 , *i.e.* alcohols, propionate and

longer chain fatty acids and aromatic acids are anaerobically oxidized to acetate or acetate and CO_2 by a group of H_2-producing acetogenic bacteria. Jeris and McCarty (1965) demonstrated that even-numbered fatty acids are β-oxidized to acetate and H_2. In β-oxidation, the β-carbon is oxidized followed by cleavage of two-carbon acetic acid fragments. Hungate (1966) and Chynoweth and Mah (1970) found the propionate and longer-chained fatty acids are more important as intermediates in anaerobic degradation than are lactate or ethanol because they are degraded by H_2-producing bacteria. Chung (1976), Bryant *et al.* (1977), and Cohen (1982) proved that in order to keep the H_2-producing reaction energetically favorable, H_2 partial pressure in an anaerobic ecosystem must be kept low by either methanogenic or sulfate-reducing bacteria.

Daniels *et al.* (1984), Wolfe (1985) and Woese and Wolfe (1985) reported that methanogenic bacteria (methanogens) are archaebacteria and represent a very ancient divergence in evolution. They are obligate anaerobes which can only live under anaerobic conditions with reducing potential below $E_0' = -330mv$. Methanogens are very unique from other living things due to their characteristic biochemistry. The methanogens have one thing in common: they use a methyl-group as their terminal electron acceptor. *Methanosarcina* and *Methanothrix* are the only two known genera of methanogens that cleave acetate (Gottschalk, 1985). *Methanothrix* only uses acetate for methanogenesis, whereas *Methanosarcina* uses H_2/CO_2, CH_3OH, methylamines and acetate.

Jeris and McCarty (1965) demonstrated that 65-70% of methane production from a complex substrate is through acetate decarboxylation accomplished by *Methanosarcina* and *Methanothrix*, while CO_2-reduction by hydrogen-oxidizing methanogens (HOM) is responsible for the rest (Harper and Pohland, 1987). Acetate cleavage is more energetically favorable when H_2 partial pressure is smaller than 10^{-4} *atm*. McInerney and Bryant (1981) reported that the formation of methane from CO_2 and H_2 even at a partial pressure of H_2 below 10^{-5} *atm*. Previous researches suggested a low half velocity constant (K_S) and maximum specific growth rate (k) for *Methanothrix*. Therefore, if the acetate concentration is kept low, the *Methanothrix* populations will dominate the *Methanosarcina* population. Harper and Pohland (1987) demonstrated that *Methanosarcina* can effectively compete with *Methanothrix* at acetate concentration > 300mg/*L*; and the maintenance of H_2 level below 10^{-4} *atm* make the *Methanosarcina* prefer acetate to H_2. Ehlinger and co-workers (1987) also reported *Methanosarcina* predominated at high acetate concentration, whereas *Methanothrix* predominated at lower acetate concentrations. Similarly, Yoda *et al.* (1987) found that sulfate-reducing bacteria (SRB) are competitive with methanogens for H_2 at low acetate concentrations.

McCarty (1970) recognized the importance of energy released per electron equivalent fermented in determining the rate-limiting step. Carbohydrate, protein and hydrogen substrates release more energy per electron equivalent fermented. This results in higher relative yields and allows these organisms to reproduce faster, while acetate and other fatty acid substrates release less energy, resulting in lower yields. However, for a complex substrate, the rate-limiting step may be dependent on the substrate composition. McInerney and Bryant (1981) showed that the fermentation of substrates containing cellulosic material is limited by the slow rate of cellulose hydrolysis.

Babbitt and Baumann (1958) first proposed the concept of phase separation which has been supported by some researchers who believed that the acidogenic and

methanogenic bacteria should not optimally coexist in a traditional single-phase digester (Andrews and Graef, 1970; Ghosh and Pohland, 1974; Cohen *et al.*, 1979). Henze and Harremoës (1983) believed a lower pH can promote polymer hydrolysis; phase separation, therefore, can provide an acid reactor with lower pH. The reported advantages of a two-phase digester are the optimization of environmental conditions for both groups of microorganisms, biogas of higher methane content (Keenan, 1976; Ghosh and Henry, 1982), and the detoxification of waste influent (Zoetemeyer, 1982; Cohen, 1983). Pohland and Ghosh (1971) suggested kinetic control for phase separation by operational adjustment of the dilution rates and recycle ratios. Cohen *et al.* (1979) proposed pH control, while Borchardt (1970) used a dialysis technique for phase separation.

Despite the claimed benefits of phase separation, the H_2 accumulation and loss in the acid reactor decreases the methane production (Kaspar and Wuhrmann, 1978; Heyes and Hall, 1981). Ward *et al.* (1978) pointed out the dependency between these two groups of bacteria because they produce required nutrients for each other. Cohen (1982) and Parkin and Owen (1986) concluded that phase separation would only be feasible for substrates where the hydrolysis step is clearly the overall rate-limiting step.

2.1.2 Growth Constants

Because the growth constants are the foundation of any kinetic study, numerous researchers have published their results on the growth constants of anaerobic fermentation. If proper values can be obtained for these constants, the performance of a reactor can be more accurately predicted through kinetic models.

Table 2-1 lists some reported values of the methanogens, most of which are from mesophilic operations. These values include the maximum specific growth rate (k), yield coefficient (Y), decay coefficient (b) and half velocity constant (K_S). The great discrepancies between values in Table 2-1 probably reflect the difference in research attitude, research method, and even analytical techniques between different research teams.

2.1.3 Stoichiometry

Buswell and Mueller (1952) proposed an empirical formula, Eq. 2-1, which still is widely accepted for predicting the gas production from the chemical composition of the substrate

$$C_nH_hO_l + \left(n-\frac{h}{4}-\frac{l}{2}\right)H_2O \rightarrow \left(\frac{n}{2}-\frac{h}{8}+\frac{l}{4}\right)CO_2 + \left(\frac{n}{2}+\frac{h}{8}-\frac{l}{4}\right)CH_4 \qquad (2\text{-}1)$$

However, this formula does not include the fraction of substrate which is converted to microorganisms. Andrews and Graef (1970) pointed out the amount of biomass, although small, cannot be ignored. McCarty (1974) proposed a stoichiometric equation for sewage sludge digestion, Eq. 2-2, which can also predict the alkalinity change.

$$C_{10}H_{19}O_3N + 4.69\,H_2O \rightarrow 5.74\,CH_4 + 2.45CO_2 + 0.20C_5H_7O_2N + 0.80NH_4^+ + 0.80HCO_3^-(alkalinity) \qquad (2\text{-}2)$$

where :

$C_{10}H_{19}O_3N$ = general formula of primary sludge
$C_5H_7O_2N$ = general formula of bacteria

Table 2-1 Growth Constants of Methanogens

Maximum Specific Growth Rate	Yield Coefficient Constant	Half-Velocity Constant	Decay Rate	Temp.	Substrate	Reference
k	Y	K_S	b			
day^{-1}	$\frac{KgVSS}{KgCOD}$	$\frac{KgCOD}{m^3}$	day^{-1}	$°C$		
>1.33	0.14		0.02	38	Synthetic	Andrews& Pearson,1965
22.0	0.022			35	Formic Acid	McCarty,1966
2.1	0.073			35	Acetic Acid	McCarty,1966
3.7	0.045			35	Propionic Acid	McCarty,1966
8.7	0.041	0.165	0.015	35	Acetic Acid	Lawrence & McCarty,1969
7.7	0.032	0.060	0.010	35	Propionic Acid	Lawrence & McCarty,1969
8.1	0.023	0.013	0.027	35	Butyric Acid	Lawrence & McCarty,1969
0.4		0.002		38	Mixed/ Acetate	Andrews& Graef,1970
8.7		0.165		35	Acetic Acid	Lawrence,1971
7.7		0.060		35	Propionic Acid	Lawrence,1971
8.1		0.013		35	Butyric Acid	Lawrence,1971
	0.044		0.019		Average value	Lawrence,1971

Table 2–1 Growth Constants of Methanogens (Continued)

Maximum Specific Growth Rate	Yield Coefficient Constant	Half–Velocity Constant	Decay Rate	Temp.	Substrate	Reference
k	Y	K_S	b			
day^{-1}	$\frac{KgVSS}{KgCOD}$	$\frac{KgCOD}{m^3}$	day^{-1}	$°C$		
3.36		0.64		37	Dextrose	Ghosh & Pohland, 1974
3.336		0.64		37	Acetate	Pohland & Massey, 1975
0.09	0.0176			35	Acetate Enrichment	van den Berg, 1977
0.49	0.2625	4.48		36.5	Acetic Acid	Ghosh & Klass 1978
0.237	0.0399	0.07499	0.0216		Acetate	Anderson & Duarate, 1980
4.38*		0.0084		35	Acetate	Wang *et al.*, 1985

*Unit : mg COD/mg $CH_2O \cdot day$

McCarty (1975) proposed a method, for construction of empirical chemical formulations for organics, which can be used to create a generalized oxidation half reaction for organics of undefined composition such as Eq. 2–2. This method can also be used to calculate the kinetic parameters. In this method, the overall stoichiometric equation (R) can be obtained by combining three oxidation half reactions, one for the electron donor (R_d), one for the electron acceptor (R_a), and one for bacterial cells (R_c). The R can be calculated by the relationship $R = R_d - f_e R_a - f_s R_c$. The fractions f_e and f_s represent the portions of electron used for energy and for cell synthesis, respectively.

2.2 Attached Microbial Growth

Attached microbial growth processes have recently become increasingly important in water and wastewater treatment. Research has significantly advanced biofilm technology over the past decade. Despite this progress, the basic conceptual assumption of a biofilm is still in question and therefore needs more investigation. The general concepts applied to biofilms and the associated kinetic models will be reviewed in the following sections.

2.2.1 Biofilm

ZoBell (1943) first suggested that nutrients in very dilute nutrient solutions may be concentrated on solid surfaces by adsorption, thus enhancing the bacterial activities. It was also pointed out by ZoBell that solid surfaces retard the diffusion of exoenzymes away from the cell thereby promoting the assimilation of those nutrients which may have to be hydrolyzed extracellularly.

Marshall *et al.* (1971) confirmed ZoBell's suggestion that bacterial sorption occurs in stages. The bacteria are first weakly attached to a surface (reversible sorption), and after several hours became firmly attached (irreversible sorption). Daniels (1972) concluded that the adsorption of cells onto surfaces is dependent upon the microorganism, the adsorbent, and the environment. Environmental factors responsible for this process include : hydrogen ion concentration, salt concentration, agitation, time of contact and temperature. Characklis (1973) postulated that initial deposition of organisms is related to the characteristics of the attachment surface and the shear force at the surface.

Sutherland (1983) demonstrated that the secretion of polysaccharides or other carbohydrate–containing polymers by many adherent microorganisms play an important role in the attachment process. The structure, function, genetics, and morphologic aspects of known proteinaceous adhesive materials of bacteria were discussed by Jones and Isaacson (1983). Audic *et al.* (1984) reported that the specific activity of bacteria increases due to attachment. Switzenbaum and Eimstad (1987) noted that 40–50% of the biofilm is due to inorganic material, with increasing amounts found at increased loading rates. This ash content is most likely due to chemical precipitation resulting from nutrient salts used in the experiments.

2.2.2 Biofilm Models

Atkinson and Davies (1974) first developed a bacterial biofilm model incorporating both diffusion and Monod–type substrate utilization equations which was subsequently modified by Williamson and McCarty (1976a,b). Harremoës (1976) simulated the

biofilm kinetics by a pore diffusion model and found that zero order heterogeneous reactions in a pore will lead to a bulk half–order reaction and that first–order heterogeneous reactions in a pore will lead to a bulk first–order reaction. Rittmann and McCarty (1981) divided the biofilm model into three categories according to the substrate concentration profiles within the biofilms. A fully penetrated biofilm is one with a constant substrate concentration which is equal to the bulk solution concentration. A deep biofilm is one in which the substrate concentration decreases asymptotically to zero within the biofilm. The flux into a deep biofilm is the maximum possible. The shallow biofilm is an intermediate case in which the substrate concentration does not decrease to zero at the wall.

The diffusion of substrate into the biofilm may be rate limiting and substrate conversion efficiency will be significantly reduced if the bacteria inside the biofilm can not be reached by the substrate. On the other hand, the out–diffusion of the products is of equal importance. Riemer (1977), Riemer and Harremoës (1978) and Arvin and Kristensen (1982) reported a pH increase in the biofilm due to alkalinity production during the denitrification process . Similarly, nitrification produces acidity and lowers the pH inside the biofilm. This build–up of alkalinity or acidity, which may inhibit microbial activity in the biofilm can not be detected from monitoring the alkalinity or acidity of the bulk liquid. The gaseous end products of anaerobic fermentation, CH_4 and CO_2, represent two completely different situations due to their difference in solubilities and their chemical reactivity. CO_2 is very soluble and its buildup will decrease the pH, whereas CH_4 is very insoluble and may form gas bubbles within the biofilm.

Harremoës *et al.* (1980) suggested that a gaseous product of low solubility may cause bubble formation and increase the sloughing of the biomass. Methane, which is much more insoluble than CO_2, can be expected to form bubbles when supersaturation in the bulk solution is reached (Henze and Harremoës, 1983). Switzenbaum and Eimstad (1987) reported channels and holes which probably occurred from gas bubbles ripping through the film. The "outgassing" of product gas from the films, therefore, deserves more recognition as one of the rate–limiting steps. How the formation of bubbles might affect the reactor performance is still unknown, but the effect may be more significant at higher organic loading rates. In fully penetrated biofilms the effect is not clear. In deep (thick) biofilms with substantial diffusional resistance, the outdiffusion of bubbles may break up the diffusional pattern. Microcurrents generated by bubbles movements may increase the apparent diffusion rate and make the diffusional resistance less significant. However, the sloughing of biofilms caused by release of the biogas bubbles may be more damaging in the deep biofilms.

2.3 Anaerobic Reactors

McCarty (1966) demonstrated that SRT is the pivotal factor in reactor design. A long SRT is essential to maintain a good biological conversion efficiency, whereas a short HRT is prerequisite to system economy. In a conventional completed–mixed anaerobic reactor without sludge recycle, the SRT is the same as the HRT. Several modified reactor types have been developed to reduce the HRT, while maintaining a fairly long SRT. These reactor types are divided into the attached–growth and the suspended–growth reactors. The former includes (1) fixed–bed reactor, (2) moving bed reactor, (3) expanded bed reactor, and (4) fluidized–bed reactor. The latter embodies the contact reactor and the sludge blanket reactor (Henze and Harremoës, 1983).

Numerous mathematical models have been developed for the purpose of defining the performance of the anaerobic reactor. Andrews (1969) developed a dynamic model to

simulate the start-up and failure of a digester. Andrews and Graef (1970) and Graef and Andrews (1973) included an inhibition function in a dynamic model in which unionized acids are the growth limiting substrate as well as inhibiting agent. Duarte (1983) studied inhibition modeling in anaerobic digestion and concluded that volatile acid inhibition does not appear to be a serious problem. Hill and Nordstedt (1977) and Hill and Barth (1977) modified dynamic models to simulate wastes with high nitrogen content, such as animal wastes. Sinechal *et al.* (1979) presented a model for single-stage anaerobic digestion of complex substrates containing no volatile acids. Kleinstreuer and Poweigha (1982) developed a transient, two-culture model focusing on the acetogenic and methanogenic stages of the three-stage scheme. Moletta *et al.* (1986) also modeled the anaerobic digestion as a two-step process. Most models described growth merely as an increase in biomass or simplistic microbial conversion reactions, and are called *unstructured* models. They ignored species dynamics in mixed cultures or changes in culture composition in response to changes in environmental conditions. Bryers (1985) used *structured* models to consider mixed-culture population dynamics and/or multiple-reaction schemes as a function of environmental conditions. Unlike these dynamic models reviewed above, Hayes *et al.* (1989) proposed an chemical equilibrium model to describe the steady-state condition of digesters.

2.3.1 Attached vs. Suspended Growth Reactor

The support media in the attached-growth reactor retains bacteria, and, therefore, improves the effluent quality by reducing the total suspended solids concentration of the effluent. These bacteria in attached-growth reactor form a biofilm and increase the SRT dramatically over the HRT, thereby reducing the reactor volume requirement for a specified conversion efficiency.

The suspended-growth reactor, on the other hand, can increase the SRT by separating and recycling of solids from the reactor effluent (contact process) or formation of sludge blanket at the bottom of an upflow reactor (upflow anaerobic sludge blanket-UASB). The chemical, microbiological, and morphological differences of biofilms in three different anaerobic reactors (packed-bed reactor, fluidized-bed reactor, and UASB) were studied by Switzenbaum and Eimstad (1987). However, they did not find significant difference among these three biofilms.

Oleszkiewicz (1981a) pointed out two major advantages of attached growth processes :

1. The loading and conversion rates can be substantially higher in attached-growth systems than in conventional completely-mixed systems. Binot *et al.* (1983) reported a volumetric loading of 42 Kg COD/ $m^3 \cdot d$ in fixed-film processes, while Chen *et al.* (1988) operated anaerobic fluidized-bed biofilm reactors under volumetric loadings as high as 72.4 Kg COD/ $m^3 \cdot d$. By contrast, the maximum loading in an UASB reactor has been reported as 36 KgCOD/ $m^3 \cdot d$ (Pette and Versprille, 1982).
2. The flexibility and stability of biofilm reactors make them very resistant to shock loadings. Kennedy and van den Berg (1982) reported an anaerobic fixed-film reactor can recover from a shock organic loading of 94 Kg COD/ $m^3 \cdot d$ within four days. Oleszkiewicz (1981b) found the long SRT makes the attached-growth system very stable and resistant to changes of temperatures, organic loading, and influent concentration or composition.

2.3.2 Upflow Fixed-Bed Biofilm Reactors

Coulter *et al.* (1957) were the first to employ an anaerobic upflow fixed-bed biofilm reactor. Rock media were used to retain solids from the effluent of an anaerobic

contact process. Young and McCarty (1968,1969) introduced the term "anaerobic filter" in which they assumed that the solids did not attach readily to the surface of the stones but lay loosely in the interstitial spaces. It was not until 1976 that Williamson and McCarty confirmed that a biofilm of closely packed bacteria formed on the surface of packing material. The substrate diffused into the biofilm where it is metabolized by the bacteria. A number of studies was conducted after Young and McCarty's work to study the applicability of this process. However, the first full-scale application was not reported until 1979 by Witt *et al.*

The fixed-bed biofilm reactors are very stable and the biofilm is not damaged by a small amount of oxygen. Norman and Frostell (1977) indicated the major drawbacks of this process is a long start-up period and possibility of the packing being clogged by inert suspended solids or chemical precipitates (metal sulfides, calcium carbonate *etc.*). Ehlinger and co-workers (1987) reported that exopolysaccharides secreted by hydrolytic and acidogenic bacteria are the main cause of clogging. van den Berg and Lentz (1979) found that one year is required to achieve the maximum capacity of a fixed-film reactor.

Switzenbaum (1983) indicated that expanded and fluidized-bed reactors have several advantages over fixed-bed reactors. These include (1) no clogging, (2) small head loss, (3) no short circuiting, (4) higher biomass concentration, (5) better efficiency, and (6) greater surface area available per unit reactor volume. In addition, Jewell and co-workers (1981) reported successful treatment of low strength waste of COD concentration down to 200 mg/*L* by a fluidized-bed reactor. However, the pumping cost is smaller in fixed-bed biofilm reactor because the effluent recycle rate is much lower than for the fluidized-bed reactor.

Lindgren (1983) successfully modeled an anaerobic packed-bed reactor by simplifying Monod kinetics into zero-order and first-order kinetics for organic nitrogen and soluble COD, respectively. This simplified kinetic model was applied to both the fermentative and methanogenic bacteria. Abramson (1987) modeled anaerobic packed-bed reactors with a dispersion equation containing terms for diffusion, convection and reaction which yields a first-order kinetic expression.

Ehlinger and colleagues (1987) studied the microorganisms inside anaerobic packed-bed reactors and noted the bacterial species in these reactors are primarily determined by the K_S of the species. High substrate concentrations inside the reactors favor the growth of the bacterial species with high K_S values and *vice versa.*

Young (1968) concluded that the hydraulic regime in an anaerobic packed-bed reactor with no recycle is almost an ideal plug flow pattern. However, as biological solids accumulate and as evolved gases cause mixing, the hydraulic regime approaches more closely a completely-mixed reactor. A recycle stream can further improve the degree of mixing in an anaerobic packed-bed reactor (Levenspiel, 1972). DeWalle and Chian (1976) used a completely-mixed model to simulate an anaerobic packed-bed reactor with a recirculated effluent. Young (1983) suggested that these reactors actually operate between plug flow and completely-mixed conditions.

2.3.2.1 Packing Material

The packing material used in a packed-bed reactor should be light weight to reduce construction cost and should be able to retain as much biomass as possible. In addi-

tion, some researchers suggested that other properties of packing medium might affect the performance of anaerobic reactors. These properties include adsorbing capability (Khan *et al.*, 1981), proton exchange ability (Sanchez and Roque-Malherbe, 1987) and surface characteristics relative to the hydrodynamics of the reactor (Verrier *et al.*, 1987).

Parker and Merrill (1984) reported that in trickling filters the cross-flow media was superior to vertical media due to more interruptions in the film flow of cross-flow media. Logan *et al.* (1987) showed that the soluble organic material removal rate in trickling filters is primarily controlled by diffusion of components to the biofilm and not uptake kinetics within the biofilm. Since fluid near the biofilm moves more slowly and has lower substrate concentration than fluid at the free surface, the media that can disrupt the fluid layer and bring substrate rich fluid into contact with the biofilm, therefore, perform better than others. Despite the aerobic nature of trickling filter, this theory is applicable to anaerobic biofilms because they share the same theoretical basis with aerobic biofilms.

Henze and Harremoës (1983) believed the type of inert support material significantly influence the type of biofilm formed. Murray and van den Berg (1981) showed that support material markedly affected the rate of attachment and growth of bacteria converting acetic acid to methane. A rough, porous surface, which offers attachment sites to microorganisms, seems to be a better support. Verrrier and co-investigators (1987) concluded that the hydrodynamics of the system is important during the establishment of the irst bacterial layer. One particular aspect of hydrodynamics is the presence of pores and crevices, on the surface of packing material, which provides quiet local areas where bacteria can first adhere.

DeWalle and Chian (1976) observed a linear relationship between substrate removal rate and specific surface area at low values of specific surface area. At high specific surface areas the increase in removal rate decreases as the specific surface area increases. This might be attributed to the bacterial growth which tends to fill up the void spaces resulting in a liquid-biofilm interface that is smaller than the specific surface area of the filter medium. van den Berg and Lentz (1980) concluded that COD removal efficiencies increased with the area/volume ratio of the packing material. However, the research conducted by Song and Young (1986) showed the specific surface area of media only slightly affected the performance of upflow anaerobic biofilm reactors. They pointed out that the ability of media to redistribute flow within the media matrix is the most important media design factor. Young and Dahab (1983) suggested that the ability of the media to entrap and prevent the washout of biological solids is a more important factor than the specific surface area. Nevertheless, their conclusion may be misleading because the suspended biomass held loosely within the media may make it a major portion of the microbial activities, concealing the importance of the fixed films. Since the activity of fixed film in an upflow reactor is less than 75 % of the total microbial activity (van den Berg and Lentz, 1981), a proper selection of packing material, enhancing the amount of bacteria attached to the packing material, can increase the total biomass in reactors and boost the removal efficiency.

Bhadra and co-workers (1987) studied the effects of three support materials in downflow stationary fixed-film bioreactors. They found that wood chips are superior to charcoal and ceramic Rasching rings as supporting material. Most studies used non-adsorbable packing media, while activated carbon and zeolites were the only ad-

sorbable media used. Khan *et al.* (1981) and Suidan *et al.* (1981) used four granular activated carbon anaerobic filters in series to treat synthetic substrates containing phenol and catechol. The activated carbon showed satisfactory results in retaining biomass and reducing adsorbable organic matter due to its absorption capability. Sanchez and Roque-Malherbe (1987) found the zeolite packing improved treatment efficiency over other supporting materials because the combined effect of zeolite's proton exchange capacity and improved biofilm attachment characteristics.

Verrier *et al.* (1987) studied adhesion of four methanogens on polymeric surfaces with different hydrophobicities and concluded that the adhesion process is influenced by both the bacterial surface and by the support characteristics. Hydrophobic surfaces favors adhesion of hydrophobic bacteria such *Methanothrix soehngenii FE*, whereas *Methanosarcina mazei MC3* does not adhere and is not a good microorganism in the start-up of fixed film reactors. Switzenbaum (1985) and co-workers used biological precoating (denitrifying biofilm) and chemical precoating (polymer precoating) as means of enhancing anaerobic biofilm development. While their results indicated the significant differences among supporting materials, bacterial precoatings and various polymer precoatings did not enhance the rate of initial anaerobic biofilm accumulation.

2.3.2.2 Recirculation

The recirculation rate is the most direct way to control the flow regime of a reactor (Levenspiel, 1972). A higher recirculation rate will increase the degree of mixing of a plug-flow reactor and also increase the degree of fluidization of a moving-bed reactor.

Chian and DeWalle (1977) showed that the buffer requirement of a plug-flow anaerobic biofilm reactor can be negated by shifting the flow regime toward a completely-stirred tank reactor (CSTR). Ferguson *et al.* (1984) also reported the benefit of effluent recycle in reducing the required base addition. Furthermore, they suggested incorporating gas-stripping of CO_2 into the process to achieve a more effective result. Joubert *et al.* (1985) found that effluent recirculation improved overall COD removal and restricted H_2 production in the first phase reactor of a two-phase anaerobic reactor. Pette and Versprille (1981) found that sudden changes are not likely to occur in the operation of a UASB reactor with an high recirculation rate because of the high reactor volume and buffer capacity.

2.4 Methane Enrichment

The composition of the gas generated in the methane fermentation system generally consists of 50 to 75% methane with the balance being carbon dioxide. The methane content is dependent upon a number of factors. Methane enrichment of this fuel gas became an important topic during the energy crisis, especially when considering this gas as a substitute natural gas. Although the attention is diminishing because of the declining oil and natural gas price, this technology is still of interest for upgrading the quality of the fuel gas generated.

There have been several systems for methane enrichment proposed over the past years; two U.S. patents are most noteworthy among them. One is the pressurized reactor concept by Ort (1976). In Ort's design, anaerobic digestion is conducted under a pressure from 2 to 5 atmospheres (about 30 to 75 *psig*), which keeps the digester

content supersaturated with respect to CO_2 at atmospheric pressure. The pressurized effluent from the reactor is depressurized, heated, degassed, and recycled back to pressurized reactor. The slurry returned to the pressurized reactor is in a unsaturated state and, therefore, absorbs CO_2 from the gas phase, and significantly reduces the CO_2 content of the gas.

The other process is the two-phase anaerobic digestion concept of Ghosh and Klass (1977). The two-phase anaerobic digestion separates acidogenesis from acetogenesis and methanogenesis.

Ferguson *et al.* (1984) suggested gas stripping to reduce CO_2 in the recycle stream for single-stage digesters. In Ferguson's design, the recycle stream is stripped of CO_2 using air prior to mixing with the influent. Since CO_2 is the major source of acidity, gas stripping has the advantage of reducing base addition. Recycle ratio is important in this operation. Without recycling, carbonate carbon is split nearly equally between the reactor gas (CO_2) and the effluent (HCO_3^{-1} and $H_2CO_3^*$). At high recycle ratios, 30% or more of carbonate carbon is removed in the stripper, thus enriching the digester gas.

Hayes and co-workers (1983, 1989) proposed a similar but more advanced technique for two-stage digesters. The conceptual design of Hayes *et al.* (1983, 1989) is a combination of the above three designs, in which a pressurized second-stage reactor (acetogenic and methanogenic reactor) with an effluent stripping is applied to a two-stage system. The carbonate carbon in a recycle stream from the second-stage reactor is converted into CO_2 and $H_2CO_3^*$ when it passes through the acid-producing first-stage fermentation reactor. The bicarbonate alkalinity in the recycle stream is converted to volatile acid alkalinity when passing through the first-stage reactor. When these volatile acid salts are returned to the second-stage reactor, the volatile acid consumption absorbs protons. The resultant alkalinity generated is converted to bicarbonate alkalinity by reacting with the CO_2 produced by the methanogens. The CO_2 is subsequently purged by a stripper before returning the recycle stream to the pressurized second-stage reactor. Because CH_4 has limited solubility, the methane loss with the liquid is small even when an elevated pressure is applied. A proper combination of the "pH swing" and the pressurized second-stage reactor make possible the production of biogas with a high methane content.

III. MODEL DEVELOPMENT

Many researchers have developed mathematical models to conceptualize the mechanisms of biofilm actions. In general, their models have yielded satisfactory but limited results. In this chapter, these biofilm models will be combined with a chemical and physical equilibrium model to fully evaluate the performance of anaerobic fixed-film reactors. The equilibrium component of the model will consider conditions where equilibrium exists between liquid and gas phases, as well as the conditions under which the equilibrium does not exist.

In order to simplify the model development, some assumptions were made :
1. The solid phase is homogeneous and liquid phase is completely mixed.
2. The rate of reaction is limited by the single substrate, *i.e.*, acetate.
3. Steady-state is assumed for the model development.
4. The suspended growth is negligible in comparison to the attached growth.
5. CO_2 and CH_4 are the only two gaseous end products of anaerobic fermentation.

3.1 Biofilm Model

Atkinson and Davies (1974) first developed a bacterial biofilm model, incorporating both diffusion and Monod-type substrate utilization equations, which was subsequently modified by Williamson and McCarty (1976a,b). Williamson and McCarty (1976a and b) used a single-substrate biofilm kinetic model in which a planar bacterial film, of thickness, L_f, and uniform microbial density, X_f, was assumed. A stagnant liquid layer of thickness L covers the biofilm. Figure 3-1 illustrates, schematically, the conception of this model. Substrate is transported from the bulk solution to the biofilm through this liquid layer by molecular diffusion. The thickness of the stagnant liquid layer, L, can be expressed in terms of liquid layer mass transport coefficient, k_L (LT^{-1}), as:

$$k_L = \frac{D_w}{L} \tag{3-1}$$

where:
D_w = molecular diffusivity of the substrate in the liquid, L^2T^{-1}

The substrate concentration is assumed to vary in the z-direction (perpendicular to biofilm surface) only. Because no microbial activity is assumed to exist in the stagnant liquid layer, the flux of substrate across this layer can be described according to Fick's law:

$$J = -D_w \frac{dS}{dz} = \frac{D_w}{L}(S_b - S_s) \tag{3-2}$$

where:
J = substrate flux, $ML^{-2}T^{-1}$
S = rate-limiting substrate concentration, ML^{-3}
S_b = bulk substrate concentration, ML^{-3}
S_s = liquid-biofilm interface substrate concentration, ML^{-3}

The substrate utilization rate within the biofilm, $(r_s)_u$, is described by the Monod relationship as:

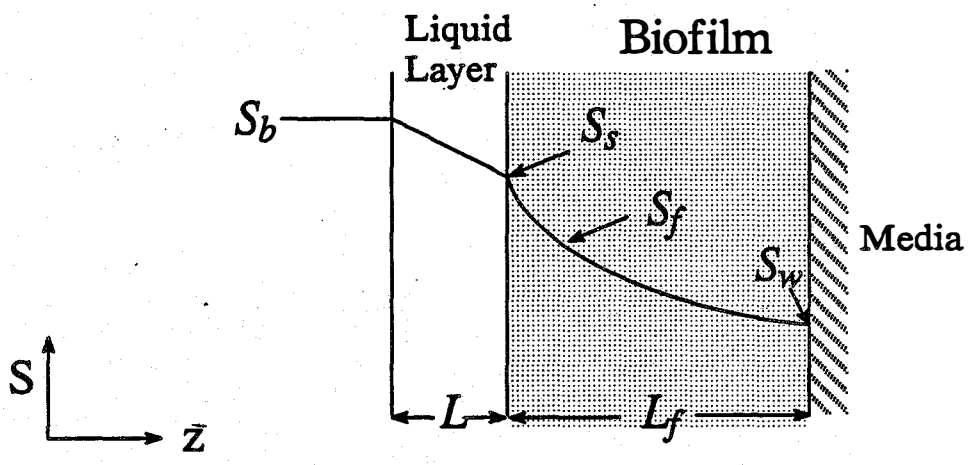

Figure 3–1 Schematic Diagram of Biofilm Model. (Williamson and McCarty, 1976a, b)

$$(r_s)_u = -\frac{kS_fX_f}{K_s + S_f} \tag{3-3}$$

where :

k = maximum specific rate of substrate utilization, T^{-1}
S_f = substrate concentration within the biofilm, ML^{-3}
X_f = biofilm density, ML^{-3}
K_s = Monod half-velocity coefficient, ML^{-3}

Molecular diffusion rate, $(r_s)_{diff}$, in the biofilm is related to substrate gradient by Fick's second law

$$(r_s)_{diff} = D_f\frac{d^2S_f}{dz^2} \tag{3-4}$$

where:

D_f = molecular diffusivity of the substrate in the biofilm, L^2T^{-1}

A second-order ordinary differential equation is obtained by incorporating Eq. 3-3 into 3-4 and assuming steady-state.

$$\frac{d^2S_f}{dz^2} = \frac{k\ S_f\ X_f}{D_f\ (K_s + S_f)} \tag{3-5}$$

with boundary conditions (B.C.)

$$B.C.1 \qquad S_f = S_s \qquad at \qquad z = 0 \tag{3-6}$$

$$B.C.2 \qquad \frac{dS_f}{dz} = -\frac{J}{D_f} \qquad at \qquad z = 0 \tag{3-7}$$

in which z is measured from the interface of the biofilm and stagnant liquid layer. Since the depth of "active biofilm" is limited by substrate mass transfer, the thickness of the active biofilm, L_f, is defined as the thickness when the concentration gradient becomes zero.

$$\frac{dS_f}{dz} = 0 \qquad at \qquad z = L_f \tag{3-8}$$

$$\int_0^{L_f} \frac{k\ S_f\ X_f}{K_s + S_f}\ dz = J \tag{3-9}$$

The number of independent variables used in the above equations can be reduced by defining dimensionless variables (Suidan, 1986).

$$S_f^* = \frac{S_f}{K_s} \qquad S_b^* = \frac{S_b}{K_s} \qquad S_s^* = \frac{S_s}{K_s} \tag{3-10}$$

$$z^* = z\sqrt{k\,X_f/D_f\,K_s} \tag{3-11}$$

$$L^* = L\sqrt{k\,X_f/D_f\,K_s} \tag{3-12}$$

$$J^* = \frac{J}{\sqrt{K_s k X_f D_f}} = \frac{D_w}{D_f}\frac{(S_b^* - S_s^*)}{L^*} \tag{3-13}$$

substituting Eqs 3-10 to 3-12 into Eqs. 3-5 to 3-9 yields :

$$\frac{d^2S_f^*}{dz^{*2}} = \frac{S_f^*}{1+S_f^*} \tag{3-14}$$

$$S_f^* = S_s^* \qquad at \qquad z^* = 0 \tag{3-15}$$

$$\frac{dS_f^*}{dz^*} = -\frac{J}{\sqrt{K_s\,k\,X_f\,D_f}} = -J^* \qquad at \qquad z^* = 0 \tag{3-16}$$

$$\frac{dS_f^*}{dz^*} = 0 \qquad at \qquad z^* = L_f^* \tag{3-17}$$

$$\int_0^{L_f^*} \frac{S_f^*}{1+S_f^*}\,dz^* = J^* \tag{3-18}$$

3.1.1 Biofilm Model Solution

Because Eq. 3-14 is a second-order, nonlinear ordinary differential equation which has no analytical solutions, it can only be solved numerically. However, analytical solutions do exist in two extreme value cases of Eq. 3-14 (Suidan and Wang, 1985). Case I - When the dimensionless substrate concentration in the biofilm, S_f^*, is everywhere much greater than one, Eq. 3-14 becomes

$$\frac{d^2S_f^*}{dz^{*2}} = 1 \tag{3-19}$$

Integration of Eq. 3-19 along with the boundary conditions given by Eqs. 3-16 and 3-17 yields the solution

$$L_f^* = J^* \tag{3-20}$$

Case II - When the dimensionless substrate concentration at the liquid-biofilm interface, S_s^*, is much smaller than 1, and since S_f^* is always less than or equal to S_s^*,

the solution of Eq. 3-14 becomes :

$$L_f^* = \tanh^{-1}\left(\frac{J^*}{S_s^*}\right) \tag{3-21}$$

Since Eqs. 3-20 and 3-21 provide analytical solutions for extreme values of S_f^*, the general solution can be expressed as

$$L_f^* = J^* + \tanh^{-1}\left(\frac{J^*}{S_s^*}\right) \tag{3-22}$$

This expression of L_f^* gave an excellent fit of the biofilm mathematical model solution for values of J^* less than or equal to 0.1. Eq. 3-22, however, did not predict the model solution for J^* values larger than 0.1. This can be corrected by changing it into

$$L_f^* = J^* + \tanh^{-1}\left\{\frac{0.5J^{*2} + J^*\left[1 + \left(\frac{J^*}{3.4}\right)^{1.19}\right]^{-0.61}}{S_s^*}\right\} \tag{3-23}$$

Rittmann and McCarty (1980) proposed an expression for steady-state biofilms, determined by the flux of substrate into the biofilm and the bacterial growth and decay rate, as

$$L_f = \frac{J\,Y}{b'\,X_f} \tag{3-24}$$

where:

Y = the true yield of bacterial mass per unit of substrate mass utilized
b' = the sum of specific decay coefficient and shear loss, T^{-1}

Eq. 3-24 can be expressed in dimensionless terms as

$$L_f^* = J^*\left(\frac{Y\,k}{b'}\right) \tag{3-25}$$

Substituting Eq. 3-25 into Eq. 3-23 and rearranging the resulting expression yields

$$S_s^* = \frac{0.5J^{*2} + J^*\left[1 + \left(\frac{J^*}{3.4}\right)^{1.19}\right]^{-0.61}}{\tanh\left[J^*\left(\frac{Yk}{b'} - 1\right)\right]} \tag{3-26}$$

Substituting Eq. 3-13 into 3-26, yields

$$S_b^* = J^*\,L^*\frac{D_f}{D_w} + \frac{0.5J^{*2} + J^*\left[1 + \left(\frac{J^*}{3.4}\right)^{1.19}\right]^{-0.61}}{\tanh\left\{L_f^* - J^*\right\}} \tag{3-27}$$

3.1.2 Completely Mixed Biofilm Reactor

A completely mixed biofilm reactor can be defined as a biofilm reactor with a spatially uniform substrate concentration in the reactor and in the effluent. A mass balance around such a reactor can be written as:

$$QS_0 - QS_b - JV\bar{a} = 0 \tag{3-28}$$

where:

S_o = substrate concentration in influent, ML^{-3}
S_b = substrate concentration in effluent, ML^{-3}
Q = wastewater flow rate, L^3T^{-1}
V = reactor volume occupied by packing media, L^3
J = substrate flux, $ML^{-2}T^{-1}$
$\bar{a}$ = specific surface area of attachment medium, L^{-1}

By defining a new dimensionless term, Eq. 3-28 can be converted into a dimensionless form as :

$$S_0^* - S_b^* - J^* \tau^* = 0 \tag{3-29}$$

$$\tau^* = \tau \bar{a} D_f \sqrt{k X_f / D_f K_s} \tag{3-30}$$

where:

τ = empty-bed retention time in biofilm reactor, T
τ^* = dimensionless empty-bed retention time in biofilm reactor

in which the dimensionless influent substrate concentration, S_0^*, is calculated by a simple mass balance relationship.

$$S_0^* = \frac{S_i^* Q_i + S_b^* Q}{Q} \tag{3-31}$$

where:

Q_i = flow rate of stock feed solution, L^3T^{-1}
S_i^* = dimensionless substrate concentration in stock feed solution

Eqs. 3-27, 3-29 and 3-31 can be solved simultaneously for J^*, S_b^*, and S_0^*. The total substrate flux, $J\bar{a}V$, can be converted into CO_2 and CH_4 flux and be incorporated into equilibrium model.

3.2 Equilibrium Model

The equilibrium model assumes an equilibrium relationship between CO_2 and CH_4 in the gaseous and liquid phase. This relationship for CO_2 and CH_4 can be described by the Henry's law.

The development of the equilibrium model starts with a stoichiometric equation of anaerobic digestion by Buswell and Mueller (1952).

$$C_nH_hO_l + \left(n - \frac{h}{4} - \frac{l}{2}\right) H_2O \rightarrow \left(\frac{n}{2} - \frac{h}{8} + \frac{l}{4}\right) CO_2 + \left(\frac{n}{2} + \frac{h}{8} - \frac{l}{4}\right) CH_4 \tag{2-1}$$

The total CO_2 and CH_4 production rate, $(CO_2)_T$ and $(CH_4)_T$ are calculated directly from the biofilm model

$$(CO_2)_T = J\,\bar{a}\,V f_c / MW_S \tag{3-32}$$

$$(CH_4)_T = J\,\bar{a}\,V f_m / MW_S \tag{3-33}$$

where:

f_c = $n/2 - h/8 + l/4$ = mole CO_2 / mole substrate
f_m = $n/2 + h/8 - l/4$ = mole CH_4 / mole substrate
MW_S = substrate molecular weight, M

The total CO_2 produced, $(CO_2)_T$, will distribute between the liquid and gaseous phase according to the following relationships

$$(CO_2)_T = Q_g \times \frac{P_{CO_2}}{P_T} \times \frac{1}{g} + Q_L \times (C_{T,out} - C_{T,in}) \tag{3-34}$$

$$P_T = P_{CH_4} + P_{CO_2} + P_w \tag{3-35}$$

in which :

Q_g = total gas flow rate, L^3T^{-1}
P_T = total pressure inside reactor, $ML^{-1}T^{-2}$
P_{CO_2} = CO_2 partial pressure inside reactor, $ML^{-1}T^{-2}$
P_{CH_4} = CH_4 partial pressure inside reactor, $ML^{-1}T^{-2}$
P_w = vapor pressure inside reactor, $ML^{-1}T^{-2}$
g = conversion factor between volume and mole, $M^{-1}L^3$
$C_{T,out}$ = total inorganic carbon concentration in effluent, ML^{-3}
$C_{T,in}$ = total inorganic carbon concentration in influent, ML^{-3}

Since the inorganic carbon concentration is the sum of the three carbonate species, Eq. 3-34 changes into Eq. 3-36 by substituting the equilibrium relationships

$$(CO_2)_T = Q_g \times \frac{P_{CO_2}}{P_T} \times \frac{1}{g} + Q_L \times [P_{CO_2} K_H (1 + \frac{K_{a1}}{10^{-pH}} + \frac{K_{a1}K_{a2}}{10^{-pH\times 2}}) - C_{T,in}] \tag{3-36}$$

where :

K_H = Henry's constant of CO_2 at the operating temperature, $L^{-2}T^2$
K_{a1}, K_{a2} = dissociation constants of H_2CO_3 at the operating temperature

Similarly, an equilibrium equation for CH_4 is developed

$$(CH_4)_T = Q_g \times \frac{P_{CH_4}}{P_T} \times \frac{1}{g} + Q_L \times (C_{CH_4,out} - C_{CH_4,in}) \tag{3-37}$$

where :

$C_{CH_4,in}$ = concentration of dissolved CH_4 in influent, ML^{-3}
$C_{CH_4,out}$ = concentration of dissolved CH_4 in effluent, ML^{-3}

Due to the relatively low solubility of CH_4 in water and the absence of CH_4 in the open atmosphere, it is reasonable to assume $C_{CH_4,in} = 0$. Eq. 3-37 is simplified further by

Henry's law.

$$(CH_4)_T = Q_g \times \frac{P_{CH_4}}{P_T} \times \frac{1}{g} + Q_L \times P_{CH_4} \times K'_H \tag{3-38}$$

where :

K'_H = Henry's constant of CH_4 at the operating temperature, $L^{-2}T^2$

Besides the above equations, an additional equation is needed to solve for the pH. Pohland and Suidan (1980) proposed the following equation, with the temperature effects incorporated into the constants, to identify the relationship between the alkalinity and the pH inside the reactor.

$$[alk] = \left[\frac{K_H K_{a1} P_{CO_2}}{10^{-pH}}\{1 + \frac{2K_{a2}}{10^{-pH}}\} + \frac{C_A}{\{\frac{10^{-pH}}{K_a} + 1\}} + \frac{C_{sul}}{\{1 + \frac{10^{-pH}}{K_{S1}} + \frac{K_{s2}}{10^{-pH}}\}}\right. \tag{3-39}$$

$$\{1 + \frac{2K_{S2}}{10^{-pH}}\} + \frac{C_N}{\{\frac{K_N 10^{-pH}}{K_W} + 1\}} + \frac{C_P}{\{1 + \frac{10^{-pH}}{K_{P2}} + \frac{K_{P2}}{10^{-pH}} + \frac{10^{-2pH}}{K_{P1}K_{P2}}\}}$$

$$\left.\{\frac{10^{-pH}}{K_{P2}} + 2 + \frac{3K_{P3}}{10^{-pH}}\} + \frac{K_W}{10^{-pH}} - 10^{-pH}\right]_{pH_f}^{pH}$$

where :

[alk] = alkalinity expressed as *mole* H^+ / L, ML^{-3}
C_A = total concentration of volatile fatty acid, ML^{-3}
C_{sul} = total sulfide concentration, ML^{-3}
C_N = total ammonia concentration, ML^{-3}
C_P = total phosphate concentration, ML^{-3}
K_a = dissociation constant of acetic acid at operating temperature
K_{S1}, K_{S2} = dissociation constants of sulfide at operating temperature
K_N = dissociation constant of ammonium at operating temperature
K_{P1}, K_{P2}, K_{P3} = dissociation constants of phosphate at operating temperature
K_W = equilibrium constant of water at operating temperature
pH_f = titration end point (4.3)

Eq. 3-39 can be simplified; for example, when the concentration of N, P and S are low, the terms related to C_P, C_{sul} and C_N can be omitted from the equation without causing major errors at low concentrations. Eqs. 3-35, 3-36, 3-38 and 3-39 provide a system of non-linear equations, from which P_{CO_2}, P_{CH_4} and Q_g and pH can be solved.

3.3 Non-Equilibrium Model

The equilibrium model assumes equilibrium exists between the gaseous and the liquid phases, however, it might not be true due to some physical constraints on the gas transfer rate from the liquid to the gas phase. Among these gas transfer theories, the two-film theory or two-resistance concept is the most widely accepted (Treybal, 1980). The pivotal factor controlling gas transfer is the gas transfer coefficient, $K_L a$, which is the product of the interfacial area of contact over the volume of liquid phase, a, and the overall liquid layer mass transfer coefficient, K_L. Shulman *et al.* (1955) defined K_L as a function of several system parameters:

$$K_L = 25.1\left(\frac{D_L}{d_s}\right)\left[D_P\frac{R_L}{\mu_L}\right]^{0.45}\left[\frac{\mu_L}{\varrho_L D_L}\right]^{0.5} \tag{3-40}$$

where :

D_L = diffusivity of solute in liquid, L^2T^{-1}
d_s = diameter of a sphere possessing the same surface area as a piece of packing, L
μ_L = liquid viscosity, $ML^{-1}T^{-1}$
ϱ_L = liquid density, ML^{-3}
R_L = superficial liquid rate, $ML^{-2}T^{-1}$

Eq. 3-40 clearly indicates that K_L is independent of gas production rate, therefore K_La is expected to vary with gas production rate as a does. The gas transfer reaction of CO_2 is expressed as Eq. 3-41, and the gas transfer of CH_4 can be described in a similar manner.

$$CO_2 \text{ gas transfer} = -K_La(K_HP_{CO_2} - C_{CO_2}) \tag{3-41}$$

in which C_{CO_2} (ML^{-3}) is the dissolved CO_2 concentration.

In non-equilibrium condition, Eqs. 3-36 and 3-38 are changed to Eqs. 3-42 and 3-43 by replacing the equilibrium concentrations of CO_2 and CH_4 with non-equilibrium concentrations C_{CO_2} and C_{CH_4}.

$$(CO_2)_T = Q_g \times \frac{P_{CO_2}}{P_T} \times \frac{1}{g} + Q_L \times \left[C_{CO_2}\left(1 + \frac{K_{a1}}{10^{-pH}} + \frac{K_{a1}K_{a2}}{10^{-pH\times 2}}\right) - C_{T,in}\right] \tag{3-42}$$

$$(CH_4)_T = Q_g \times \frac{P_{CH_4}}{P_T} \times \frac{1}{g} + Q_L \times C_{CH_4} \tag{3-43}$$

where C_{CH_4} (ML^{-3}) is the dissolved CH_4 concentration.

Since steady-state was assumed, the rates of CO_2 and CH_4 produced are equivalent to their respective mass transfer rates, as Eq. 3-44 and 3-45.

$$Q_g \times \frac{P_{CO_2}}{P_T} \times \frac{1}{g} = -K_La(K_HP_{CO_2} - C_{CO_2}) \tag{3-44}$$

$$Q_g \times \frac{P_{CH_4}}{P_T} \times \frac{1}{g} = -K'_La(K'_HP_{CH_4} - C_{CH_4}) \tag{3-45}$$

where :

K'_L = overall liquid layer mass transfer coefficient of CH_4, LT^{-1}

The alkalinity equation in the equilibrium model needs some modification for the non-equilibrium condition accordingly.

$$[alk] = \left[\frac{K_{a1}C_{CO_2}}{10^{-pH}}\left\{1 + \frac{2K_{a2}}{10^{-pH}}\right\} + \frac{C_A}{\left\{\frac{10^{-pH}}{K_a} + 1\right\}} + \frac{C_{sul}}{\left\{1 + \frac{10^{-pH}}{K_{S1}} + \frac{K_{s2}}{10^{-pH}}\right\}}\right. \tag{3-46}$$

$$\{1+\frac{2K_{S2}}{10^{-pH}}\}+\frac{C_N}{\{\frac{K_N 10^{-pH}}{K_W}+1\}}+\frac{C_P}{\{1+\frac{10^{-pH}}{K_{P2}}+\frac{K_{P2}}{10^{-pH}}+\frac{10^{-2pH}}{K_{P1}K_{P2}}\}}$$

$$\{\frac{10^{-pH}}{K_{P2}}+2+\frac{3K_{P3}}{10^{-pH}}\}+\frac{K_W}{10^{-pH}}-10^{-pH}\Big]_{pH_f}^{pH}$$

Eqs. 3-35, 3-42, 3-43, 3-44, 3-45, 3-46 form a similar system of non-linear equations, as in the previous model, of which P_{CO_2}, P_{CH_4}, C_{CO_2}, C_{CH_4}, pH and Q_g are the output parameters. The non-equilibrium model should be more accurate than the equilibrium model because it takes the gas transfer process into consideration. However, the determination of K_La would be the major uncertainty involved in model solving even though Eq. 3-40 can predict the K_L. Macroscopically, a is the contact area between liquid and gaseous phases over the volume of reactor. Since this model idealized the gas transfer process into a two-phase system in which biogas was evenly distributed, a can be regarded as related to the specific surface area of packing material ($\bar{a}$).

IV. DIFFUSIONAL MODEL DEVELOPMENT

Bird *et al.* (1960) modeled the diffusion of a gas into a liquid with a homogeneous first–order chemical reaction. Levenspiel (1972) used the same method to simulate a first–order diffusion reaction into a pore, while Harremoës (1976) modeled the pore diffusion of the denitrifying biofilms with zero– and first–order kinetics and obtained satisfactory results. Riemer (1977) used a diffusional model to simulate the out–diffusion of denitrification products and successfully predict the pH profile in denitrification biofilms. These studies have presented modeling techniques to describe the diffusion of gases. As a result, a diffusional model is developed in this chapter to simulate the diffusion of end products, CO_2 and CH_4, in anaerobic biofilms.

4.1 Zero–Order Kinetics

Riemer and Harremoës (1978) assumed that the out–diffusion of products of denitrification is zero–order and these products do not react with the substrates. This assumption is reasonable and applicable to the anaerobic biofilms because CO_2 (inorganic carbon) and CH_4 are also inactive to other compounds in anaerobic biofilms.

Figure 4–1 illustrates the idealized biofilm for in–diffusion of the substrate and the out–diffusion of the product. Since CH_4 does not readily react with other compounds, its out–diffusion can be assumed to be zero–order. It is also assumed that acetate is the only rate–limiting substrate. The rate of change of substrate flux (J_S) can be expressed as :

$$\frac{d\,J_S}{d\,z} = -\,k_{0f} \tag{4–1}$$

$$J_S = -\,D_f \frac{dC_S}{dz} \tag{4–2}$$

where :

J_S = the substrate flux, $ML^{-2}T^{-1}$
C_S = the substrate concentration, ML^{-3}
k_{0f} = the zero–order rate of substrate removal per unit volume of the biofilm, $ML^{-3}T^{-1}$
D_f = the substrate diffusivity in biofilm, L^2T^{-1}

At steady–state a mass balance for the elementary sections gives :

input – output + reaction = 0

$$AJ_S(in) - AJ_S(out) - k_{0f}A\Delta z = 0 \tag{4–3}$$

where :

A = total surface area of biofilm, L^2

rearranging:

$$\frac{d^2C_S}{dz^2} = \frac{k_{0f}}{D_f} \tag{4–4}$$

The substrate profile can be solved for 2 boundary conditions

$B.C.1 \qquad z = 0 \qquad C_S = C_S^B$

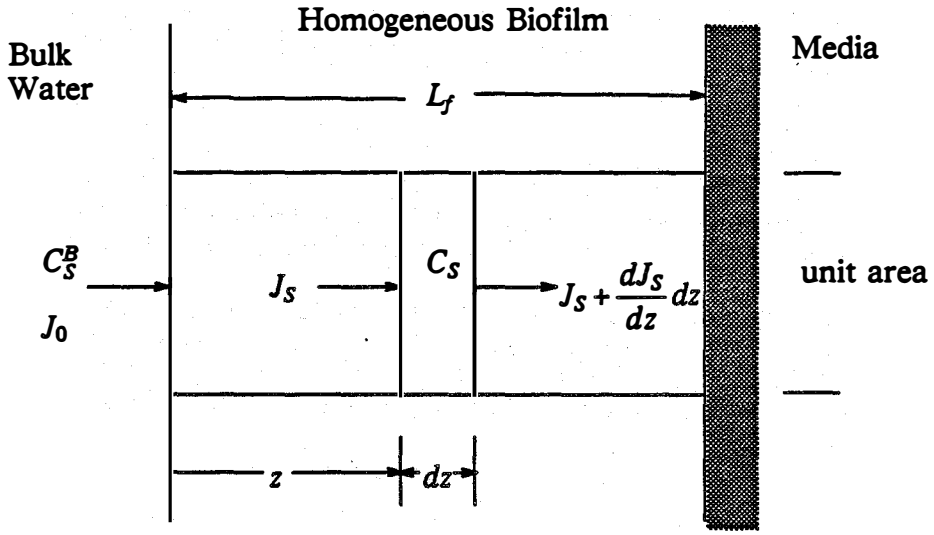

Figure 4–1 Geometry and Definition of Symbols for an Idealized Biofilm in Diffusional Model.

$$B.C.2 \qquad z = L_f \qquad \frac{dC_S}{dz} = 0$$

$$C_S = \frac{k_{0f}}{2D_f} z^2 - \frac{k_{0f}}{D_f} L_f z + C_S^B \tag{4-5}$$

in which :

L_f = the biofilm thickness, L

C_S^B = the substrate concentration in the bulk liquid, ML^{-3}

In which the superscript B represents the concentration at the biofilm surface. A dimensionless penetration parameter for substrate, β_S , and other dimensionless parameters can convert Eq. 4-5 into a dimensionless form.

$$\xi = \frac{z}{L_f} \qquad c_s = \frac{C_S}{C_S^B} \qquad \beta_S = \sqrt{\frac{2D_f C_S^B}{k_{0f} L_f^2}}$$

$$c_s = \frac{\xi^2}{\beta_S^2} - \frac{2}{\beta_S^2}\xi + 1 \tag{4-6}$$

The total substrate removal at the surface of the biofilm, if the biofilm is shallow, *i.e.* $\beta_S > 1$, can be expressed as

$$J_{S,T} = -D_f\left(\frac{dC_S}{dz}\right)_{z=0} A = k_{0f} L_f \bar{a} V \tag{4-7}$$

Eq. 4-7 shows that if zero-order kinetics exist in a shallow biofilm, the reactor should also follows zero-order kinetics.

The total substrate removal at the surface of a deep biofilm, $\beta_S \leq 1$, as given by Eq. 4-6 is incorrect because negative concentrations might result from negative $\beta_S$values. If the depth of substrate penetration is defined as ξ', then the boundary conditions become:

$$B.C.1 \qquad \xi = 0 \qquad c_s = 1$$

$$B.C.2 \qquad \xi = \xi' \qquad \frac{dc_s}{d\xi} = 0$$

$$B.C.3 \qquad \xi = \xi' \qquad c_s = 0$$

The solutions are :

$$\xi' = \beta_S$$

$$c_s = \frac{\xi^2}{\beta_S^2} - \frac{2}{\beta_S}\xi + 1 \tag{4-8}$$

The total substrate flux

$$J_{S,T} = -D_f\left(\frac{dC_S}{dz}\right)_{z=0} A = -D_f\left(\frac{dc_s}{d\xi}\right)_{\xi=0} \frac{C_S^B}{L_f} A = \bar{a} V \sqrt{2k_{0f} D_f} (C_S^B)^{\frac{1}{2}} \tag{4-9}$$

Eq. 4-9 shows that if zero-order kinetics exist in a deep biofilm, the reactor should follow half-order kinetics. Harremoës (1976) observed this behavior for diffusion limited zero-order reactions.

4.2 Out-Diffusion of Methane

A similar zero-order kinetic mass balance equation can be derived for CH_4

$$\frac{dJ_{CH_4}}{dz} = k_{0f} \tag{4-10}$$

$$J_{CH_4} = -D_{CH_4}\frac{dC_{CH_4}}{dz} \tag{4-11}$$

where :

J_{CH_4} = the CH_4 flux, $ML^{-2}T^{-1}$
C_{CH_4} = the CH_4 concentration, ML^{-3}
D_{CH_4} = the CH_4 diffusivity in biofilm, L^2T^{-1}

$$\frac{d^2C_{CH_4}}{dz^2} = -\frac{k_{0f}}{D_{CH_4}} \tag{4-12}$$

In dimensionless terms :

$$\eta = \frac{z}{\beta_S L_f} \qquad c_{CH_4} = \frac{C_{CH_4}}{C^B_{CH_4}} \qquad \beta_{CH_4} = \sqrt{\frac{2D_{CH_4}C^B_{CH_4}}{k_{0f}L_f^2}} \qquad \gamma = \frac{C^B_S D_f}{C^B_{CH_4}D_{CH_4}}$$

The CH_4 profile can be solved for 2 boundary conditions (B.C.)

$B.C.1 \qquad \eta = 0 \qquad c_{CH_4} = 1$

$B.C.2 \qquad \eta = 1 \qquad \frac{dc_{CH_4}}{d\eta} = 0$

$$c_{CH_4} = -\gamma\eta^2 + 2\gamma\eta + 1 \tag{4-13}$$

The concentration in the rear of the effective biofilm, $\eta = 1$, is :

$$c_{CH_4,rear} = \gamma + 1 \qquad C_{CH_4,rear} = C^B_{CH_4} + \frac{D_f}{D_{CH_4}}C^B_S \tag{4-14}$$

4.3 Out-Diffusion of Inorganic Carbon and pH Profile

If the product reacts in the biofilm, estimation of the concentration profile of the product becomes very complicated. Since no researchers have reported the reversible reaction of methane formation, the assumption of irreversibility should be quite acceptable. By contrast, the concentration profile of the other end product of anaerobic digestion, CO_2, is much more difficult to simulate because of its interchangability with HCO_3^{-1} and CO_3^{-2} . In addition, pH also affects the equilibrium relationship between these inorganic carbon species. Therefore, the out-diffusion of alkalinity produced should play a key role in determining the pH and concentration profile of inorganic carbon in the biofilm.

The stoichiometric equation for methane fermentation of acetate is :

$$CH_3COO^- + H_2O \rightarrow CH_4 + HCO_3^- \tag{4-15}$$

For each mole of acetate removed, one mole of CH_4 and of alkalinity is produced.

Riemer (1977) used a total inorganic carbon balance, an alkalinity balance and the equations of the carbonate system to model the alkalinity out-diffusion. Szwerinski *et al.* (1986) used a similar method to model nitrifying biofilms, while Liehr *et al.* (1988) used similar method to model the algal biofilm. The model development is based on the following assumptions :

(1) The intrinsic reaction rate is zero-order, which was proposed by Harremoës (1976).
(2) The rate of diffusion of reactants and products is described by Fick's first law of diffusion.
(3) The biofilm is homogeneous with no biogas bubbles and no bacterial filaments on the surface.
(4) The zero-order reaction is not pH-dependent.
(5) Steady-state conditions are considered.

The profiles of the inorganic carbon species and pH are developed as follows :

$$[H^+][OH^-] = K_W \tag{4-16}$$

$$[H^+]C_{HCO_3^-} = K_{a1}C_{CO_2} \tag{4-17}$$

$$[H^+]C_{CO_3^{-2}} = K_{a2}C_{HCO_3^-} \tag{4-18}$$

$$\Delta C_T = \Delta(C_{CO_3^{-2}} + C_{HCO_3^-} + C_{CO_2}) \tag{4-19}$$

$$\Delta ALK = \Delta\,(\,2C_{CO_3^{-2}} + C_{HCO_3^-} + [OH^-] - [H^+]\,) \tag{4-20}$$

Carbon balance :

$$\frac{dJ_{C,T}}{dz} = k_{0f} \tag{4-21}$$

$$D_{CO_2}\frac{\partial^2 C_{CO_2}}{\partial z^2} + D_{HCO_3^-}\frac{\partial^2 C_{HCO_3^-}}{\partial z^2} + D_{CO_3^{-2}}\frac{\partial^2 C_{CO_3^{-2}}}{\partial z^2} = -k_{0f} \tag{4-22}$$

Alkalinity balance :

$$\frac{dJ_{ALK}}{dz} = k_{0f} \tag{4-23}$$

$$D_{HCO_3^-}\frac{\partial^2 C_{HCO_3^-}}{\partial z^2} + 2D_{CO_3^{-2}}\frac{\partial^2 C_{CO_3^{-2}}}{\partial z^2} = -k_{0f} \tag{4-24}$$

The pH is assumed to stay within a range such that the change of $[H^+]$ and $[OH^-]$ can be neglected. The changes in C_{CO_2} and $C_{CO_3^{-2}}$ are also small because the inorganic carbon is predominantly present in the bicarbonate form at the operational pH in most anaerobic fermentations.

$$D_{CO_2}\frac{\partial^2 C_{CO_2}}{\partial z^2} = 0 \tag{4-25}$$

$$D_{HCO_3^-}\frac{\partial^2 C_{HCO_3^-}}{\partial z^2} = -k_{0f} \tag{4-26}$$

$$D_{CO_3^{-2}}\frac{\partial^2 C_{CO_3^{-2}}}{\partial z^2} = 0 \tag{4-27}$$

The concentration profiles of these inorganic carbon species therefore are solved for the B.C.s as :

$$C_{CO_2} = C^B_{CO_2} \tag{4-28}$$

$$C_{HCO_3^-} = -\frac{1}{2}\frac{k_{0f}}{D_{HCO_3^-}}z^2 + \frac{\sqrt{2D_f C^B_S k_{0f}}}{D_{HCO_3^-}}z + C^B_{HCO_3^-} \tag{4-29}$$

$$C_{CO_3^{-2}} = C^B_{CO_3^{-2}} \tag{4-30}$$

By defining the dimensionless depth as ;

$$\eta = \frac{z}{\beta_S L_f} = z\sqrt{\frac{k_{of}}{2D_f C^B_S}} \tag{4-31}$$

The pH profile :

$$pH(z) = -\log(K_{a1}\frac{C_{CO_2}(z)}{C_{HCO_3^-}(z)}) \tag{4-32}$$

$$pH(\eta) = -\log K_{a1} - \log\frac{d_1}{d_0} - \log\frac{C^B_0 d_0}{(-\eta^2 + 2\eta + C^B_1 d_1)} \tag{4-33}$$

in which:

$C^B_0 = C^B_{CO_2}/C^B_S$

$C^B_1 = C^B_{HCO_3^-}/C^B_S$

$d_0 = D_{CO_2}/D_f$

$d_1 = D_{HCO_3^-}/D_f$

Eq. 4-33 is useful in predicting the pH profile of anaerobic biofilms since the only information needed is the bulk concentrations of $C^B_{CO_2}$ calculated from the equilibrium model.

V. MATERIALS AND METHODS

Three anaerobic upflow fixed-bed reactors were chosen to experimentally verify the biofilm models developed. Three packing materials with different specific surface areas were used to examine the effect biomass has on the reactor performance, while different operating conditions were conducted in an attempt to test the equilibrium and non-equilibrium models.

5.1 Experimental Reactor System Design

The schematic configuration of the experimental reactor system is shown in Figure 5-1. The substrate was fed at the bottom of the reactor through a conical inlet followed by a distribution plate. Effluent was withdrawn from the top for recirculation and disposal. The liquid level was maintained at 4 inches above the packing material, while 4 inches of head space was allowed for gas-liquid separation. Biogas, passing through a pressure control valve, exited from the top of the reactor and was collected by a wet-test gas meter (*Precision Scientific*, cat. no. 63126).

An internal recirculation stream was set at a recycle ratio of 20 in order to ensure an influent concentration of less than 3000 mg/L COD even when the feed concentration was as high as 40 g/*L* of COD. Although the reactors were operated in a plug-flow pattern, mixing action in the reactor produced by the gas bubbles and hydraulic dispersion and the high recycle ratio made the flow regime approach an ideal CSTR (Levenspiel, 1972). An external recirculation stream, used for diluting the concentrated feed solution, was pumped at 5 *L*/d to control the HRT at 3 days. Before being fed into the reactor, the external recirculation stream, after being mixed with the acid feed solution, was passed through a CO_2 stripper where the CO_2 was removed, facilitated by a "pH swing". In the stripper, the pH was depressed by the addition of the acid feed solution, thus converting the inorganic carbon species in the effluent into CO_2. An air stream of 1.85 *L/min* was used to strip this CO_2 prior to returning this stream to the reactor.

The reactors were made from 1/4 inch thick 8 inch diameter Plexiglas columns and 1/2 inch thick stainless steel end plates. All reactors were maintained at mesophilic condition, *i.e.* $35 \pm 2\,^{\circ}C$, by heat tapes monitored by automatic temperature controllers (*Cole Parmer*, model 2157). Three different packing materials, of different specific surface areas, were placed into three reactors. The packing materials include : Berl saddle, light-weight aggregate (Haydite) and activated carbon. Table 5-1 lists the physical dimensions and characteristics of the packing materials. The surface area to volume ratios are calculated by the following equation :

$$\frac{A}{V} = \frac{6}{d_s}\,\frac{(1-\epsilon)}{\phi_s} \qquad (5\text{-}1)$$

where :

- A = total surface area of packing material, L^2
- V = the total effective reactor volume, L^3
- d_s = the diameter of equivalent-volume sphere, L
- ϕ_s = sphericity = ratio of the surface area of the equivalent-volume to the actual surface area
- ϵ = porosity

van den Berg and Lentz (1979) pointed out that upflow reactors behave in part as fluidized or expanded bed reactors. They also proved that the activity of the fixed

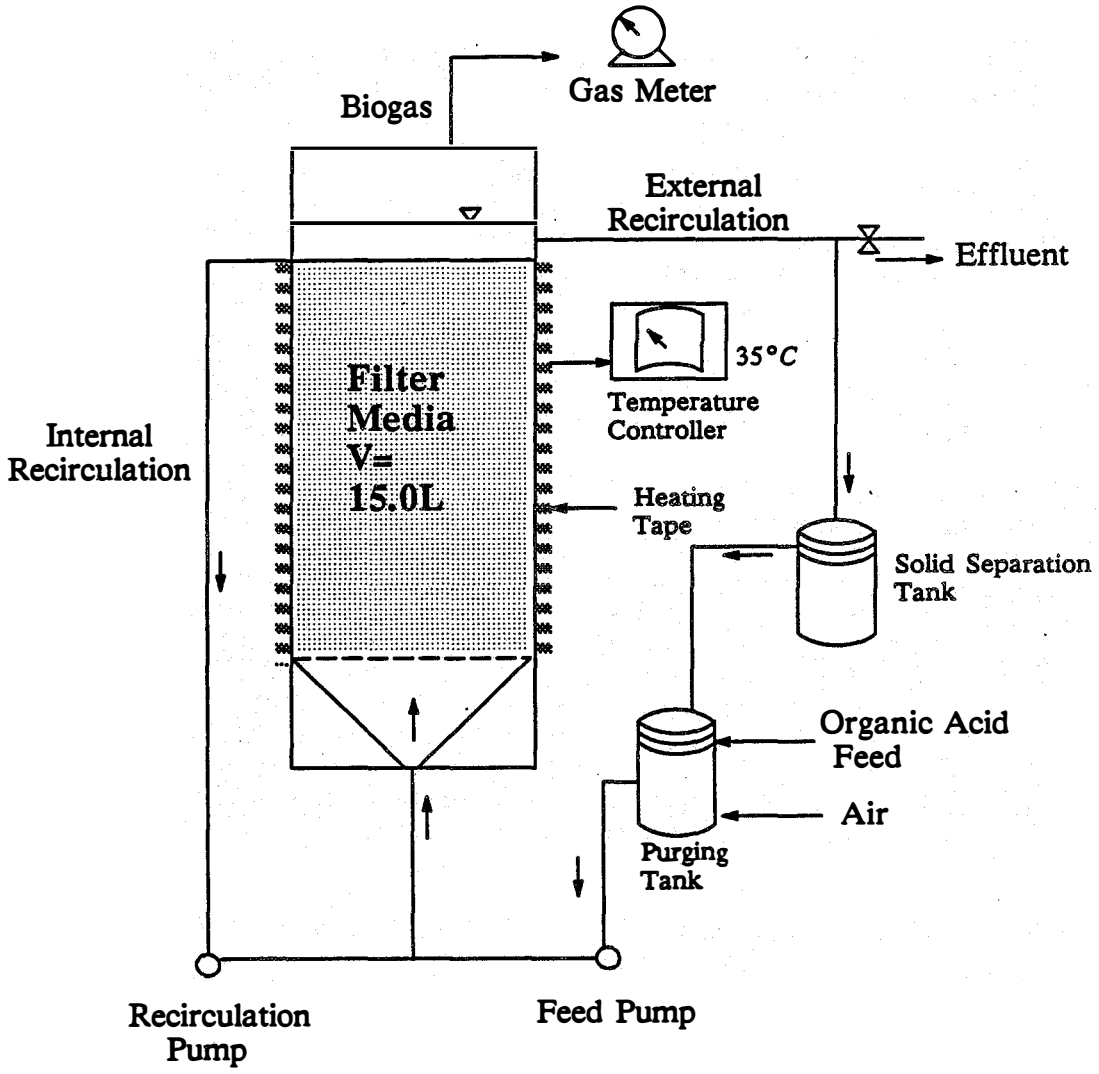

Figure 5-1 The Schematic Diagram of Experimental Set-up.

Table 5-1 Physical Dimensions and Characteristics of Packing Materials

Media	Filtrasorb 400 Activated Carbon (12×14)	Mid-Size Aggregate (Haydite)	Berl Saddle
Surface area(a) (m^2 /g)	1091.65	0.3669	
Area / volume (cm^{-1})	26.79	12.92	1.87(b)
Porosity	0.4 - 0.5	0.4925	0.80
Size(*mm*)	1.41 - 1.68	2.38 - 4.76	
Bulk Density, (lb/ft^3)	25	5.1	
Particle density, Wetting in water	1.3 - 1.4	1.5	
Sphericity	0.8	0.70(c)	0.3(d)

(a) N_2 BET method
(b) Provided by manufacturer
(c) Visual comparison from Fair *et al.* (1973)
(d) Perry and Green, 1984.

film in an upflow reactor is less than 75% of the total microbial activity. Consequently, the biological solids held loosely within the void space of the media may make the suspended growth a major portion of the microbial activity and therefore conceal the importance of the attached biomass. Young (1983) indicated that this increased bed activity, caused by unattached (suspended) growth, is greater toward the inlet. In addition, the internal recycle stream brings the suspended solids back to the bottom of the reactors where these solids are trapped in the influent cones. These conical bottoms should have sufficient slope for drainage of the sludge. Therefore, a periodical (biweekly) removal of these solids, by draining a portion of the reactor contents from the inlet, was practiced to meet the assumption of negligible suspended growth in the reactor.

5.2 Feed Solution

A mixture of organic acids and a nutrient feed solution was used to simulate the leachate from the acid fermentation phase of a two-stage fermentation. Because the simulated feed does not contain suspended solids (SS) and its composition limits the microbial growth to low polysaccharide-secretion syntrophic and methanogenic bacteria, the media clogging problem is eliminated (Ehlinger, 1987). The composition of the concentrated feed solution, simulating the typical anaerobic fermentation products of a carbohydrate substrate (Hungate, 1966), is listed in Table 5-2.

5.3 Experimental Procedure

The experimentation included three major parts, *i.e.* the start-up, batch experiments and the model verification. These components are elucidated in the following sections.

5.3.1 Start-up

The reactors were started with a low organic loading while the initial biofilm development occurred. The organic loading was increased incrementally until the initial loading conditions were achieved. All three reactors were started up with effluent of existing anaerobic fluidized-bed reactors. The Berl saddle reactor had been operating for about three years before the activated carbon- and aggregate-packed reactors were started in August and December 1987, respectively. These reactors were first operated at an organic loading of 3.33 KgCOD/$m^3 \cdot d$ until a pseudo-steady state was reached. The steady state is called pseudo-steady-state because while the hydraulic retention time and COD loading rate are constant, the biomass concentration is continuously and slowly increasing (Guiot and van den Berg, 1985). Evaluation of pseudo-steady-state conditions was considered completed when the effluent quality remained consistent for a period over five times the hydraulic retention time.

5.3.2 Estimation of Biofilm Activity

Yoda *et al.* (1987) proposed the use of batch experiments to estimate biomass activity in the reactors. This is similar to the progress curve experiment used by Dolfing (1985) to evaluate the kinetics of methanogenesis. Dolfing's technique follows Fick's first law for estimating the concentration gradient which controls the substrate flux through a biofilm. This method also assumes the relationship between activity and substrate concentration follows Monod kinetics. Linear dependency between activity and substrate concentration is observed at concentrations around and below the K_S

Table 5-2 Composition of (Concentrated) Acid Feed Solution

Component	mg/L	COD Equivalent-g/L
Acetic Acid	150000.0	160.0
Propionic Acid	60000.0	91.0
Butyric Acid	60000.0	110.0
Valeric Acid	15000.0	31.0
Caproic Acid	5000.0	11.0
Total		403.0
N (NH_4Cl)	200.0	
P ($K_2HPO_4 \cdot 3H_2O$)	40.0	
S ($(NH_4)_2SO_4$)	50.0	
Co ($CoCl_2$)	0.5	
Zn ($ZnCl_2$)	0.1	
Fe ($FeSO_4 \cdot 7H_2O$)	5.0	
Ni ($NiCl_2$)	0.5	

value. The batch experiments, by contrast, were conducted at high substrate concentration in order to measure the maximum substrate utilization rate. Provided that the specific activities of the organisms are constant throughout the test period, the maximum rate of reaction is proportional to the biomass responsible for the reaction. This technique may have some limitation in the fixed-film systems because the completely-mixed state is unlikely to be attained. However, batch experiments are very useful in estimating the amount of biomass in each reactor. Since CH_4 formation is much easier to determine than the disappearance of COD, CH_4 production rates were used to calculate the substrate utilization rate. The relationship between the substrate utilization rate and total biomass, M_T, is :

$$r_{sub} = k\, M_T \qquad (5\text{–}2)$$

where :

r_{sub} = the substrate utilization rate, MT^{-1}
k = the maximum specific rate of substrate utilization, T^{-1}

The estimated maximum CH_4 production rate from batch experiment is converted to r_{sub} to calculate the total biomass as Eq.5–2. The attached biomass M_{Bio} is estimated as :

$$M_{Bio} = M_T - VSS \times V_T \qquad (5\text{–}3)$$

where :

M_{Bio} = the total attached biomass, M
VSS = the volatile suspended solids in effluent, ML^{-3}
V_T = the total reactor volume, L^3

The relationship between the biofilm thickness, L_f, and M_{Bio} is expressed as follows:

$$M_{Bio} = X_f\, L_f\, \bar{a}\, V \qquad (5\text{–}4)$$

in which :

X_f = the biofilm density, ML^{-3}
L_f = the biofilm thickness, L
V = the reactor volume occupied by packing media, L^3
$\bar{a}$ = specific surface area of attachment medium, L^{-1}

The feed was routinely stopped four hours before the test to ensure all substrate had been reduced to the minimum level by the microorganisms. A slug of feed solution was injected into the reactor which allowed the substrate concentration to sufficiently exceed the K_S value so that the microorganisms can utilize the substrate at the maximum rate. The slug dose of 15 g COD was selected to ensure an excess of 1,000 mg COD/L initial concentration for the whole reactor. During the experiment the flow rate of recycle pumps was raised to 175 L/d to ensure better mixing. Acetic acid was replaced by sodium acetate of equivalent COD strength in the feed solution to minimize pH drop. After the slug injection, the biogas production, biogas content, COD and pH were measured at regular intervals.

5.3.3 Experimental Tasks

The following tasks were designed to generate data that can verify the models.

Task I. The validity of the biofilm model.
In order to confirm the biofilm model, one set of experiments was conducted upon all three reactors. This condition included a feed solution of 10 g COD/L, HRT of 3 days, pH 7 and COD loading of 3.33 Kg COD/$m^3 \cdot d$. After the steady-state conditions had been reached for each reactor, batch experiments were conducted to measure the maximum rate of methane production of the entire reactor. The maximum substrate utilization rate, calculated from the CH_4 production rate, can estimate the biomass through Eq. 5-1.

Task II. The effect of supporting media on the performance of anaerobic filters. After the initial set of experiments, the COD loading was step increased in each reactor, with other operational parameters remaining constant, until system failure was reached. Chen *et al.* (1988) reported that a COD loading of 72.4 Kg COD/ $m^3 \cdot d$ was treated successfully by an anaerobic fluidized-bed reactor containing activated carbon. Therefore, the step increase of COD loading in the activated carbon reactor was selected as 13.32 KgCOD/ $m^3 \cdot d$. Since there is no report on the performances of the other two packing materials, the step increase of the COD loadings was initially set at a more conservative value of 3.33 KgCOD/ $m^3 \cdot d$. Steady-state condition and biomass content were assessed after each increment to inspect the biomass-holding capacity of each material and determine the correlation between the total biomass and organic loadings.

Task III. The effectiveness of the equilibrium model.
Two key input parameters of the equilibrium model, alkalinity and HRT, were varied on one reactor to test the accuracy of the model. Since the Berl saddle reactor was the first to achieve a steady-state condition for the initial experiments, the alkalinity level was changed on it before Task II. was initiated to examine the chemical equilibrium described by the equilibrium model. Three steady states were reached with alkalinity of 2600, 3600 and 4600 mg $CaCO_3$ /L, respectively, to test the accuracy of equilibrium model. At an organic loading of 5.0 KgCOD/ $m^3 \cdot d$ and pH 7 , the HRT was reduced by a step of 1 day until an HRT of 1 day was reached. The HRT was then reduced by a step of 0.25 day until failure was reached. The steady-state condition was evaluated at each step to validate the equilibrium model as well as determine the conditions at which the non-equilibrium modification is necessary.

5.4 Analytical Methods

Several parameters were measured routinely to monitor the performance of the reactor. The total gas production rate, feed rate and pH were measured daily. Alkalinity, chemical oxygen demand (COD), biogas composition and volatile fatty acids (VFA) were measured twice weekly, while total dissolved inorganic carbon was measured during steady-state operation.

pH The pH of the effluent was measured by a *CORNING* pH meter model 7 immediately after samples were withdrawn from the reactors. The pH should be read without delay to minimize pH shift due to the release of dissolved CO_2 into the atmosphere.

Total Inorganic Carbon The total inorganic carbon was analyzed by using a *Dohrman* Model DC-80 carbon analyzer (made by *Environtech/Dohrman*). All samples were filtered through 0.45 μm membrane filters. Analyses were conducted on the same sample before and after it was acidified to pH 2 with concentrated phosphoric acid and purged with nitrogen gas for 5 minutes to remove all inorganic carbon. The total inorganic carbon was estimated as the difference between these two values.

Alkalinity The alkalinity analysis followed the procedure in section 403 of *Standard Methods for the Examination of Water and Wastewater,* 15th edition (1981). Samples were titrated to an end point of pH 4.3 with standardized 0.02N H_2SO_4.

COD The COD was determined by *Hach* COD procedure which is a modification of the traditionally-used dichromate reflux method. Soluble CODs were determined on samples filtered through 0.45 μm membrane filters. Two milliliters of filtered sample was put into a COD digestion reagent vial, digested for 2 hours at 150°C. The COD was read by a *Busch & Lomb* Spectrometer at 420 nm.

VFA Samples for volatile fatty acid analysis were first filtered through 0.45 μm membrane filters and acidified to pH 2 by phosphoric acid. A *Hewlett-Packard* 57[illegible] gas chromatograph, equipped with a flame ionization detector (FID), with a 92 cm long, 2 mm ID glass column packed with 0.3 % Carbowax with 0.1% phosphoric acid on 60/80 Carbopack were used in the analysis. Nitrogen was used as the carrier gas at an average flow rate of 30 *mL/min.* An air to hydrogen ratio of 2.7 was maintained. The detector temperature was maintained at 200 °C. Standard solutions of volatile fatty acids were used for calibration.

Gas Analysis The biogas composition was analyzed by a *Fisher* Gas Partitioner Model 1200 which employs gas chromatography to separate and measure the components of gas mixtures containing H_2, N_2, O_2, CH_4 and CO_2. When a sample of 500 μl was injected into the gas partitioner with a hypodermic syringe, it was carried through the instrument's two chromatographic columns by a continuous flow of helium carrier gas at a flow rate of 250 *ml/min.* The components of the sample traveled through the two chromatographic columns at different rates and were consequently separated before they reached the detector. Each component produced an electrical signal which was plotted by a strip chart recorder.

Total and Volatile Suspended Solids The glass fiber filter method, using Gooch crucibles, to measure suspended solids is described in Section 209D of *Standard Methods for the Examination of Water and Wastewater,* 15th edition (1981). The method to determine the volatile suspended solids is described in Section 209E of the same reference.

VI. RESULTS AND DISCUSSIONS

The numerical results of the models and the experimental results are presented in this chapter. All mathematical models are solved by the ZSPOW subroutine of IMSL (1984) library on a personal computer (IBM-AT).

6.1 Biofilm Model verification

The effects of specific surface area of packing materials on biomass retention and on reactor performance were tested by using three different supporting materials, including : Berl saddle, light-weight aggregate (Haydite) and activated carbon. Each reactor was operated at pseudo-steady state, under increasing organic loadings, until the systems failed. The biomass-retaining capacity of each material was evaluated through a series of batch experiments (see Section 5.3.2). The methane production rates were evaluated from the batch tests and the total biomass and biofilm thickness were calculated from Eqs. 5-2 to 5-4.

6.1.1 Parameter Estimation

As assumed in the model development, substrate reaches the biofilm through a stagnant liquid layer by molecular diffusion. As a result, the thickness of this layer, L, controls the diffusional resistance. Estimation of L is summarized in this section.

The liquid layer thickness, L, for deep beds of packed spheres is predicted by a correlation proposed by Wilson and Geankoplis (Skelland, 1974).

$$L = \frac{\epsilon\, d_s}{1.09(Re)^{1/3}(Sc)^{1/3}} \qquad (6\text{-}1)$$

For

$$0.0016 < Re < 55$$
$$0.35 \leq \epsilon \leq 0.75$$
$$165 \leq Sc \leq 70,600$$

in which:

Re = the Reynolds number = $\varrho d_s v/\mu$
Sc = the Schmidt number = $\mu/\varrho D$
D = molecular diffusivity of the substrate in the liquid, L^2T^{-1}
v = the empty-bed flow velocity through the reactor, LT^{-1}
μ = absolute viscosity of the liquid, $ML^{-1}T^{-1}$
ϱ = density of the liquid, ML^{-3}
ϵ = bed porosity
d_s = diameter of sphere of the same surface area as a single particle, L

Sherwood and Holloway (Treybal, 1980) established a relationship for liquid layer thickness for Berl saddles, which is given by :

$$L = \frac{d_s\,(\mu / d_s\, v\, \varrho)^{0.45}}{25.1\, Sc^{0.5}} \qquad (6\text{-}2)$$

The diffusivity of the substrate, acetate, is calculated by the empirical correlation of Wilke and Chang (Treybal, 1980). Table 6-1 presents all the parameters used in

Table 6-1 Parameters Used in Biofilm Model and Biomass Assessment

Parameter	Value	References
K_S	0.05 mg COD/ cm^3	Suidan, 1986
k	8.7 day^{-1}	Lawrence & McCarty, 1969 Lawrence, 1971
X_f	10.0 mg/cm^3	Suidan, 1986
D_w	1.37 cm^2/day	Wang, 1984
D_f	1.1 cm^2/day	Wang, 1984
L (Haydite)	1.87×10^{-2} cm	
L (Activated Carbon)	3.44×10^{-2} cm	
L (Berl Saddle)	4.73×10^{-3} cm	
d_s(Haydite)	0.337 cm	
d_s(Activated Carbon)	0.154 cm	
d_s(Berl Saddle)	3.385 cm	
Sc	456.43	
v	350.85 cm/day	
ϱ	0.994 g/cm^3	CRC Handbook of Chemistry and Physics, (Weast, 1985)
	$7.194 \times 10^{-2} g\ cm^{-1}\ sec^{-1}$	

these equations except for bed porosity which is given in Table 5–1. The d_s values for Haydite and activated carbon were calculated as the geometric means of the upper and lower limits of their particle sizes.

6.1.2 Haydite Reactor

The pseudo–steady state conditions for the Haydite reactor, for each organic loading, are listed in Table 6–2. The operation of this reactor was stopped after obtaining data for the 19.98 Kg COD/ $m^3 \cdot d$ loading. At this loading rate the reactor showed signs of instability, such as a substantial increase in the effluent soluble COD and volatile suspended solid (VSS). Figure 6–1 illustrates the results of the batch experiments conducted to estimate the total biomass in the reactor. All batch experiments were performed by spiking the reactor with 15g COD except at the loading of 19.98Kg COD/ $m^3 \cdot d$. A slug feed of 45g COD was injected at that loading to ensure an extended period of maximum biological activity because the substrate utilization rate was much higher than at the lower loadings.

The total biomass is computed with the maximum substrate utilization rate from Figure 6–1 and Eq. 5–2. The biofilm thickness is computed by Eqs. 5–3 and 5–4, while Eqs. 2–27, 3–29 and 3–31 are used to compute the total substrate flux and effluent soluble COD. Table 6–3 summarizes the model predictions. Figure 6–2 shows the effect of the COD loading rate on the thickness of the biofilm and the total biomass in the reactor. The lower portion of Figure 6–2 demonstrates the biomass–holding capacity of this reactor, which reaches the maximum biofilm biomass at the loading of 13.32 KgCOD / $m^3 \cdot d$. The corresponding biofilm thickness, shown in the top part of Figure 6–2, indicates the same fact that the L_f has reached its maximum value at the same loading. The reactor did not completely fail at the loading of 19.98 KgCOD / m^3 d because the suspended–growth biomass was making a significant contribution to the COD reduction. It was, however, operating at a reduced efficiency as indicated by the increase in the effluent COD (Table 6–2). Figure 6–2 shows the possible deviation of the biomass estimation which occurs at the COD loading of 10.0 KgCOD / $m^3 \cdot d$. Because the estimations are made from the slopes of the plot of batch experiments, the results may vary depending on the interpretation of these slopes. The difficulty in defining the proper slopes is demonstrated in Figure 6–1.

The validity of the biofilm model is further substantiated by the effluent COD results in Figure 6–3. Because the suspended–growth kinetics were not considered in the model development, the model might deviate from reality when the suspended–growth biomass concentration is high. The model prediction, however, shows very good agreement with the experimental values when suspended biomass is low. While the model prediction and experimental value differ at the higher loading, the biofilm biomass is predominantly responsible for the activity in the anaerobic reactor even at elevated concentrations of suspended–growth biomass. The assumption that the suspended–growth is negligible compared to the attached growth is, consequently, justified.

Since the biomass loss in the form of dispersed biomass can reduce the reactor SRT, the biomass controlling the SRT should be regarded as a combination of the biofilm and the suspended–growth biomass. The biofilm biomass will remain large even at higher suspended–growth biomass concentration, whereas the suspended–growth biomass will be lost in the effluent thereby reducing the reactor SRT. This hypothesis is supported by Figure 6–2, which shows that the amount of biofilm biomass remained

Table 6-2 Steady-State Condition in Haydite Reactor
HRT (empty bed) = 3 days

COD Loading $Kg/m^3 \cdot d$	Biogas Rate L/day	pH	Effluent Soluble COD mg/L	CH_4 %	Alkalinity mg $CaCO_3$/L	VSS* mg/L	$C_{T,in}$ mole/L	$C_{T,out}$ mole/L
3.33	24.86	7.0	52.06	72.07	2667.54	45	0.00479	0.0549
6.66	59.93	6.95	135.8	64.27	3604.58	41	0.0178	0.0586
9.99	91.24	6.98	124.84	63.31	3730.65	50	0.01173	0.0729
13.32	132.57	6.93	136.37	60.63	3135.15	95	0.02209	0.0604
19.98	187.13	7.0	1729.0	57.70	4202.92	943	0.02981	0.0583

* Volatile Suspended Solid.

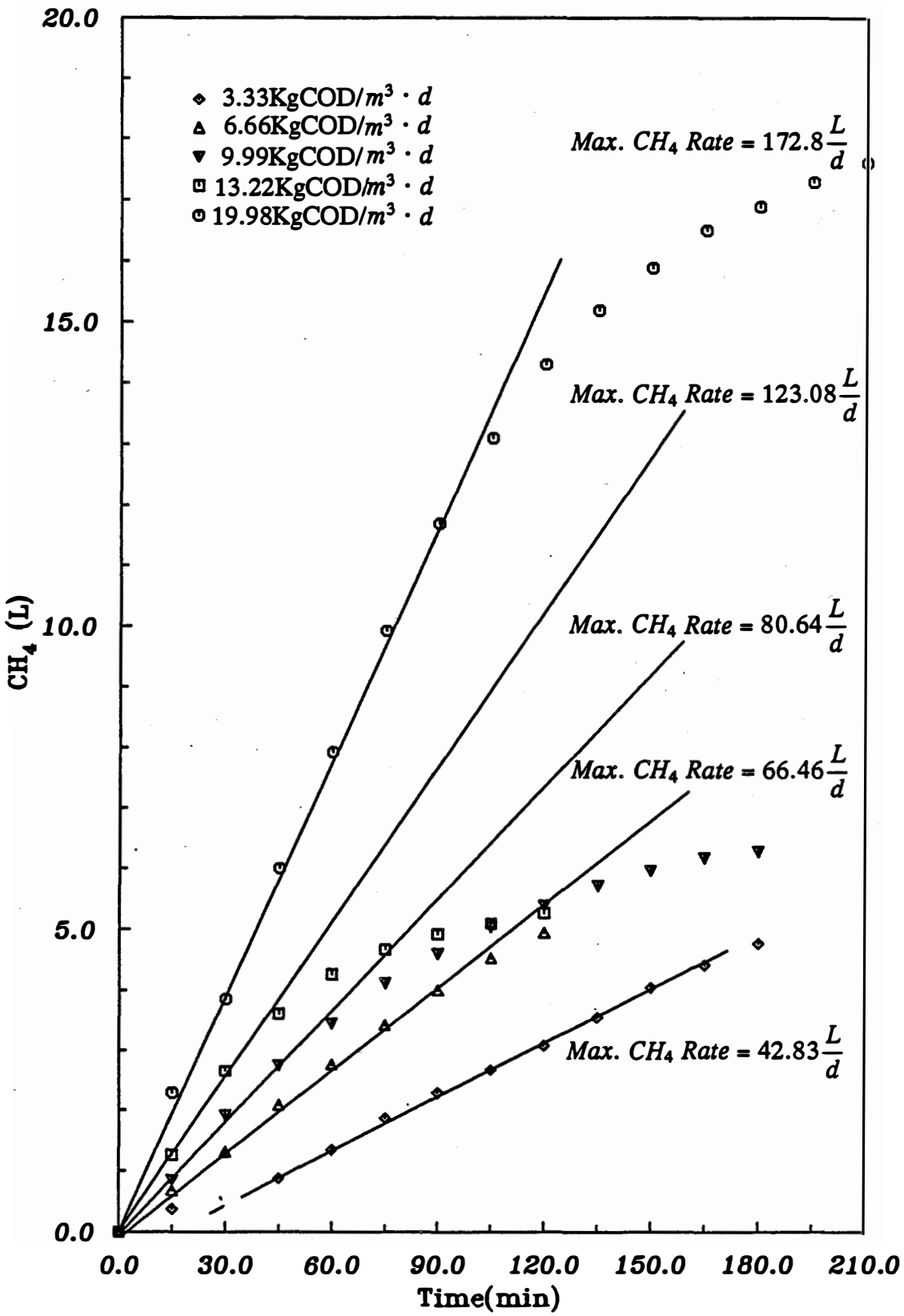

Figure 6–1 Results of the Batch Experiment of Haydite Reactor.

Table 6-3 Biofilm Model Outputs for Haydite Reactor

COD Loading $KgCOD/m^3day$	Maximum CH_4 Production Rate, L/d	Total Biomass mg	Biofilm Biomass mg	L_f * cm	J ** $gCOD/d$	Effluent COD mg/L
3.33	42.83	12860.1	12095.5	6.24E-3	50.4	51.95
6.66	66.46	19955.1	19258.1	9.94E-3	100.8	90.28
9.99	80.64	24212.8	23362.8	1.21E-2	151.1	185.47
13.32	123.08	36955.8	35340.8	1.82E-2	201.9	141.67
19.98	172.80	51884.6	35853.6	1.85E-2	302.3	2026.03

* Biofilm thickness estimated from Eq. 5-4.
**Total Substrate Flux.

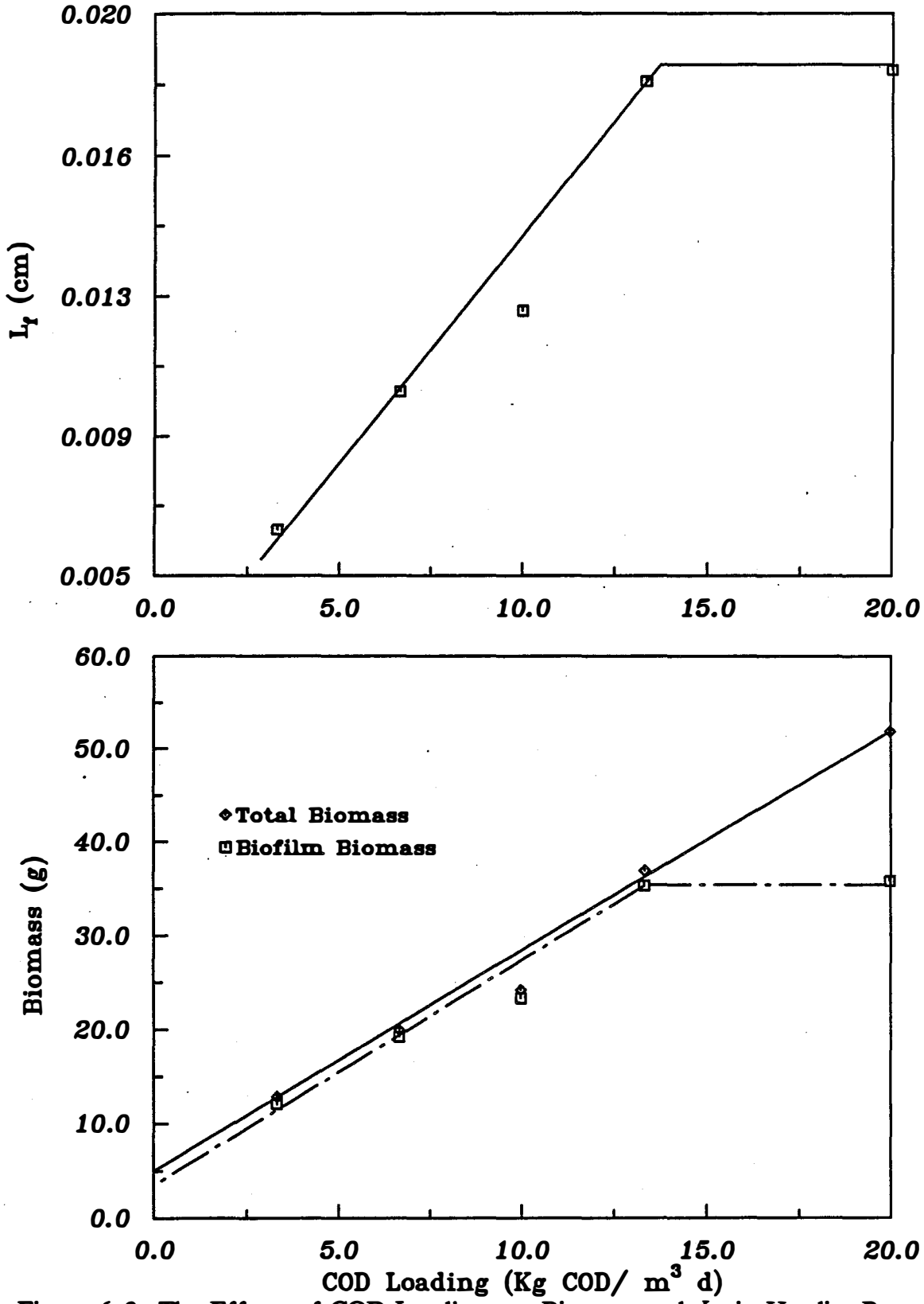

Figure 6-2 The Effects of COD Loadings on Biomass and L_f in Haydite Reactor.

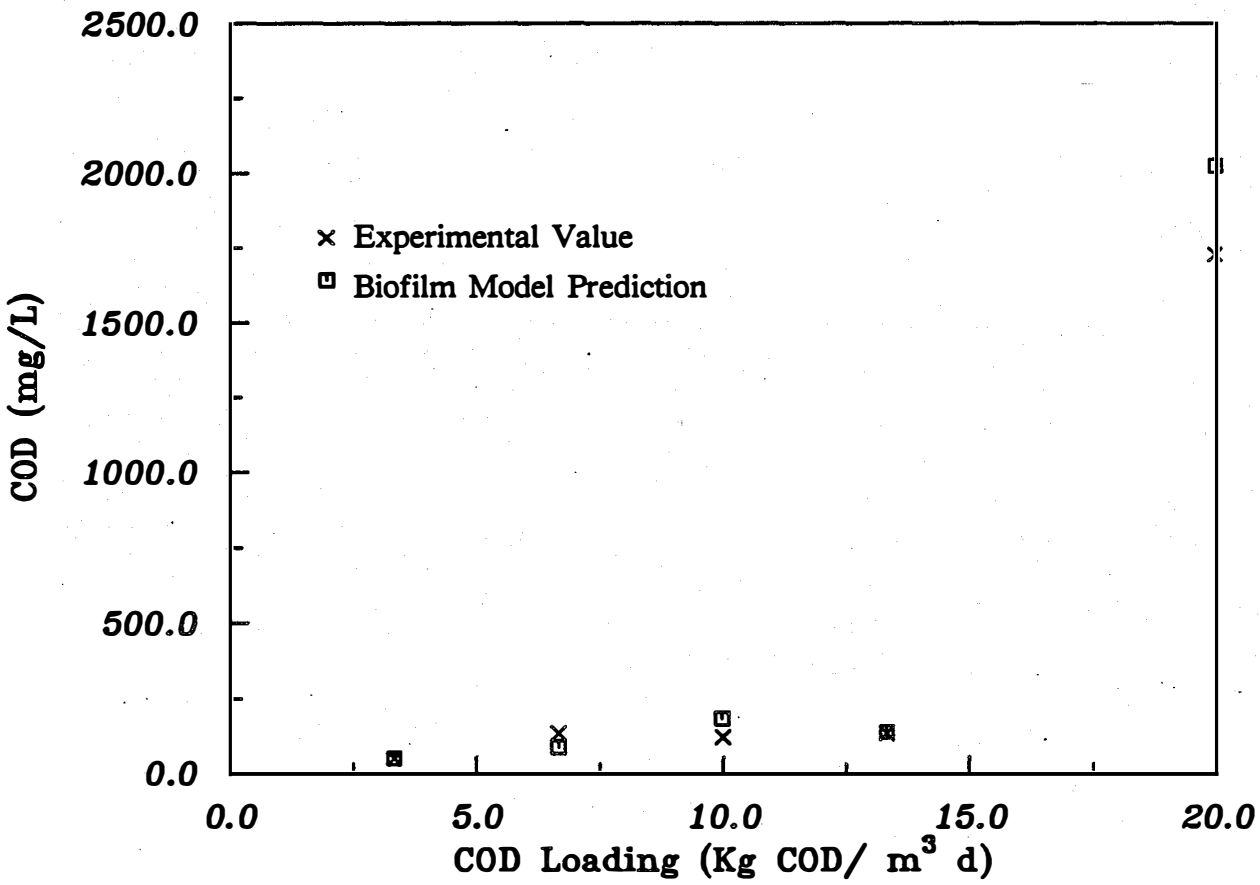

Figure 6-3 The Effects of COD Loadings on Effluent Soluble COD.

constant whereas suspended-growth biomass increased when the loading was greater than 13.32 Kg COD / $m^3 \cdot d$.

The sludge retention time (SRT) is an important factor for determining the treatment efficiency, and is expressed as :

$$SRT = \frac{Mass\ of\ Cells\ in\ Reactor}{Mass\ of\ Cells\ Wasted\ per\ Day} = \frac{M_T}{VSS \times Q_i} \qquad (6\text{-}3)$$

The SRT at different organic loadings are tabulated in Table 6-4. These numbers are substantially higher than those commonly observed in a CSTR, thereby ensuring the excellent performance over the conventional reactors. The SRT increased with organic loading until the maximum biofilm biomass capacity of the reactor had been reached at a loading of 13.32 Kg COD / $m^3 \cdot d$. The declining SRT matched the increasing VSS data in Table 6-2, suggesting that the rate of biomass loss had increased because there was more suspended-growth biomass in the effluent. Since the biofilm thickness remained the same after the loading of 13.32Kg COD / $m^3 \cdot d$ had been reached, additional loading either supported the growth of more suspended biomass or increased the biofilm loss rate. Data in Table 6-4 also indicate that the SRT decreased dramatically at the loading when the reactor efficiency exhibited a significant decrease.

The concentration profile of a biofilm is important in determining the biofilm thickness because the depth of substrate penetration can dictate whether the biomass can receive proper nutrition at the attachment wall. Biofilm has been classified into three categories, by Rittmann and McCarty (1980), according to the characteristics of its concentration profile. A *fully penetrated* biofilm is one in which the decrease in substrate concentration throughout the full thickness is negligible. A deep biofilm is one in which the substrate concentration decreases asymptotically to zero within the biofilm. A *shallow* biofilm is the intermediate case, in which the substrate concentration decreases within the biofilm but does not reach zero at the attachment wall.

The extent of substrate penetration in a biofilm can be determined by the dimensionless substrate concentration at the wall ($z^* = L_f^*$), S_w^*, which follows the relationship derived by Suidan *et al.* (1987) and Suidan and Wang (1985) as :

$$\frac{J^{*2}}{2} = (S_s^* - S_w^*) + \ln\left(\frac{1 + S_w^*}{1 + S_s^*}\right) \qquad (6\text{-}4)$$

The substrate-utilization penetration was defined according to a new rate modules, $Q_{modulus}$, which is the ratio of the dimensionless substrate utilization rate at the attachment surface to that for the bulk substrate concentration :

$$Q_{modulus} = \frac{S_w^* / (1 + S_w^*)}{S_b^* / (1 + S_b^*)} \qquad (6\text{-}5)$$

A deep biofilm has $Q_{modulus} = 0$, as S_w^* approaches zero, while a fully penetrated biofilm has $Q_{modulus} = 1$. Table 6-5 lists the S_w^* and $Q_{modulus}$ at each organic loading. The high $Q_{modulus}$ values suggests that the biofilms were very close to fully penetrated.

Since the biofilms approached fully-penetrated, the mass transport resistance within the biofilm can be neglected to simplify the rate expression as (Wang, 1984) :

$$\frac{Q(S_o - S_b)}{\bar{a} V X_f L_f} = \frac{k S_s}{K_s + S_s} \qquad (6\text{-}6)$$

Table 6–4 Sludge Retention Time Estimation for Haydite Reactor

COD Loading $KgCOD/m^3 \cdot day$	Total Biomass mg	VSS mg/L	Q_i L/day	SRT day
3.33	12860.1	45	0.175	1633
6.66	19955.1	41	0.175	2781
9.99	24212.8	50	0.175	2767
13.32	36955.8	95	0.215	1809
19.98	51884.6	943	0.300	183

Table 6–5 Substrate Utilization Penetration in Haydite Reactor

COD Loading $KgCOD/m^3day$	S_b^*	S_s^*	S_w^*	$Q_{modulus}$
3.33	1.04	0.97	0.95	0.9579
6.66	1.81	1.66	1.62	0.9604
9.99	3.71	3.32	3.23	0.9698
13.32	2.83	2.31	2.15	0.9229
19.98	40.52	39.74	39.48	0.9994

If the mass transfer resistance in the liquid layer, L, is also neglected, Eq. 6–6 can be further simplified to:

$$\frac{Q\,(S_o - S_b)}{\bar{a}\,V\,X_f\,L_f} = \frac{k\,S_b}{K_s + S_b} \qquad (6\text{–}7)$$

Eq. 6–7 along with Eq. 3–31 can be solved for S_b, which is less complicated than the biofilm model. Therefore, the removal of COD in an anaerobic biofilm reactor can be described by a Monod–type simple expression when mass transport resistances are disregarded.

Comparison between the outputs of these two models, Figure 6–4, shows that the simplified model slightly underestimates the bulk COD concentration. Because the simplified model assumes $S_b = S_w$, it neglects the transfer resistances and does not require a concentration gradient for substrate transport. However, the simplified model still satisfactorily describe the bulk COD, especially at the lower loadings.

Since the biofilms are nearly fully penetrated, it is likely that they have not yet reached their maximum possible depth even at the highest organic loading. However, many factors dictate the depth of biofilm. The shearing stress of the fluid flow will remove the biomass externally, whereas the sloughing associated with biogas bubble formation in the biofilm will internally dislodge the biomass from the attachment media. The normal bacterial decay will also impact the depth. The detailed mechanism of the biofilm sloughing will be discussed in a later section.

The experimental data and modeling results clearly demonstrate that the biofilm is the biomass responsible for the substrate utilization in these anaerobic packed beds. When high suspended–growth biomass was present, the loss of this biomass in the effluent decreased the SRT and reduced the substrate removal efficiency of the reactor. Additionally, these results show that there is an upper limit on the organic loading beyond which the biofilm biomass in the reactor will not increase. This upper limit of organic loading also coincided with the maximum biofilm thickness, thus confirming the assumption that the biofilm biomass accounted for all the bio–activity at the lower loading rates. Once the maximum biofilm depth has been reached the fixed–bed biofilm reactor will not be able to efficiently accommodate additional loadings. Higher organic loadings will elevate the bulk substrate concentration and increase the suspended–growth biomass. The VSS concentration, at the same time, will increase significantly causing an increase loss of biomass in the effluent. However, this high concentration of VSS effluent will reduce the treatment efficiency by causing a reduction in the SRT. It is likely that the biofilm growth rate does not decrease with the higher loading, but the biofilm loss rate may increase with the biofilm thickness. Therefore, more biofilm may be sloughed from the media, contributing to effluent VSS and causing the effluent quality to deteriorate.

6.1.3 Activated–Carbon Reactor

The pseudo–steady state operating conditions of the activated–carbon reactor are tabulated in Table 6–6. The operation of this reactor was terminated at the loading of 16.65 Kg COD/ $m^3 \cdot d$, even though the reactor was still functioning. However, because of operational difficulties and system instability, steady–state was not achieved and it was clear that the loading rate could not be increased above 16.65 Kg COD/ $m^3 \cdot d$. The effluent COD and VSS were consistently increasing at this loading.

Figure 6–5 illustrates the batch experiments, the results of which are listed in Table 6–7. Only two sets of batch experimental results are used. The batch experiments

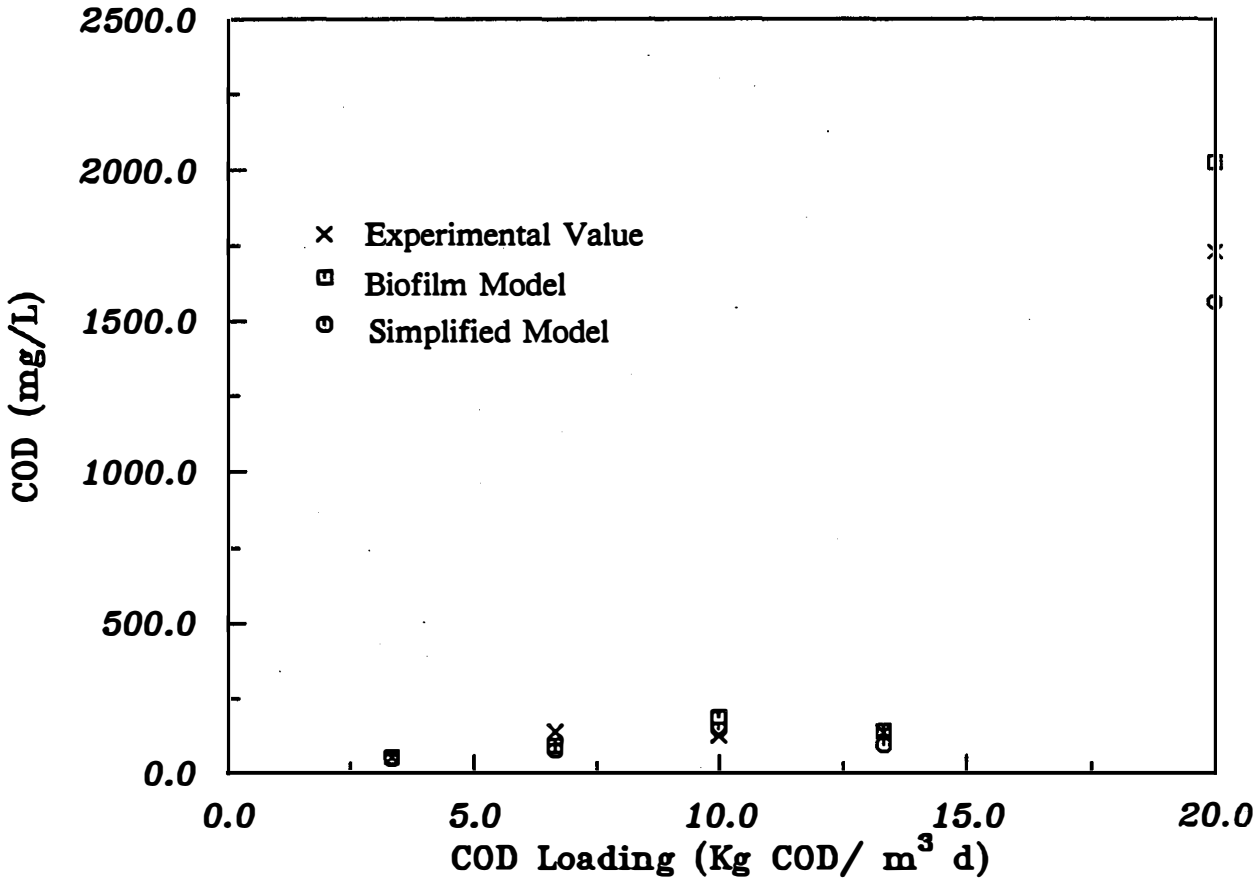

Figure 6–4 Comparison Between Biofilm and Simplified Models.

Table 6-6 Steady-State Operations in Activated-Carbon Reactor
HRT (empty bed) = 3 days

COD Loading $Kg/m^3 \cdot d$	Biogas Rate L/day	pH	Effluent COD mg/L	CH_4 %	Alkalinity mg $CaCO_3$ /L	VSS mg/L	$C_{T,in}$ mole/L	$C_{T,out}$ mole/L
3.33	27.44	6.99	47.01	69.29	2461.45	232.5	6.15E-3	5.01E-2
6.66	59.72	7.0	113.48	64.27	3454.44	747.6	1.21E-2	6.46E-2
13.32	127.56	6.93	107.13	58.20	2847.39	749.3	2.58E-2	5.67E-2

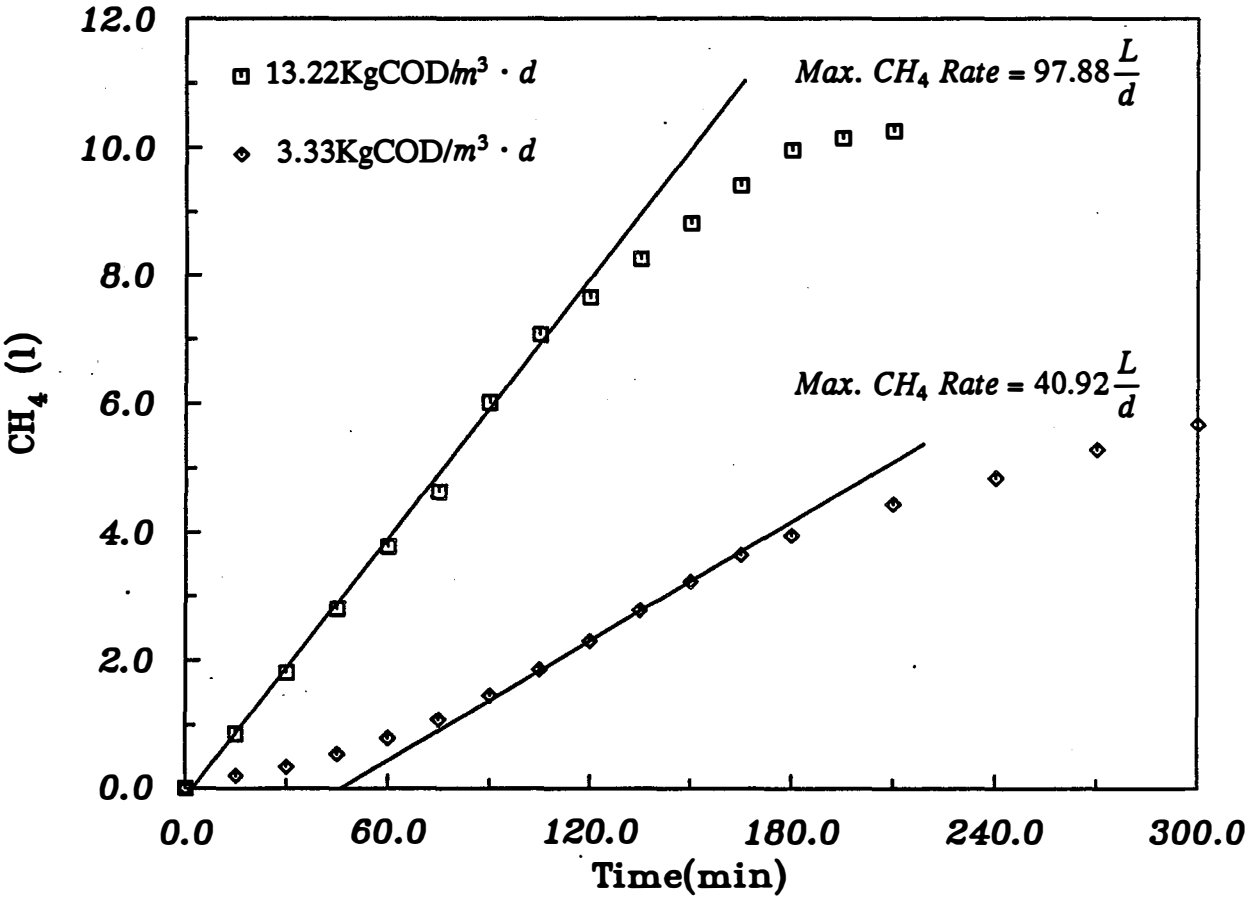

Figure 6-5 Results of the Batch Experiments of Activated-Carbon Reactor.

Table 6–7 Biofilm Model Outputs for Activated–Carbon Reactor

COD Loading $KgCOD/m^3day$	Maximum CH_4 Production Rate, L/d	Total Biomass mg	Biofilm Biomass mg	L_f * cm	J $gCOD/d$	Effluent COD mg/L
3.33	40.92	12286.56	8334.06	2.07×10^{-3}	50.38	118.27
13.32	97.88	29389.26	16651.26	4.14×10^{-3}	NC**	NC**

* Biofilm thickness estimated from Eq. 5–4.
**Biofilm model does not converge.

conducted at other organic loadings were discarded because the surface active properties of activated carbon were not considered during the experimental processes. The apparent adsorptive effect of this medium was discovered because of the inconsistent results of the batch experiments. Unlike the other two reactors, the biogas production rate decreased slowly in the activated-carbon reactor after the feed stream had been stopped. In addition, the maximum CH_4 production rate varied from one test to another depending on the amount of time between when the feed was shut off and the spiked was added. Therefore, several batch tests were conducted to examine the cause of this difference.

The adsorptive effect of activated carbon on the results of batch experiments is demonstrated in Figure 6-6. The batch experiments were performed at 13.32 Kg COD/ $m^3 \cdot d$ with influent solution stopped four hours prior to the start of two experiments (non-continuous feed) and stopped when the spike of organic feed was added to the reactor for the other two experiments (continuous feed). Adsorption apparently affects the substrate available to microorganisms during the batch experiments. The substrate utilization rate of the two experiments with the four hour resting period was considerably less than the rate obtained without the rest period. In the two non-continuous feed experiments, the adsorbed substrate was released and utilized when the feed was stopped before the spike was added. The substrate spiked for the batch experiments, consequently, was re-adsorbed by the carbon, resulting in a lower bulk solution concentration and a lower utilization rate. In the other two experiments, when the feed was continued until the spike was injected, the maximum rate of methanogenesis was obtained due to the undisturbed absorptive capacity. However, the batch experiment performed at 3.33 Kg COD/ $m^3 \cdot d$ is considered valid because the substrate was completely utilized in less than one hour after the feed solution was stopped. Since the stop period before the spike was only half an hour, the desorption-adsorptive effect was regarded as negligible. This discrepancy was not found in the Berl-saddle and Haydite reactors because the media do not have significant surface active properties.

The data presented in Table 6-7 show that the biofilm model, at the loading of 13.32 Kg COD/ $m^3 \cdot d$, are numerically insoluble because the L_f^* is close to J^* and therefore yields a negative S_b^*. The relationship between S_b^* and J^* for the L_f^* of 0.165 at 13.32 Kg COD/ $m^3 \cdot d$, given in Figure 6-7, verifies that the biofilm model does not converge when $J^* = L_f^*$. A criteria developed by Suidan *et al.* (1987) also confirmed that $J^* = L_f^*$ when the biofilm is fully-penetrated and $S_b^* \gg 1$. Furthermore, the substrate penetration tabulated in Table 6-8 reveals the fully-penetrated nature of the biofilm. In addition, the experimental S_b of 107 mgCOD/L and the VSS of 749.3 mg/L leads to the conclusion that suspended-growth biomass may be accountable for significant substrate utilization. Similarly, the SRT summarized in Table 6-9 and the high VSS also indicate that the reactor was losing biomass to effluent. This information suggests that this reactor may behave more like a suspended-growth reactor.

Eq. 6-7, instead of the biofilm model, is used to model the activated carbon reactor. Because of the high concentration of VSS, Eq. 6-7 should include the suspended-growth biomass as well as the biofilm biomass.

$$\frac{Q\,(S_o - S_b)}{M_T} = \frac{k\,S_b}{K_s + S_b} \qquad (6\text{-}8)$$

in which M_T is the total biomass inside the reactor. Eq. 6-8 includes all bio-activities, whereas Eq. 6-7 only considers the biofilm fraction of biomass and may signifi-

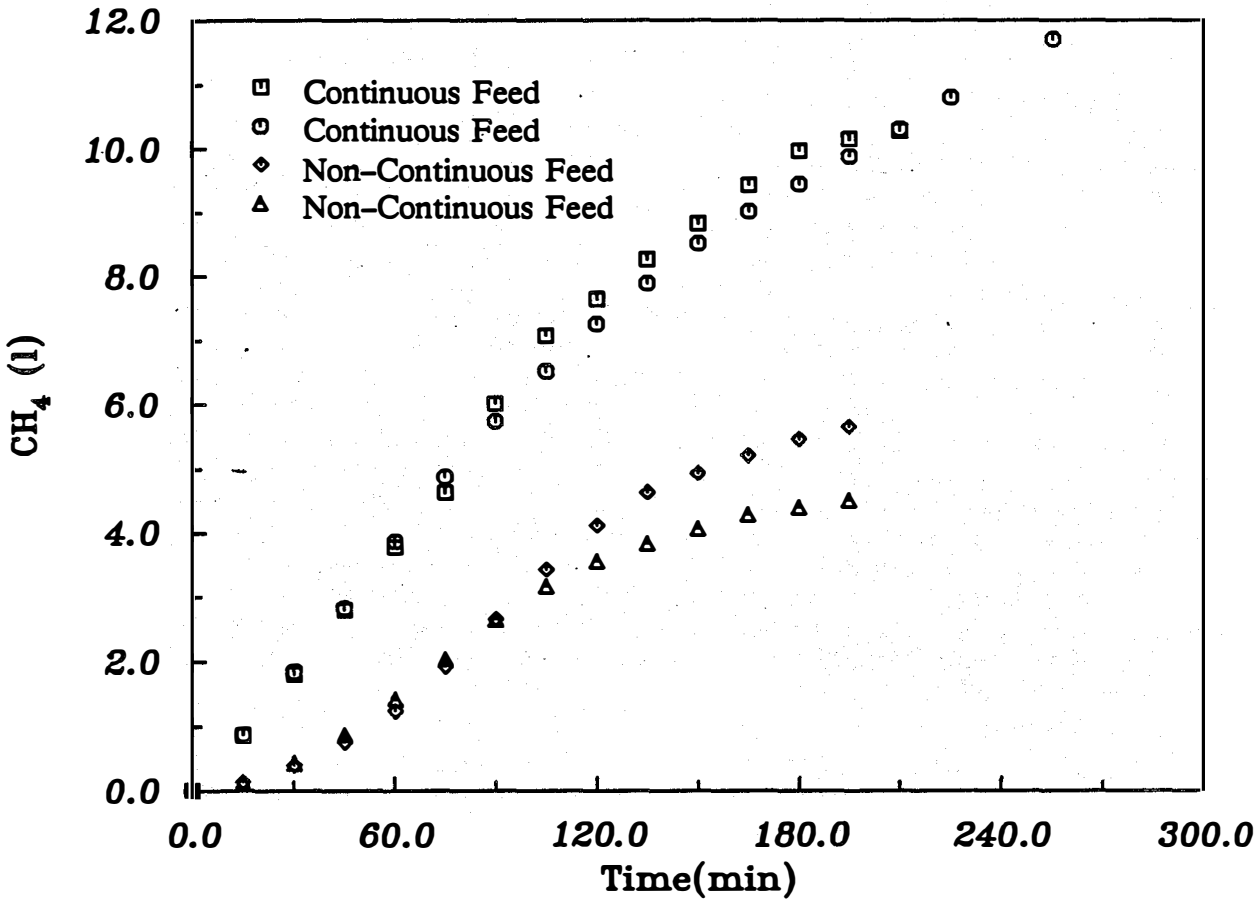

Figure 6-6 Effect of Adsorption of Activated Carbon on Batch Experiments

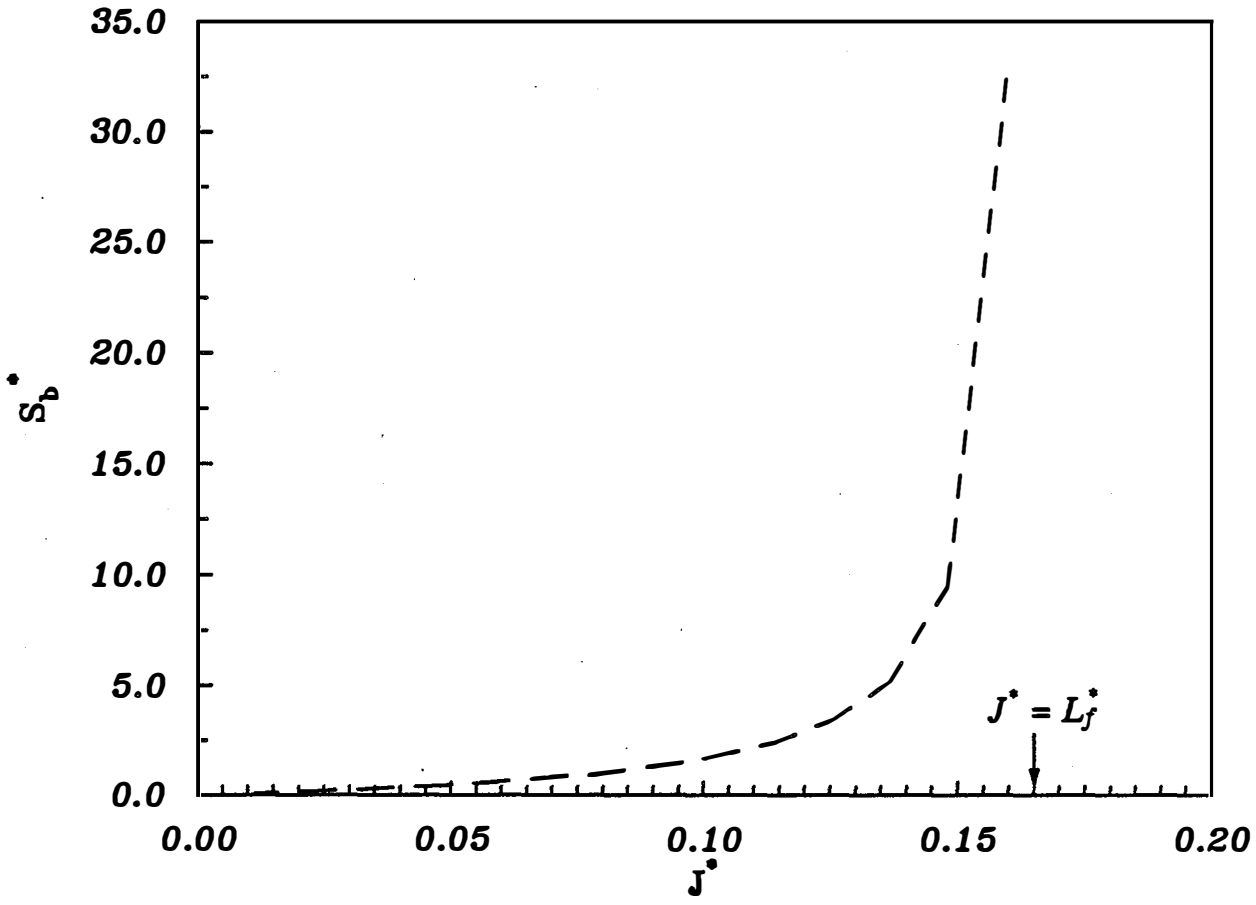

Figure 6–7 Relationship Between J^* and S_b^*, $L_f^* = 0.165$, Loading =13.32 $KgCOD/m^3 \cdot d$

Table 6–8 Substrate Utilization Penetration in Activated-Carbon Reactor

COD Loading $KgCOD/m^3day$	S_b^*	S_s^*	S_w^*	$Q_{modulus}$
3.33	0.9481	0.9139	0.9105	0.9792

Table 6-9 Sludge Retention Time Estimation for Activated-Carbon Reactor

COD Loading $KgCOD/m^3day$	Total Biomass mg	VSS mg/L	Q_i L/day	SRT day
3.33	12286	232.5	0.175	302
13.32	29389	749.3	0.215	182

cantly underestimate the activities when the suspended-growth biomass concentration is high. Results of Eqs. 6-7 and 6-8 are compared to experimental data in Table 6-10. These results indicated that biofilm biomass alone is not enough to model the COD removal, whereas total biomass simulate the process satisfactorily.

The short SRT of the activated-carbon reactor suggests that activated carbon is not an ideal media for a packed-bed anaerobic reactor despite its tremendous surface area. Compared to the other two media, activated carbon is smaller and lighter. As a consequence, the biogas bubbles agitated the carbon particles to escape from the tightly packed media. This motion caused abrasion between carbon particles and shearing of the attached biofilm. The abrading effect nullified the advantages of tremendous surface area provided by activated carbon. The effect of shear stress on the biofilm thickness will be discussed in a later section.

The design of these experimental reactors assumed good distribution of the influent across the column. Considerable emphasis was placed on effluent recycle and substrate diffusion through the reactor void spaces to insure the total volume of the reactor was active. The gas release played a very important role in the hydraulics of the reactors. The Berl-saddle reactor had a very high porosity, so it was easy for gas bubbles to escape. The Haydite medium had a porosity similar to the activated carbon, but was about 2.3 times as large as the carbon. The void spaces were larger which permitted the gas bubbles to move through the bed with relative ease. This was not true for the activated carbon reactor. Visual observations indicated that the bubbles would aggregate into larger bubbles that could force their way up through the column. It was originally assumed that this bubble activity would keep the bed mixed. However, it appeared the these bubbles created a path for influent short circuiting and a significant part of the reactor was not a active.

A comparison of the results of the batch tests in Figures 6-1 and 6-5 show that the total activity of the carbon reactor was substantially less than the Haydite reactor, especially at the higher loading rate. The Haydite reactor had an activity that was 25 percent greater than the carbon reactor. Since this rate is used to compute the total biomass, this same relationship is observed in Table 6-3 and Table 6-7. However, this dispersed growth was much higher in the activated carbon reactor. From these tables, it can be seen that at the 3.33 Kg COD/ $m^3 \cdot d$ loading rate, the biofilm biomass in the Haydite reactor was 54 percent greater than in the activated carbon reactor. At the 13.32 Kg COD/ $m^3 \cdot d$ loading biofilm biomass in the Haydite reactor was 2.1 times that the the carbon reactor.

The activated carbon has a larger specific surface area and better attachment properties than Haydite. However, the Haydite was much superior for this particular reactor design. Clearly, the hydraulic characteristic of the reactor design was the determining factor in the performance of the activated carbon. Short circuiting appeared to be a major problem suggesting that carbon is not a suitable medium for a packed-bed biofilm reactor.

6.1.4 Berl-Saddle Reactor

The Berl-saddle reactor was operated under three different loadings - 3.33, 5.0 and 6.66 Kg COD/ $m^3 \cdot d$. Since the effluent soluble COD continued to slowly increase at the loading of 6.66 Kg COD/ $m^3 \cdot d$, it is assumed that the system has reached its maximum loading. The operation of this reactor was terminated after completing the

Table 6–10 Model Outputs of Effluent COD Prediction for Activated–Carbon Reactor.

COD Loading $KgCOD/m^3day$	Experimental Value mg/L	Eq. 6–7 mg/L	Eq. 6–8 mg/L	Biofilm Model mg/L
3.33	47.01	113.81	44.57	118.27
12.32	107.13	NC*	187.70	NC*

*Model does not converge.

batch experiments estimating the biomass content at the highest loading rate. Table 6–11 lists the pseudo–steady state operating conditions. Figure 6–8 illustrates the data obtained from the batch experiments. Table 6–12 shows the results of the biofilm model predictions.

The computed biomass inventory and biofilm thickness are illustrated in Figure 6–9. The biofilm biomass and biofilm thickness only slightly increased with increased organic loading. This implies that this reactor was operating under organic loadings close to its maximum capacity. Figure 6–9 also shows a larger fraction of suspended–growth biomass compared to the Haydite reactor. This may be attributable to the high porosity of the Berl saddle that permits the retention of more suspended biomass. The substrate utilization penetration, in Table 6–13, shows the fully–penetrated nature of the biofilm. This reactor is modeled with the biofilm model and the simplified model to examine their applicability. The outputs of these models are given in Table 6–14. Neither model precisely described the effluent COD of this reactor, while the biofilm model predicts the highest effluent soluble COD.

The difference between Eq. 6–8 and the other two models is that the suspended–growth biomass was included, thus being closer to real situation. The larger deviation from the experimental values for the other two models also suggests that the suspended biomass played an important role in determining the effluent COD. However, estimation of biomass and total available surface area may be inaccurate because the Berl saddles were not packed in a certain pattern. The interlocking structure formed by the Berl saddles can retain more suspended–growth biomass than measured by the effluent VSS. At the same time, several pieces of media can arrange themselves in a continuous series and form smaller columns of stack elements and decrease the available area. In either way, the experimental values do not reflect the true biofilm kinetics because the total surface area and biofilm biomass were not estimated properly. In addition, the porosity may be greatly decreased depending on the packing method, thereby changing the flow velocity and biomass–holding capacity. Similarly, the SRT at different organic loadings, summarized in Table 6–15, may be significantly in error because of the dispersed growth retained by the characteristics of the reactor packing.

In summary, the Berl–saddle reactor seemed to be operable over a very limited loading range. This mainly is due to the lower specific surface area. Because of the irregular characteristics of this medium, biofilm kinetics are difficult to evaluate.

6.1.5 Shear Stress

The main function of the media in anaerobic filters is to immobilize as much biomass as possible, hence increasing the treatment efficiency. It is, therefore, logical to theorize that packing material with higher specific area can retain more biomass and lead to higher total biomass content. Experimental results of the three reactors indicate that Berl saddle does not provide enough surface area for the required biofilm growth at 6.66 Kg COD/ $m^3 \cdot d$, while the Haydite reactor, due to its larger specific surface area, can accommodate an organic loading four times higher. In contrast, the activated–carbon reactor could not support organic loadings as high as the Haydite reactor despite having the highest specific surface area.

At 3.33 Kg COD/ $m^3 \cdot d$, the Berl–saddle reactor had the highest biofilm thickness (L_f), whereas the activated–carbon reactor's L_f was less than one–tenth of the Berl saddle's. Rittmann (1982) stated that the shear stress is important in determining the

Table 6-11 Steady-State Condition in Berl Saddle Reactor
HRT (empty bed) = 3 days

COD Loading $Kg/m^3 \cdot d$	Biogas Rate L/day	pH	Effluent Soluble COD mg/L	$CH_4\%$	Alkalinity $mgCaCO_3/L$	VSS mg/L	$C_{T,in}$ $mole/L$	$C_{T,out}$ $mole/L$
3.33	26.72	7.0	66.63	69.21	2577.57	100.8	0.00243	0.05295
5.00	40.56	7.1	448.46	67.61	3545.02	66.0	0.00767	0.0685
6.66*	59.72	7.03	580.61	63.22	3131.63	156.0	0.011	0.05795

* Typical value (Non-Steady State Condition).

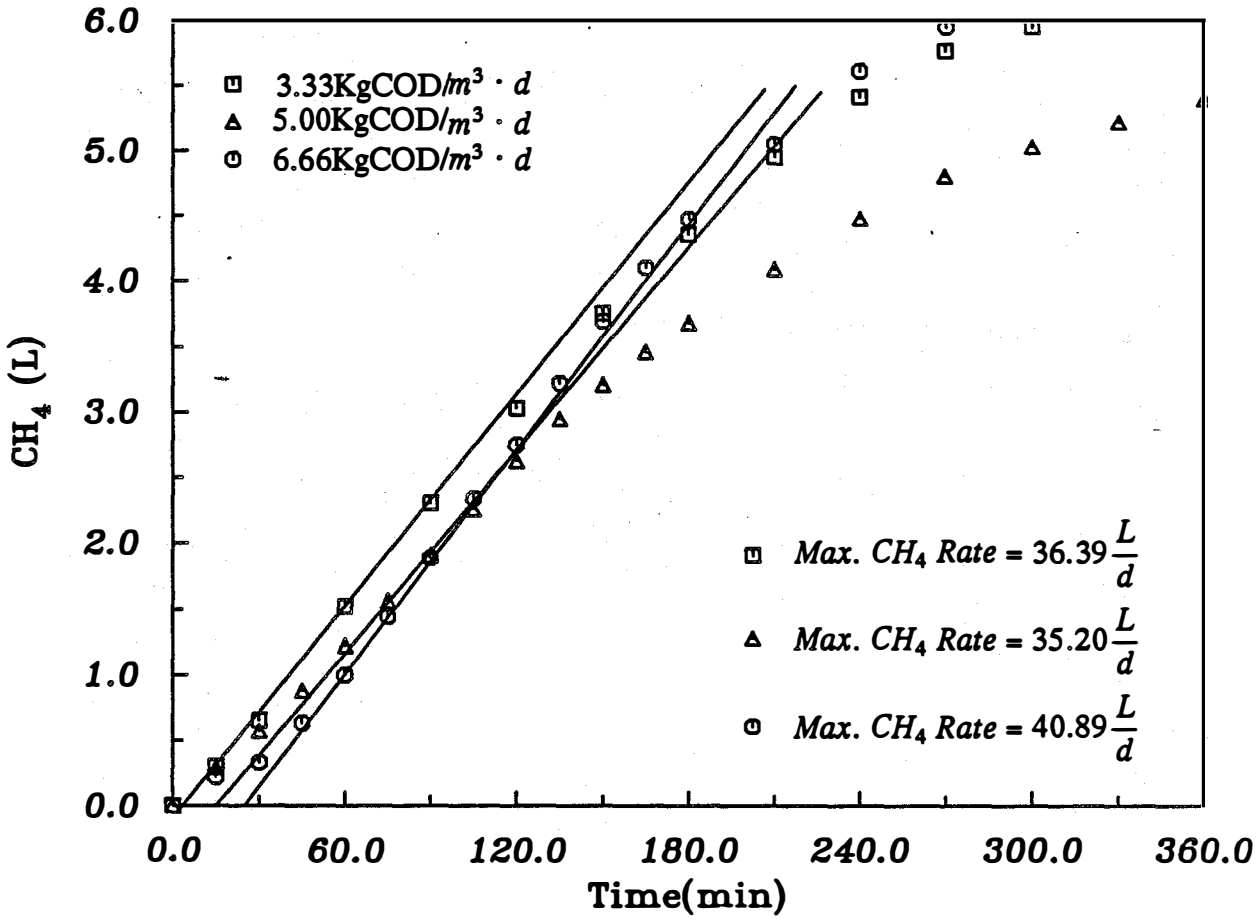

Figure 6–8 Results of the Batch Experiments of Berl–Saddle Reactor.

Table 6-12 Biofilm Model Outputs for Berl-Saddle Reactor

COD Loading $KgCOD/m^3day$	Maximum CH_4 Production Rate, L/d	Total Biomass mg	Biofilm Biomass mg	L_f * cm	J ** $gCOD/d$	Effluent COD mg/L
3.33	36.39	10926.39	9212.79	3.28E-2	50.34	125.80
5.00	35.20	10569.08	9447.08	3.37E-2	75.56	849.69
9.99	40.89	12277.55	9625.55	3.43E-2		

* Biofilm thickness estimated from Eq. 5-4.
**Total Substrate Flux.

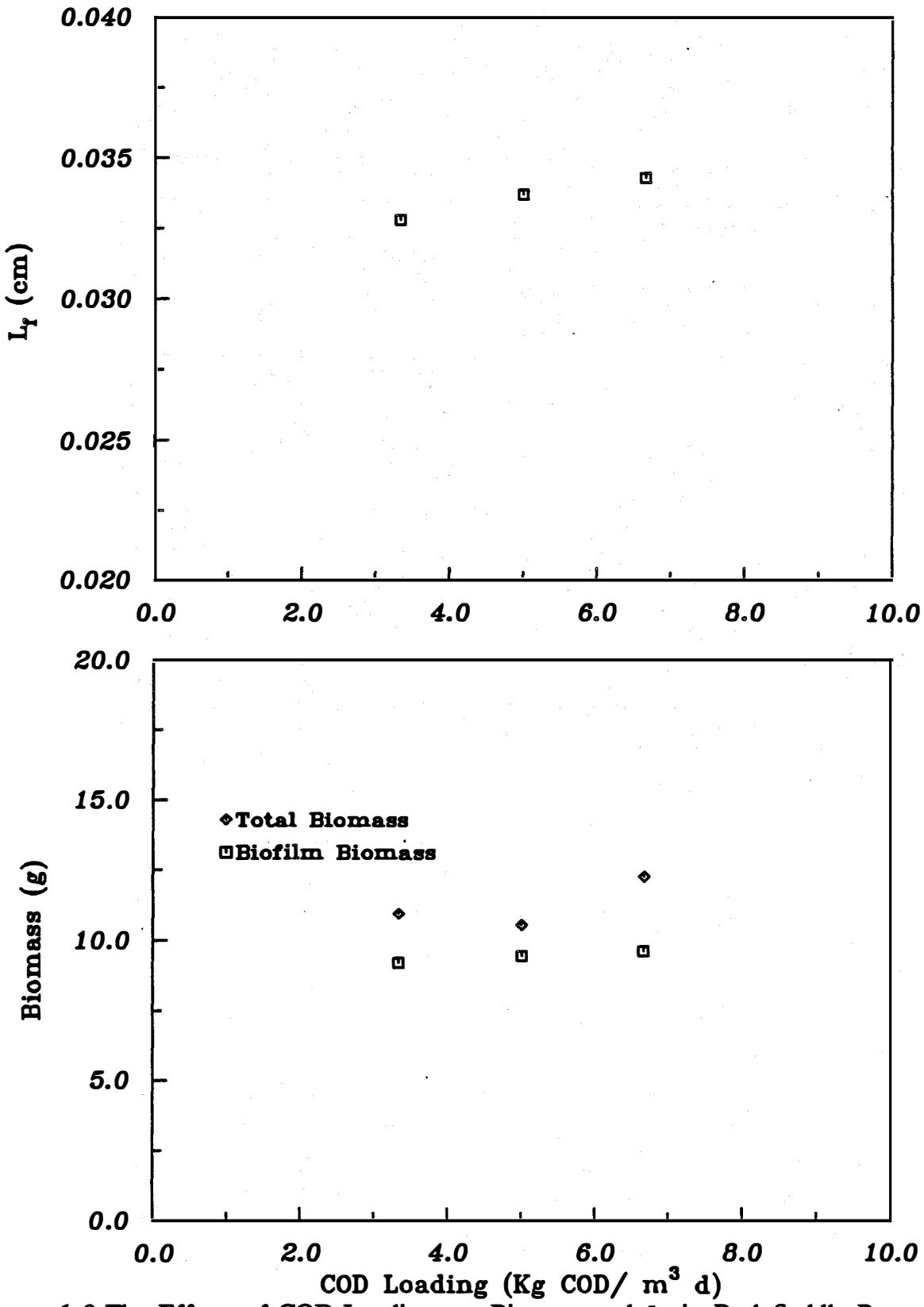

Figure 6–9 The Effects of COD Loadings on Biomass and L_f in Berl–Saddle Reactor.

Table 6–13 Substrate Utilization Penetration in Berl–Saddle Reactor

COD Loading $KgCOD/m^3day$	S_b^*	S_s^*	S_w^*	$Q_{modulus}$
3.33	2.52	2.39	1.90	0.9151
5.00	16.99	16.81	16.00	0.9966

Table 6-14 Model Outputs of Effluent COD Prediction for Berl-Saddle Reactor.

COD Loading $KgCOD/m^3day$	Experimental Value mg/L	Eq. 6-7 mg/L	Eq. 6-8 mg/L	Biofilm Model mg/L
3.33	66.63	84.59	56.36	125.80
5.00	448.46	570.10	230.53	849.69

Table 6–15 Sludge Retention Time Estimation for Berl–Saddle Reactor

COD Loading $KgCOD/m^3day$	Total Biomass mg	VSS mg/L	Q_i L/day	SRT day
3.33	10926.39	100.8	0.175	619
5.0	10569.08	66	0.175	915
6.66	12277.55	156	0.175	450

total biofilm loss rate and the steady-state thickness. The purpose of this section is to demonstrate that the biofilm loss rate caused by shear stress can be significantly affected by the medium type. Perry and Green (1984) documented a correlation given by Leva to estimate the pressure drop for flow through an imcompressible bed of granular solids. This correlation is modified to calculate the shear stress over the biofilm surface, σ ($dyne\ cm^{-2}$), as :

$$\sigma = \frac{2 f_a v^2 \mu^2 \varrho (1 - \epsilon)^{3-n}}{d_s \dot{a} \epsilon^3 \phi_s^{3-n}} \qquad (6\text{–}9)$$

in which n = dimensionless exponent, which is a function of Re.
In laminar flow ($Re < 10$)

$$f_a = 100/Re \qquad (6\text{–}10)$$

$$\sigma = \frac{200 v \mu (1 - \epsilon)^2}{d_s^2 \dot{a} \epsilon^3 \phi_s^2} \qquad (6\text{–}11)$$

Eq. 6–11 is appropriate for laminar flow in fixed-bed reactors. Table 6–16 lists the parameters necessary to calculate as well as the calculated value of the shear stress. The activated-carbon reactor has the highest calculated shear stress, 200 times that of the Berl-saddle reactor.

Rittmann (1982) derived a simple functional relationship for the rate of biomass loss due to shear stress, R_S ($mg\ cm^{-2} day^{-1}$), from Trulear and Characklis' (1982) results as

$$R_S = -8.42 \times 10^{-2} (X_f L_f) \left(\frac{\sigma}{1 + 433.2(L_f - 0.003)}\right)^{0.58} \qquad L_f \geq 0.003 \qquad (6\text{–}12)$$

$$R_S = -8.42 \times 10^{-2} (X_f L_f)\ \sigma^{0.58} \qquad L_f \leq 0.003 \qquad (6\text{–}13)$$

The development of Eqs. 6–12 and 6–13 were based on X_f = 11.4 mg/cm^3. However, Trulear and Characklis' data showed that results from X_f = 11.4 mg/cm^3 and X_f = 20.2 mg/cm^3 are actually indistinguishable. As a consequence, it is assumed that these equations are correct when X_f = 10.0 mg/cm^3. The calculated rate of biomass loss due to shear stress is also listed in Table 6–16. The overall rate of biofilm loss due to shear stress $R_{T,S}$($mg\ day^{-1}$), can be obtained by multiplying the R_S by the total surface area. The $R_{T,S}$ values in Table 6–16 imply that the activated-carbon reactor had a biofilm loss rate about 50 times more than that of the Haydite reactor, which may in part explain the inefficiency of the activated-carbon reactor.

Previous research by Chen *et al.* (1988) has shown that activated-carbon medium is capable of treating organic loading up to 72.4 Kg COD/ $m^3 \cdot d$ in a fluidized-bed reactor. There are two factors that may reduce the treatment efficiency of a fixed-bed activated-carbon reactor as contrasted to a fluidized-bed reactor.

1. The degree of mixing is severely limited in a fixed-bed reactor when granular activated carbon is used. The porosity of activated carbon, 0.45, was measured on virgin carbon, but the porosity decreases as the biofilm grows thicker. According to Eq. 6–9, shear stress rises with the decreasing porosity, making the actual biomass loss rate even higher than those presented in Table 6–16. Poor mixing, resulting from reactor plugging due to small porosity, may limit the amount of packing material available for biofilm growth and thereby reduce the treatment efficiency.

Table 6-16 Effect of Shear-Stress Losses on Various Reactors at 3.33 $KgCOD/m^3 \cdot d$

Media	Filtrasorb 400 Activated Carbon (12×14)	Mid-Size Aggregate (Haydite)	Berl Saddle
$d_s(cm)$	0.154	0.33658	3.385
ϵ	0.45	0.4925	0.8
Temperature($^\circ C$)	35.0	35.0	35.0
μ ($g\ cm^{-1}\ sec^{-1}$)	7.194×10^{-3}	7.194×10^{-3}	7.194×10^{-3}
X_f ($mg\ cm^{-3}$)	10.0	10.0	10.0
L_f (cm)	2.07×10^{-3}	7.04×10^{-3}	3.28×10^{-2}
v ($cm\ sec^{-1}$)	4.06×10^{-3}	4.06×10^{-3}	4.06×10^{-3}
σ ($dyne\ cm^{-2}$)	0.0477	0.01756	2.367×10^{-4}
$R_S(mg\ cm^{-2} day^{-1})$	2.98×10^{-4}	3.16×10^{-4}	4.73×10^{-4}
$R_{T,S}(mg\ day^{-1})$	3206.8	61.24	1.33

2. It was observed in this study that carbon particles were violently agitated by the escaping biogas bubbles. The bubbles forming in the bottom of the reactor had to move through the bed to exit from the top. The channeling effect caused by the biogas release is more damaging to the reactor performance than is the poor mixing because the short circuiting caused by channeling will substantially reduce the active volume. These bubbles also carried the carbon particles along and caused friction between the particles. This abrasion could be expected to remove more biofilm from the surface than is predicted by the shear-stress loss. The combined effect of channeling and excess biofilm loss due to abrasion will considerably reduce the effectiveness of activated carbon as a medium for a packed-bed reactor.

On the other hand, there is less abrasive force between carbon particles in fluidized bed owing to the cushion effect provided by the liquid. The fluidized-bed reactors, therefore, can support more biofilm biomass and a higher organic loading.

In summary, a medium of larger specific surface area is necessary to retain more biofilm biomass in anaerobic packed-bed reactors. However, this criterion does not always hold when the medium is comprised of small particles, such as granular activated carbon. The abrasion caused between particles during the release of biogas bubbles will increase biofilm loss causing a substantial reduction in the biofilm biomass. This will reduce the maximum allowable organic loading that the reactor can accommodate.

6.2 Equilibrium and Non-Equilibrium Model Verification

The experimental results used for verification of the equilibrium and non-equilibrium models are presented in this section. These results are compared with the numerical outputs from both models. Operating conditions in the experimental units were such that most of the data were generated under equilibrium conditions. Consequently, this section will focus on the verification of both models under equilibrium conditions and Section 6.3 will discuss the conditions necessary for application of the non-equilibrium model. All parameters used in these models are tabulated in Table 6-17.

6.2.1 Effects of pH

The pseudo-steady state conditions of different alkalinity levels in the Berl saddle reactor are listed in Table 6-18. Figures 6-10 and 6-11 show the results of the model prediction which demonstrate good agreement with the experimental values. Model predictions were based on the substrate flux $J = 50.34$ gCOD/day calculated from the biofilm model. In order for the model to compute a continuous result over the range of alkalinities selected, it was necessary to use a constant value for the influent total inorganic carbon. Therefore, this value was taken to be 4.2×10^{-3} $mole/L$, which is the average value of experimental measurements for the condition tested. By assuming this value, the effect of alkalinity was modeled continuously from 1000 to 6000 mg $CaCO_3$ $/L$. The models clearly demonstrates the effects of alkalinity on the reactor pH and the related gas composition (Figure 6-10). The alkalinity appears predominantly in the form of bicarbonate at the normal pH range of operation, *i.e.* 7.0 - 8.0. A higher alkalinity, therefore, requires that more inorganic carbon be dissolved in the liquid phase as bicarbonate, and more of the CO_2 being produced by the biofilm is dissolved owing to the equilibrium relationship. Consequently, the methane content in biogas increases. In addition, the reactor pH also increases because of the elevated concentration of carbonate and bicarbonate. The close match between the data and the model outputs demonstrates the validity of these models.

Table 6-17 Parameters Used in Equilibrium and Non-Equilibrium Models

Parameter	Value	References
P_w	5.549E-2 *atm* at 35 °C	*
g	25.272 *L/mole* at 25 °C and 1 *atm*	Ideal Gas Law
pK_{a1}	6.3 at 35 °C	**
pK_{a2}	10.25 at 35 °C	**
pK_a	4.76 at 35 °C	**
pK_{S1}	6.825 at 35 °C	**
pK_{S2}	11.3706 at 35 °C	**
pK_N	4.7 at 35 °C	**
pK_{P1}	2.1 at 35 °C	**
pK_{P2}	7.2 at 35 °C	**
pK_{P3}	12.3 at 35 °C	**
pK_W	13.6801 at 35 °C	**
pH_f	4.3	
K_H	2090.0 *mole / atm L* at 35 °C	**
K'_H	48600.0 *mole / atm L* at 35 °C	*

* Perry and Chilton, 1973.
** Snoeyink and Jenkins, 1980.

Table 6–18 Steady–State Conditions of Different Alkalinity in Berl–Saddle Reactor
HRT (empty bed) = 3 days, COD loading = 3.33 Kg COD/ $m^3 \cdot d$

Alkalinity mg$CaCO_3$/L	pH	Biogas L/day	CH_4* atm	Effluent COD mg/L	Effluent Acetic Acid mg/L	$C_{T,in}$ mole/L	$C_{T,out}$ mole/L
2577.57	7.0	26.72	0.6534	66.63		2.43E–3	0.05295
3526.26	7.34	22.67	0.7289	90.70	11.84	4.55E–3	0.07099
4601.38	7.63	20.31	0.8090	119.24	22.50	5.62E–3	0.08679

* Partial Pressure.

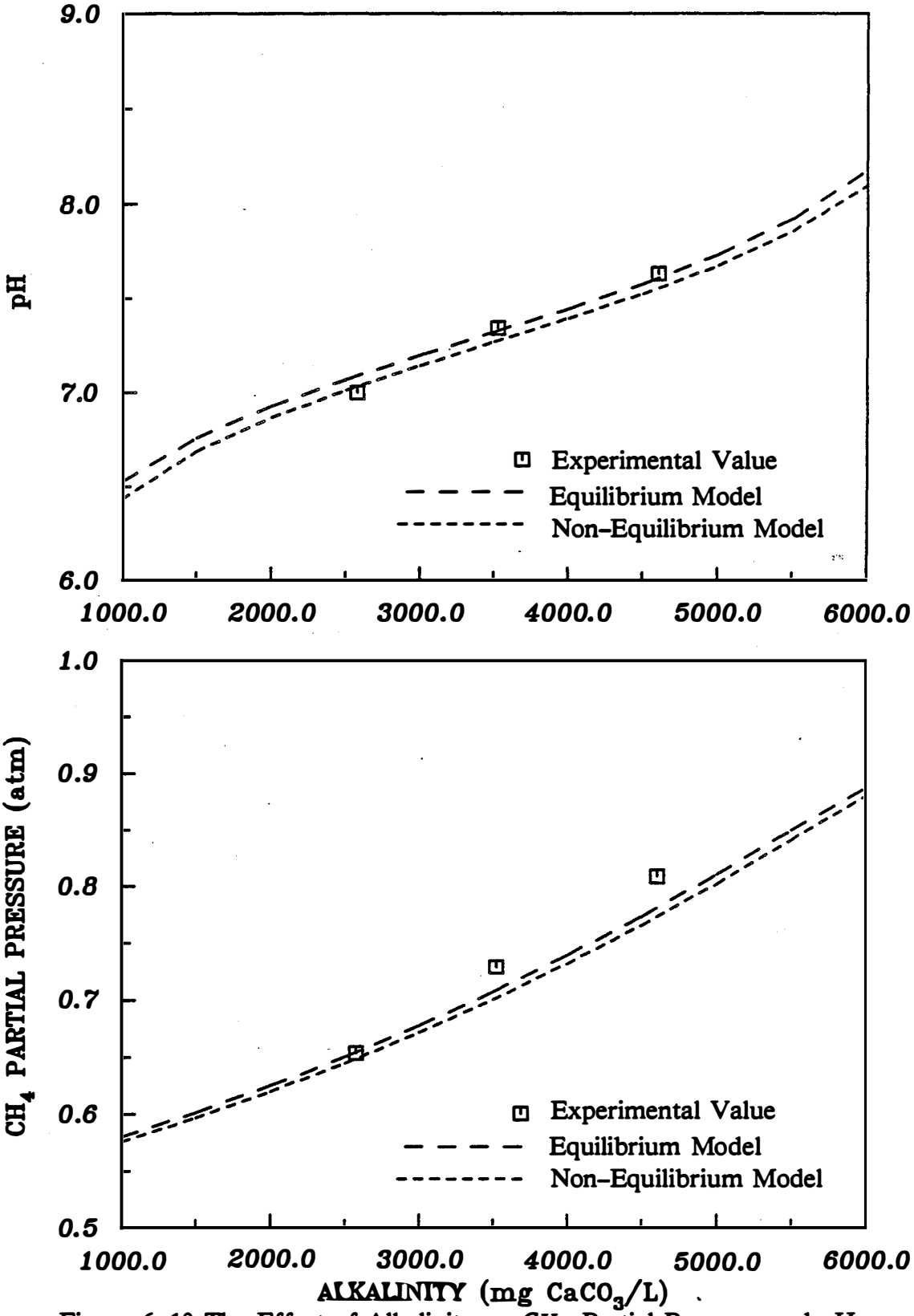

Figure 6-10 The Effect of Alkalinity on CH_4 Partial Pressure and pH.

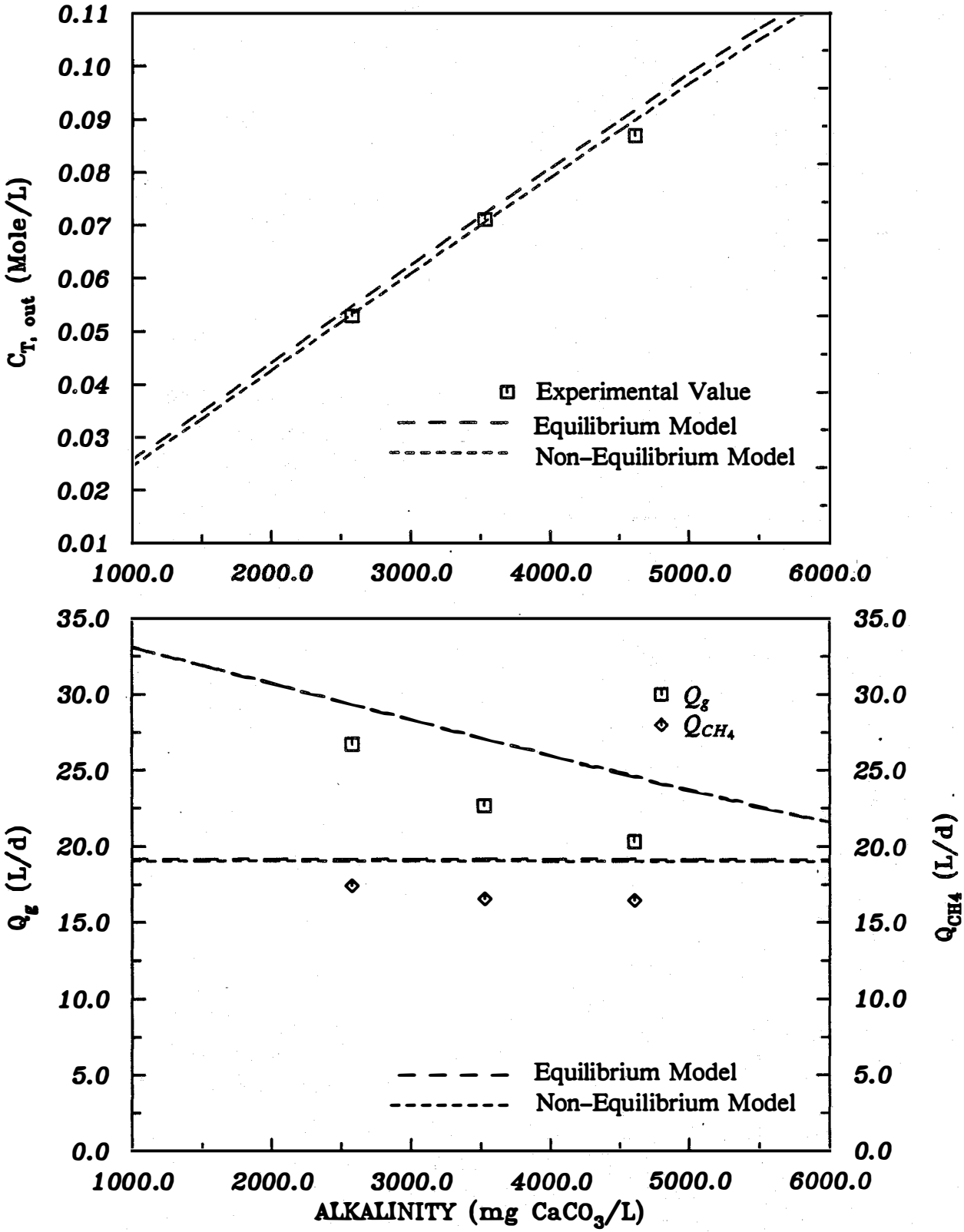

Figure 6–11 The Effects of Alkalinity on Q_g and $C_{T,out}$

The effects of alkalinity on total inorganic carbon in the effluent, $C_{T,out}$, are shown in the top part of Figure 6–11. Despite the loss of CO_2 during the process of sample preparation, which is unavoidable, the predicted values still closely model the experimental $C_{T,out}$ values.

The experimental total biogas production rates, Q_g, in the bottom half of Figure 6–11, deviate from the model prediction; the degree of the deviation increases with the alkalinity. Since Q_g includes water vapor and CO_2 which varies with reactor pH, the CH_4 production rate (Q_{CH_4}) was also plotted in Figure 6–11 to exclude the confusion in data interpretation. The trend of the increasing difference between the experimental and the predicted values with alkalinities coincides with the rising effluent soluble COD (Table 6–18). This digression is mainly due to the J value which was calculated on the condition for the alkalinity of 2600 $mg\ CaCO_3/L$, and J apparently decreased with increasing alkalinity because the effluent COD increased. Since reactor pH and alkalinity were the only two parameters different in each operation, they must be accountable for the COD increase.

One possible explanation is that the substrate can only be utilized in the protonated form (CH_3COOH) and the amount of which is a function of the pH inside the reactor. The CH_3COOH decreases as pH increases, thus reducing the substrate available for methanogenesis. Although most substrate was in the CH_3COO^- form when the pH was near neutrality, the amount of CH_3COOH differs significantly according to the relationship :

$$\frac{[CH_3COOH]}{[CH_3COO^-]} = \frac{[H^+]}{K_a} \qquad (6\text{–}14)$$

At 35 °C, the ratio of $[CH_3COOH]/[CH_3COO^-]$ diminishes by a factor of 1/3 when the pH increases by 0.5 unit. Because of the lower availability of CH_3COOH, the treatment efficiency decreased accordingly. The model simulation did not reflect the decline in substrate fluxes, which consequently overestimated the biogas production rates. Moreover, since the predicted CH_4 partial pressures in Figure 6–10 underestimate the experimental values, the corresponding Q_g values were overestimated.

The outputs of the non–equilibrium model are very close to that of the equilibrium model. It is obvious from these results that all the operations were under equilibrium conditions.

6.2.2 Effects of HRT

In the non–equilibrium model, the gas transfer takes place due to the difference between the equilibrium concentration between the gas and liquid phase and the actual bulk concentration of the dissolved gas. The rate of gas transfer, therefore, should be a function of this concentration difference. Since the equilibrium concentration is fixed by the system operating conditions, the concentration of dissolved gas in the bulk liquid controls the gas transfer rate. It is hypothesized that the magnitude of the deviation of the operating condition from true equilibrium depends on the concentration difference between these two conditions. The larger the difference between the equilibrium concentration and the dissolved biogas concentration, the greater the system deviates from the equilibrium. In order to examine how much, if any, the dissolved gas concentration affects the degree of equilibrium, the HRT of the reactor was changed to adjust the bulk concentration of dissolved biogas. By varying the HRT, the amount of inorganic carbon removed by the stripper and the average residence time of

the external recycle stream in the stripper can be drastically changed. These combined effect may change the bulk concentrations of CH_4 and CO_2 and, eventually, the degree of deviation from equilibrium. Because of the different solubilities of CH_4 and CO_2 and the chemical activity of CO_2, these gases may be expected to respond differently to changes in HRT.

The effects of empty-bed HRT on reactor performance were studied on the Berl saddle reactor of an organic loading of 5.0 Kg COD/ $m^3 \cdot d$ by keeping other parameters constant. The HRT was reduced from 3 days to 2, 1, 0.5 and 0.25 days for pseudo-steady state operation. The experimental results of the steady state operation are listed in Table 6-19, from which the data were plotted in Figures 6-12 and 6-13 to compare the outputs of the equilibrium and non-equilibrium models. The biofilm model predicted the biofilm thickness of the Berl saddle reactor to be 3.37×10^{-2} cm for organic loading of 5.0 Kg COD/ $m^3 \cdot d$. The total substrate flux was 75.56 g COD/day.

In Figures 6-12 and 6-13, the model predictions show an unusual trend at the HRT of 1 day, at which the reactor pH was abnormally high and the CH_4 partial pressure and Q_g were correspondingly different. This unusual result might be caused by erroneous experimental data, as shown in Table 6-19, at HRT of 1 day. A COD of 392.23 mg/L, recorded at that HRT, was lower than the CODs observed at other HRTs. Additionally, the alkalinity of 3589 $mg\ CaCO_3/L$ was also higher than alkalinities at other HRTs. The combined effects of a high alkalinity and a low COD make the results deviate from the normal trend of the model prediction at different HRTs. It was noted from the daily record that the operational temperature was about $5\,^{\circ}C$ higher than usual during the 1 day HRT operation. This higher temperature might have enhanced the microbial activity, hence decreasing the effluent COD. However, both models followed the same trend and, in general, show good agreement with the experimental data. In addition, the models did not show that the equilibrium model is invalid even at the lowest HRT of 0.25 day. It is, therefore, concluded that the equilibrium condition is valid at operations at low HRTs with the COD load applied.

The lower Q_g values at the two shortest HRTs, 0.5 and 0.25 day, reflected the limitation of the experiment. The shorter HRTs decreased the retention time of the feed stream in the purging tank accordingly, and diluted the feed strength because the COD loading remained constant. The pH inside the purging tank increased from 4.3 at HRT of 3 days to 8.5 at 1 day. This elevated pH not only decreased the amount of inorganic carbon appearing as CO_2, but also provided an optimum environment for aerobic bacterial growth. Since some organics were oxidized aerobically, the total gas produced by anaerobic fermentation decreased.

Both models follow the same trend with the experimental data, showing the model effectiveness. The slight difference between the outputs of these two models, mainly due to the mathematical formulation, suggests that the decrease in HRT did not shift the operation into a non-equilibrium state. Basically, the reactor was still operated under equilibrium condition even though the HRT had been reduced to less than one-tenth of its original value. Since the HRT was not further reduced, it is practical to summarize that the HRT does not change the state of equilibrium under normal operational conditions at this loading rate.

6.2.3 Effects of Pressure

Hayes *et al.* (1989) verified that biogas with high CH_4 content can be obtained from pressurized reactors. Experiments determining the effects of the total pressure, P_T,

Table 6–19 The Effect of HRT in Berl Saddle Reactor
COD Loading = 5.0 $KgCOD/m^3 \cdot d$

HRT Day	Biogas Rate L/day	pH	Effluent COD mg/L	CH_4* atm	Alkalinity mg $CaCO_3/L$	$C_{T,in}$ mole/L	$C_{T,out}$ mole/L
3	40.56	7.1	448.46	0.6386	3545.02	7.667E–3	0.0685
2	36.89	7.2	476.58	0.6936	3491.61	6.53 E–3	0.0686
1	31.07	7.5	392.23	0.8252	3589.46	1.75 E–2	0.0686
0.5	27.58	7.5	472.37	0.8255	3447.79	4.47 E–2	0.0652
0.25	27.38	7.51	476.58	0.8253	3446.57	5.38 E–2	0.0637

* partial pressure.

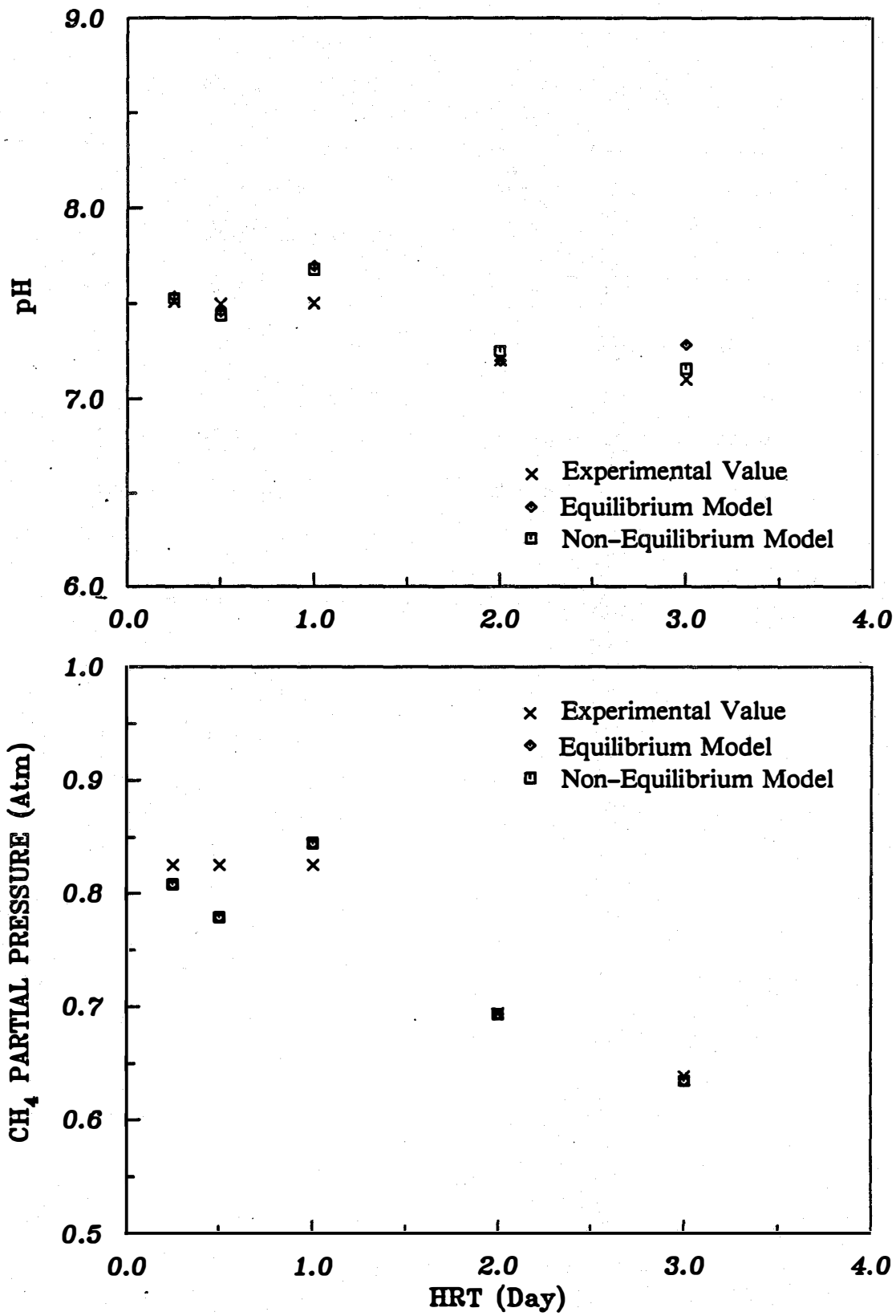

Figure 6-12 The Effect of HRT on CH_4 Partial Pressure and pH.

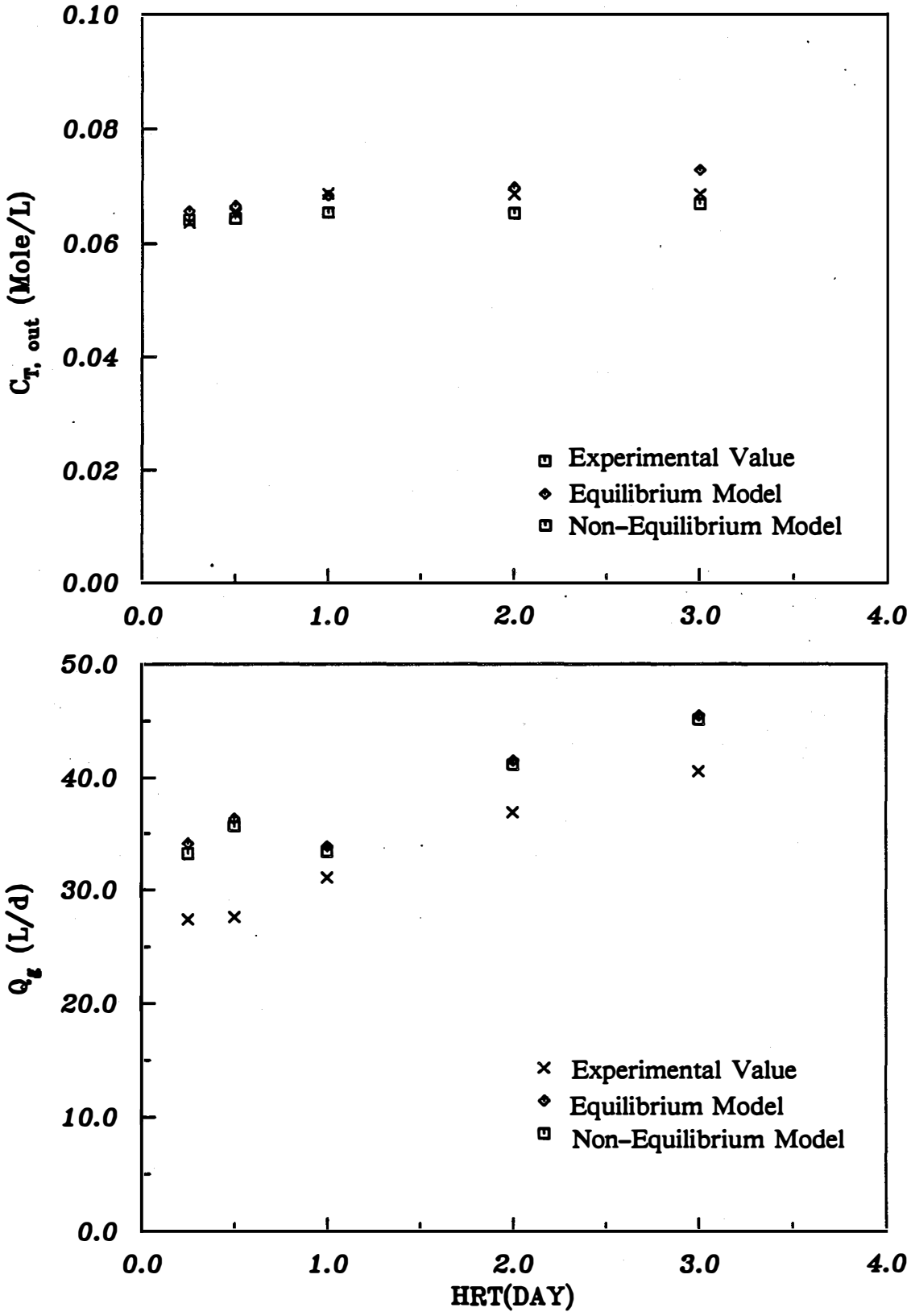

Figure 6-13 The Effects of HRT on Q_g and $C_{T,out}$

were not conducted in the present study because of the difficulties associated with pressurized reactors, such as special pumps and tubing. However, the equilibrium model prediction conclusively demonstrates the effects of P_T. In this section, a flux of 50g/d was used to simulate the equilibrium model for different P_T values.

The higher pressure can enrich methane in biogas by dissolving more CO_2 than CH_4 into the liquid, but pH is also decreased because higher CO_2 partial pressure in the reactor head space results in a higher $H_2CO_3^*$ concentration in the liquid phase. Figure 6–14 shows the effects of P_T on the methane content in the biogas and the reactor pH. The dissolved CO_2 and CH_4 concentrations, shown in Figure 6–15, explain the enrichment mechanism in greater detail because more CO_2 than CH_4 is dissolved into the liquid phase. When the alkalinity increases, more inorganic carbon is present in the HCO_3^{-1} and CO_3^{-2} forms, thus increasing the pH inside the reactor. The dissolved CO_2 concentration in the liquid is higher when the alkalinity and pH are both lower because there is less HCO_3^{-1} and CO_3^{-2} to restrain the CO_2 concentration. It was also demonstrated that 1 *atm* increase of P_T can elevate C_{CO_2} by 0.01 *mole/L* at 1000 mg $CaCO_3/L$, while only 0.002 *mole/L* at 6000 mg $CaCO_3/L$. This is because most of the inorganic carbon is present at lower alkalinities as CO_2, whereas less inorganic carbon exists as CO_2 at higher alkalinities. This follows Henry's law and the partial pressure of CO_2 in the gas phase increases as concentration of CO_2 in the liquid phase increases.

The bottom part of Figure 6–16 further illustrates the role played by alkalinity, which dictates the form and the amount of inorganic carbon which will be dissolved in the liquid. Although there is more CO_2 available at lower alkalinities, the allowable amount of $H_2CO_3^*$ in equilibrium with CO_2 is also limited. In contrast, more total inorganic carbon, $C_{T,out}$, can be dissolved into the liquid phase because higher HCO_3^{-1} and CO_3^{-2} concentrations also lift the equilibrium constraint of $H_2CO_3^*$. The upper half of Figure 6–16 shows that Q_g decreased with increased pressure because the extra biogas absorbed into the liquid. The decrease of Q_g with increasing alkalinity also coincides with the increase of $C_{T,out}$ and C_{CH_4}. As a result, the methane content in biogas is not only a function of P_T, but also a function of total alkalinity. Figure 6–14 demonstrates that alkalinity alone can raise the CH_4% to 90%, while an additional 4 *atm* of total pressure can only increase an extra 8 to 5 % depending on the alkalinity. Therefore, it is reasonable to conclude that a pressurized reactor is effective in enriching CH_4 in the biogas, but the total alkalinity has a more pronounced effect.

Comparison between the experimental results of Hayes *et al.* (1989) and the model predictions are given in Table 6–20. The equilibrium model prediction, based on the assumption of $C_{T,in} = 3.43 \times 10^{-3}$ *mole/L*, agreed with the experimental results well. As documented, biogas of 93.2 % CH_4 can be obtained under the operational condition of 2 *atm* and a total alkalinity of 5581 $mgCaCO_3/L$.

6.3 Non-Equilibrium Model

As discussed in 6.2.1 and 6.2.2, the equilibrium model satisfactorily described the behavior of the experimental anaerobic fixed-bed reactor under the conditions tested. Consequently, it is concluded that the reactors operate under equilibrium conditions in normal operational situations. However, the conditions under which the equilibrium does not exist are worth exploring.

Since the equilibrium is controlled by the rate of mass transfer between the liquid and the gas phase, the gas mass transfer coefficient (K_La) is assumed to play a major role

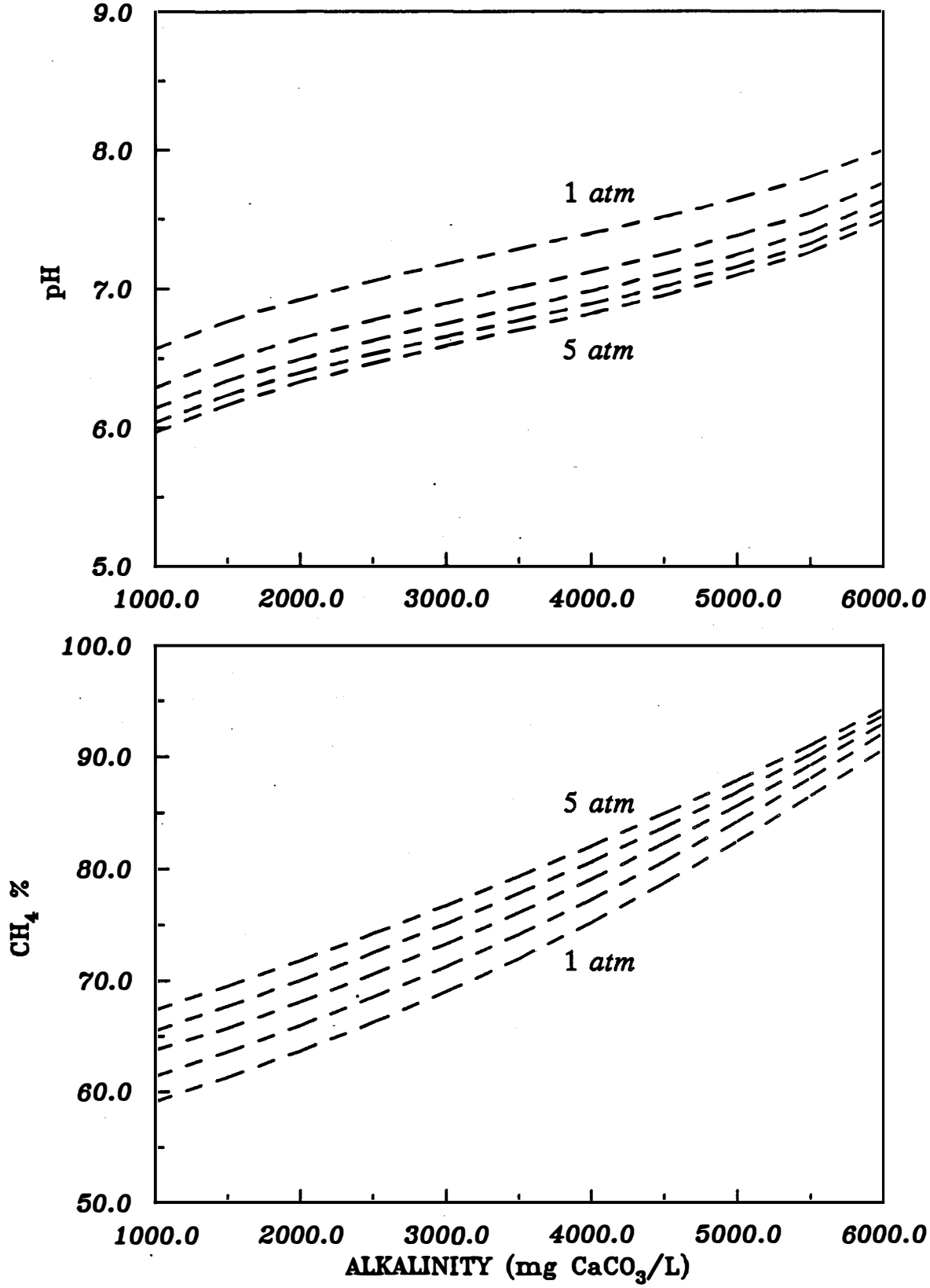

Figure 6-14 The Effects of Total Pressure on pH and CH_4%

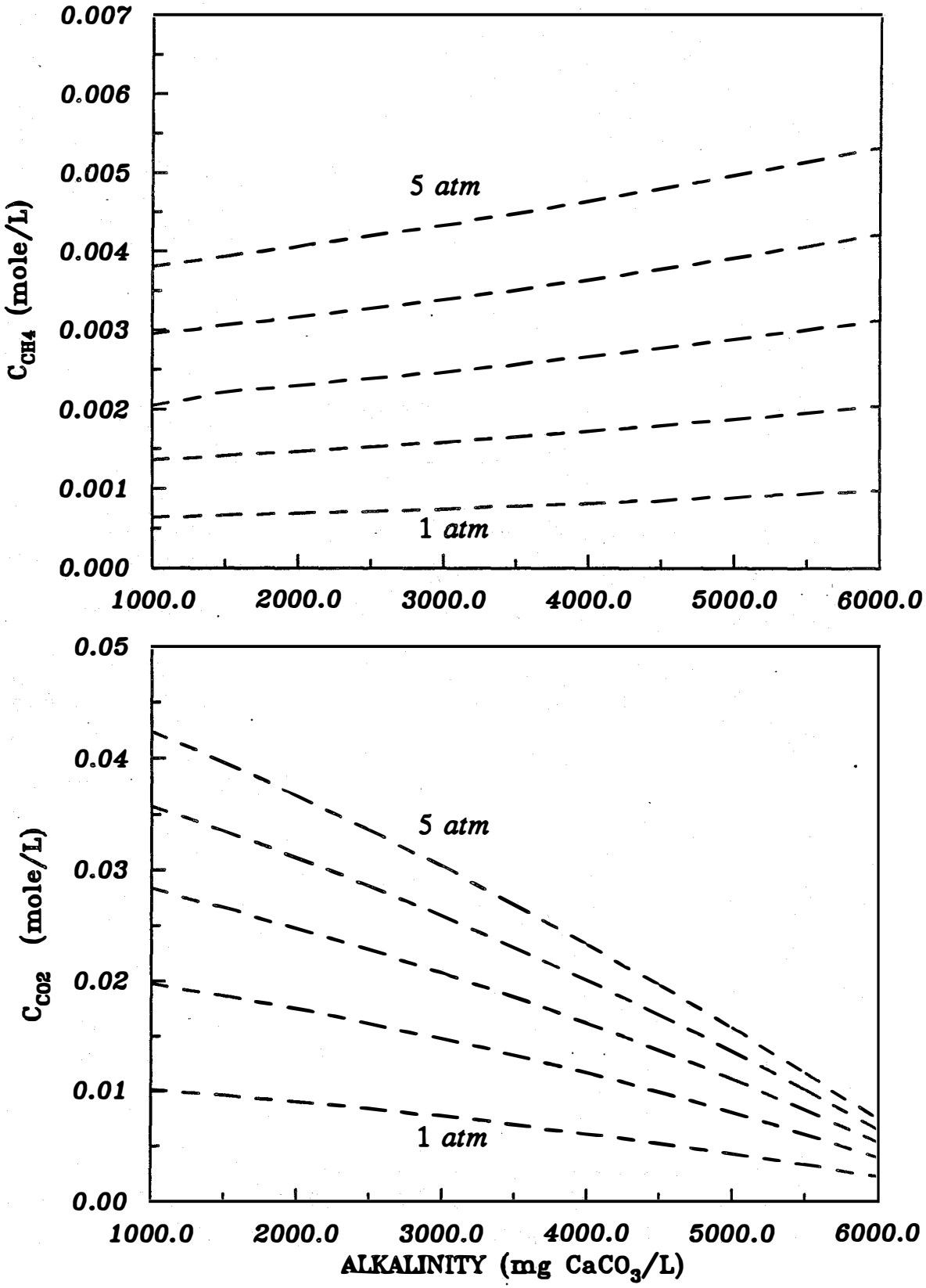

Figure 6-15 The Effects of Total Pressure on C_{CO_2} and C_{CH_4}

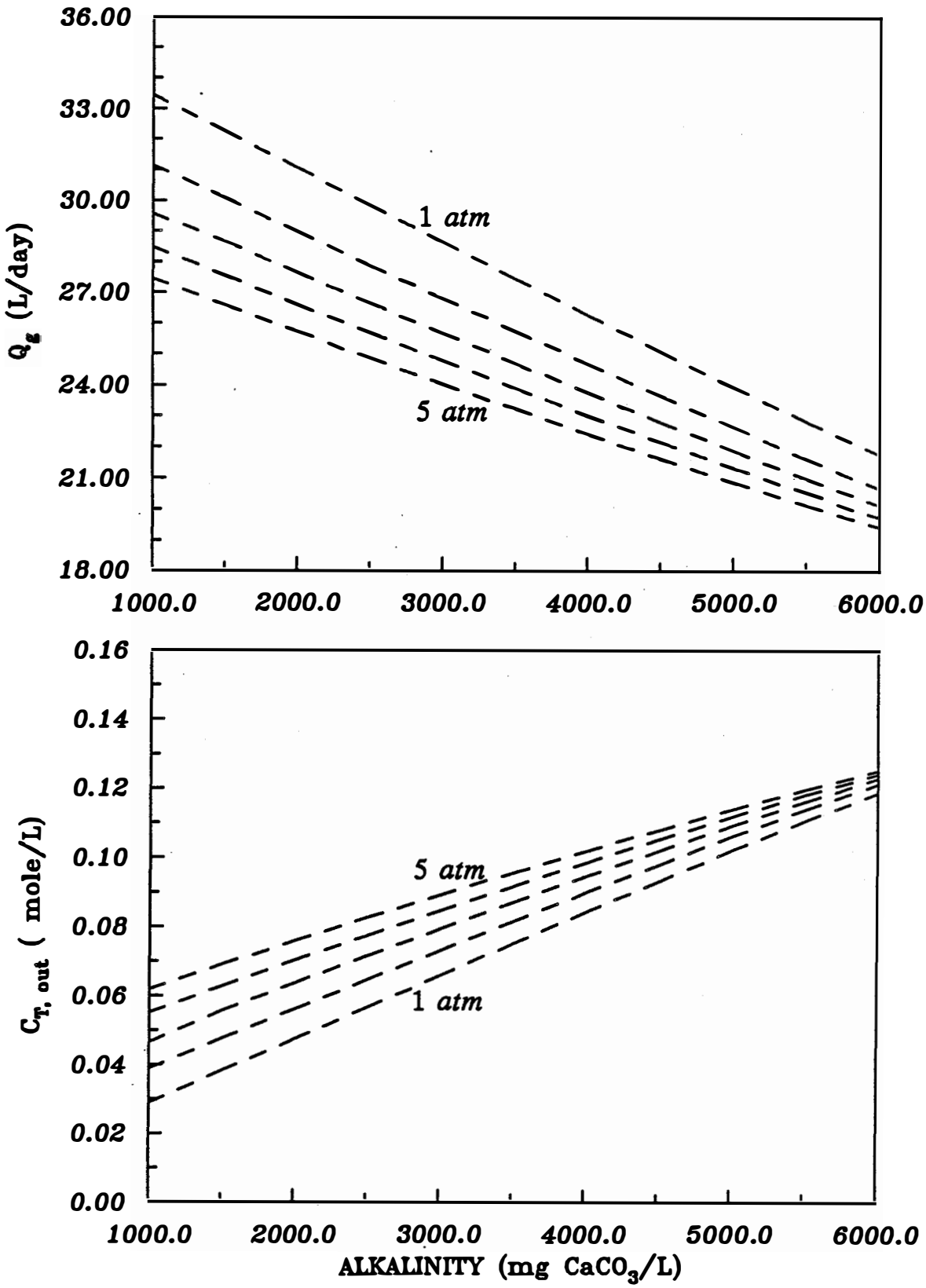

Figure 6-16 The Effects of Total Pressure on Q_g and $C_{T,out}$

Table 6–20 Comparison Between the Model Predictions and the Results of Hayes *et al. (1989)*

	Experimental Result		Equilibrium Model	
$P_T(atm)$	0	30	0	30
Alkalinity ($mg\ CaCO_3\ /L$)	4733	5581	4733	5581
COD				
$S_b(mg/L)$	269.4	265.3		
$S_o(mg/L)$	10000	10000		
$Q(L/day)$	5.0	5.0		
J (gCOD/day)			48.65	48.65
$CH_4\%$	81.05	93.20	80.55	93.02
pH	7.5	7.5	7.69	7.94
$C_{T,out}(mole/L)$	0.975	0.115	0.0933	0.0113

in determining the degree of equilibrium. The significance of K_La is illustrated in Figure 6–17, in which the operational condition is assumed to be 2600 mg $CaCO_3$ / L and 50.0 g COD /day of total COD flux in the Berl saddle reactor. Since K_L, according to Eq. 3–40, is a function of several system parameters and is independent of gas production rate, K_La is expected to vary with the gas rate as a does. In Figure 6–17, the values at a=1 were calculated as if a was the same as the specific surface area of the packing material - Berl saddle, *i.e* a = 1.87 cm^{-1}. The corresponding gas mass transfer coefficients are K_La = 693.93 day^{-1} and K'_La = 723.39 day^{-1}. The x–axis in Figure 6–17 represents the logarithmic multiplication of this a value. When the K_La and K'_La are greater than the calculated value, all parameters reach constant levels, which are very close to the equilibrium values, according to Figures 6–1 and 6–2.

A larger a value represents more contact area between liquid and gas phases and consequently a potential for higher mass transfer rates. At lower a values, there is not enough contact between gas and liquid; thus the concentration of gases in the liquid phase increase and more gas is lost in the effluent. When the mass transfer rate is limited due to insufficient contact area, the upper part of Figure 6–17 displays a low Q_g and reactor pH. The low Q_g simply reflects the limitation of gas transfer into the gas phase, thus accumulating CH_4 and CO_2 in the liquid phase and the increased CO_2 lowers the pH. Because the alkalinity is a fixed input of the model, lower a values increase the amount of dissolved CO_2, C_{CO_2}, and shift the inorganic carbon from CO_3^{-2} into HCO_3^- thus lowering the pH. The high concentration of dissolved CO_2 and CH_4 in the lower part of Figure 6–17 exemplifies the restricted area for mass transfer to take place. The higher C_{CH_4}, compared to C_{CO_2}, is largely due to the constraint of alkalinity, which confines the amount of dissolved CO_2. Whereas C_{CO_2} is bounded by alkalinity, the C_{CH_4} does not have any restraints. At the lower a values, the larger C_{CH_4} makes the P_{CH_4} slightly higher.

Figure 6–17 clearly indicates that the gas transfer is substantially restricted at very small a values. One possible cause for this lack of contact between the gas and liquid phases in the high rate of biogas production, thereby leading to the assumption that at high organic loadings, the biogas escaped into the bulk liquid in the form of big bubbles. The non–equilibrium model simulated the possible operational conditions at higher loadings, the results of which are illustrated in Figures 6–18 to 6–21. All of these figures were calculated by assuming a constant alkalinity of 2600 mg $CaCO_3$ / L in the Berl saddle reactor at different organic fluxes. All other assumptions are the same as those made in Figure 6–17.

The higher organic flux increase the biogas production rate, as in Figure 6–18, and the amount of CO_2 in the liquid, which leads to lower pH values as well as CH_4 partial pressure, as shown in Figure 6–19. As illustrated in Figures 6–20 and 6–21, the dissolved CO_2 and CH_4 concentration also increase with the organic flux. Despite the additional biogas produced by the elevated fluxes, the equilibrium states were not affected at high a values. In fact, all simulated results seem to converge to equilibrium when a is larger than that of the Berl saddle, *i.e.* 1.87 cm^{-1}.

The biogas production rate, shown in Figure 6–18, increases as the organic flux does at higher a values, while Q_g reduces dramatically at lower a values, especially for higher organic loadings. These low Q_g values at the lowest a value show that the gas transfer is so greatly restricted that the Q_g is also limited. As shown in Figure 6–18 , it is likely that the Q_g values will converge to a uniform value if the contact area, a, declines further. The low Q_g values, regardless the COD fluxes, demonstrates that

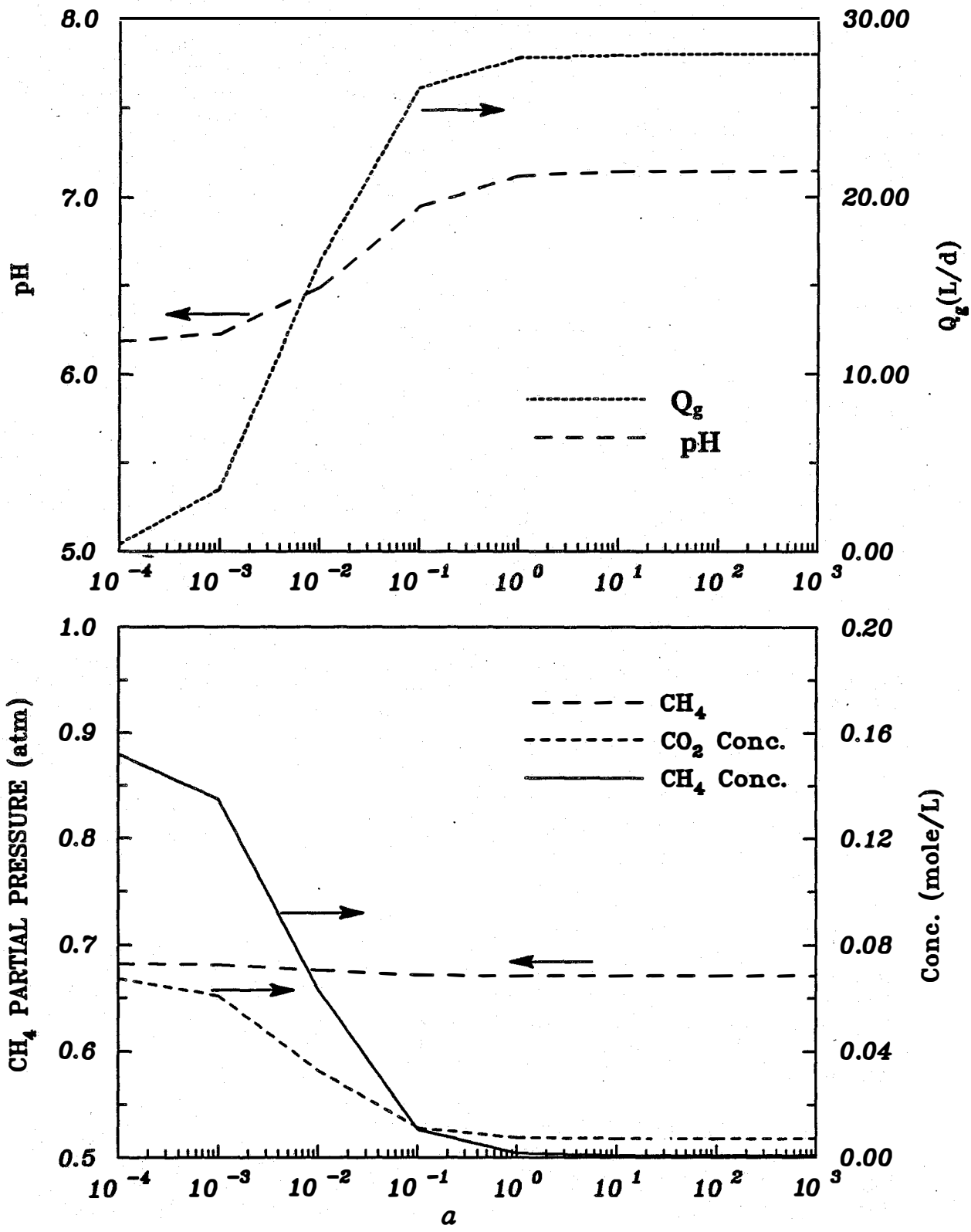

Figure 6-17 The Effects of a on Reactor Performance.

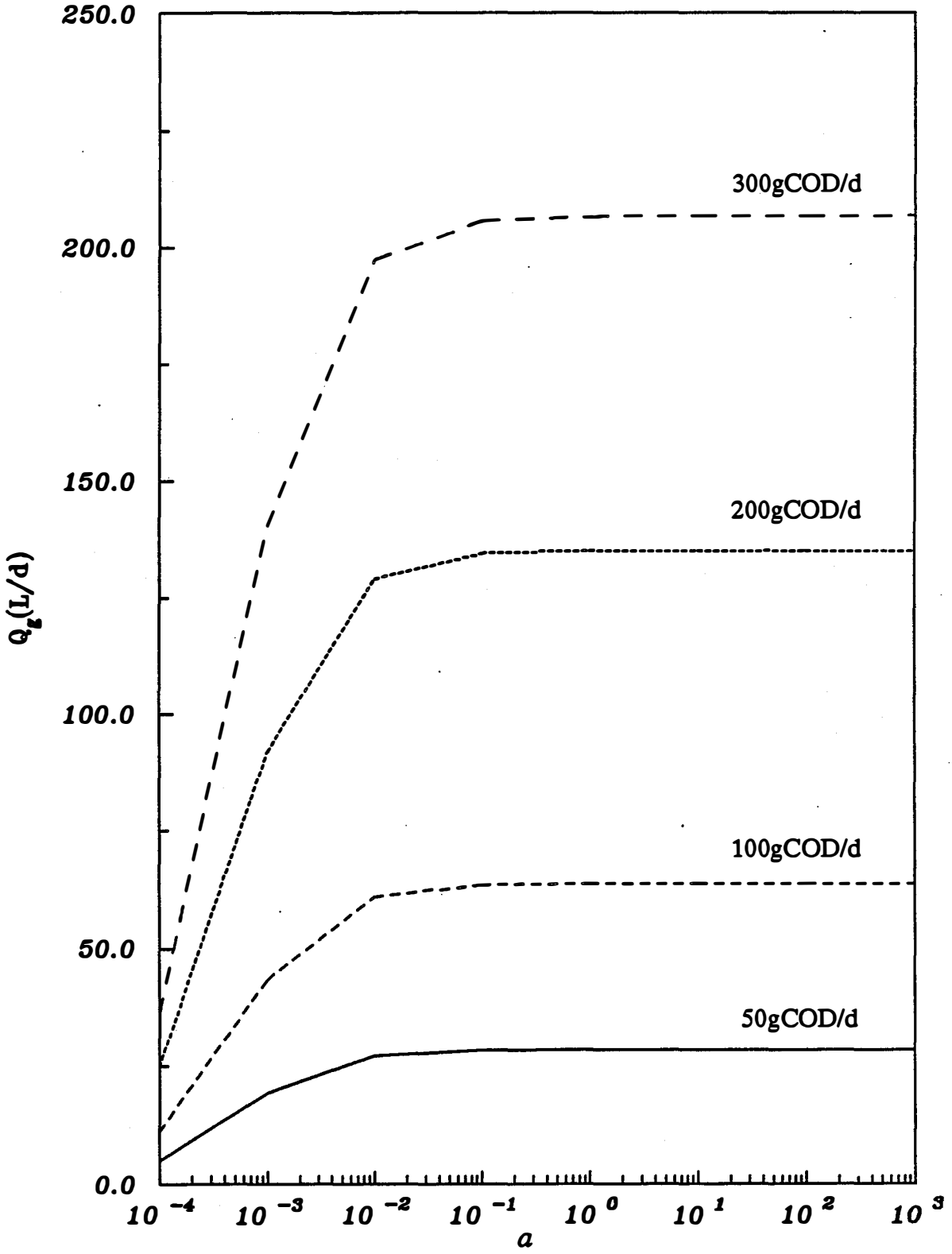

Figure 6-18 The Effects of Organic Flux and a on Q_g.

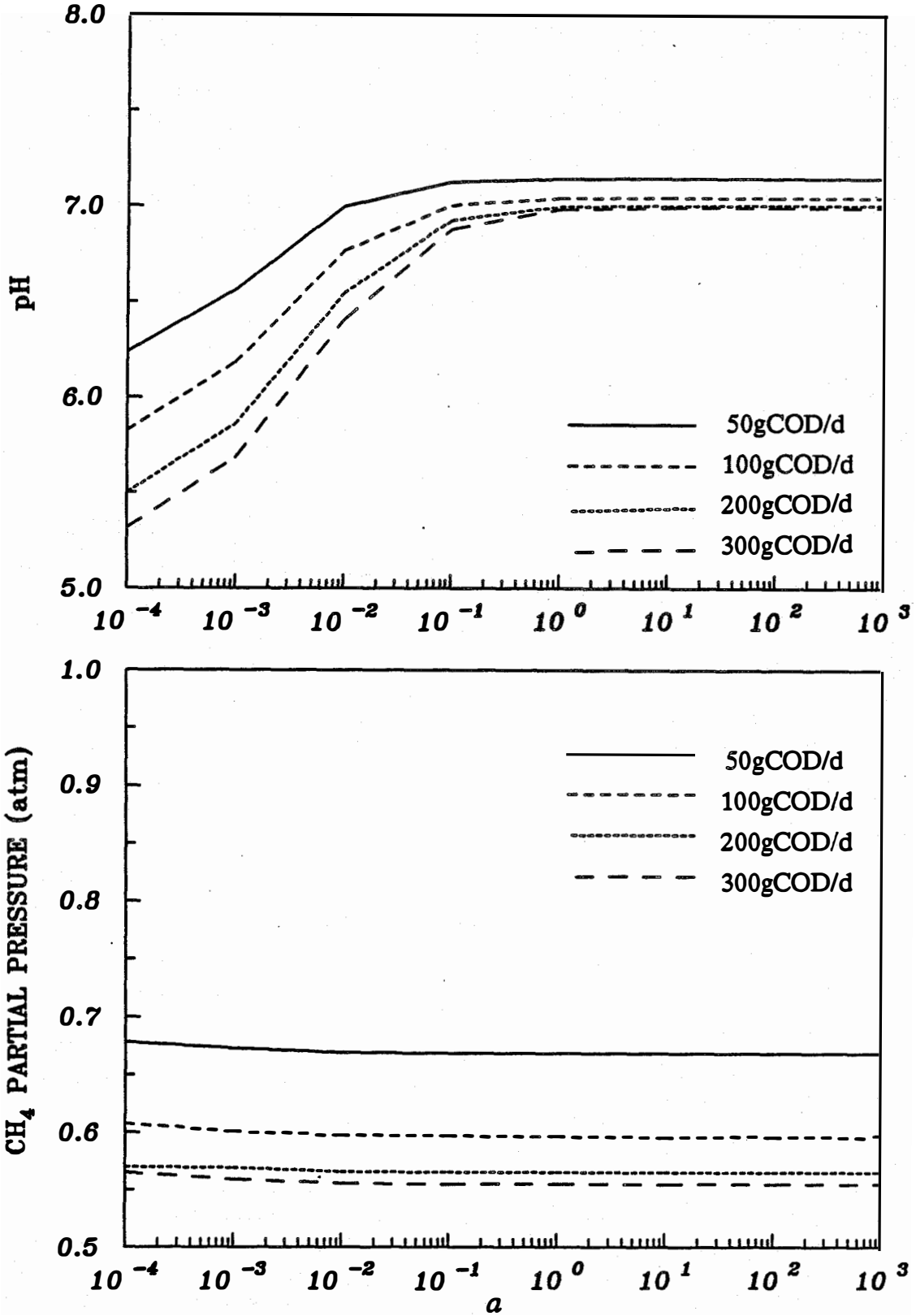

Figure 6-19 The Effects of Organic Flux and *a* on pH and Methane Partial Pressure

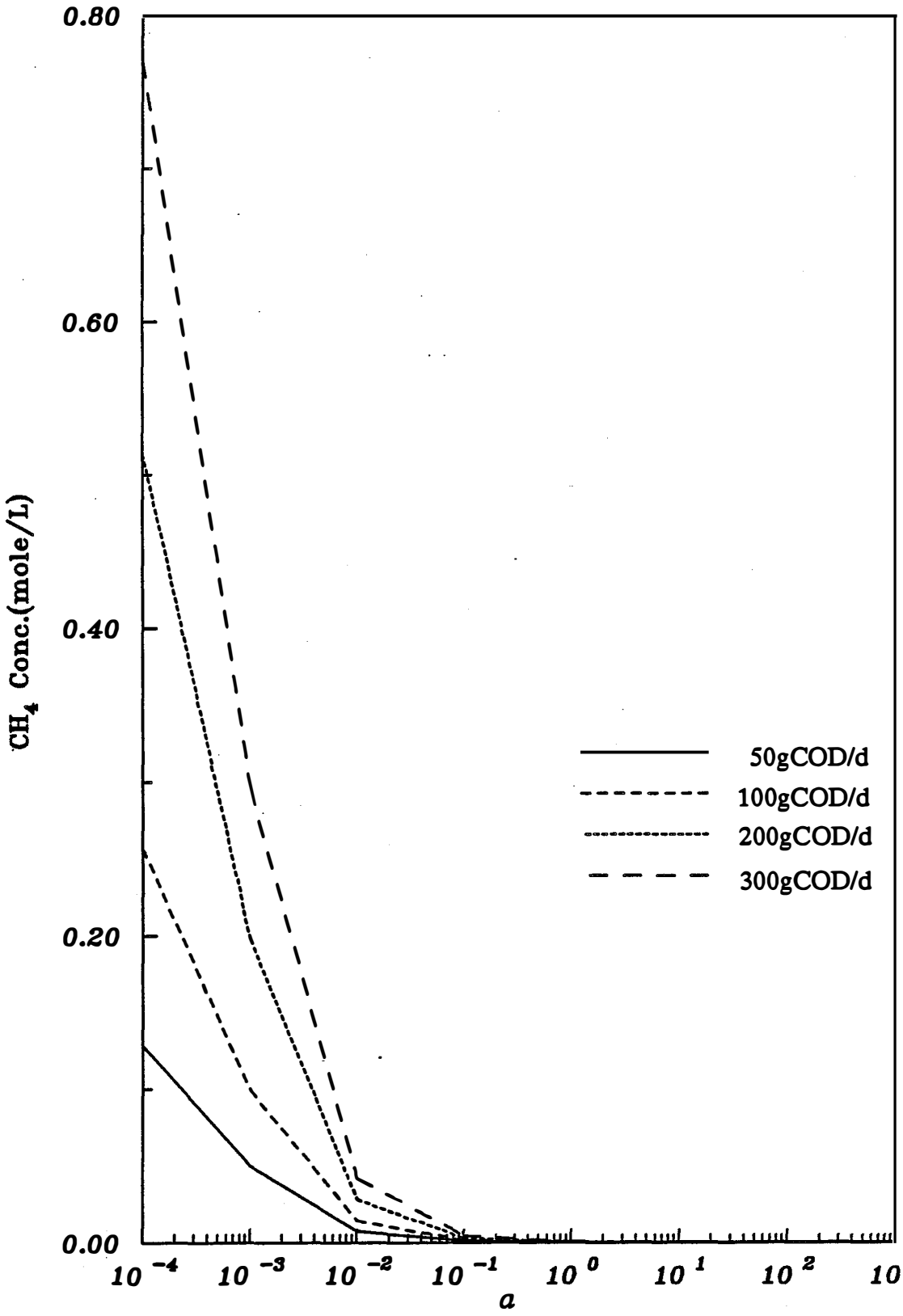

Figure 6–20 The Effects of Organic Flux and a on Methane Concentration.

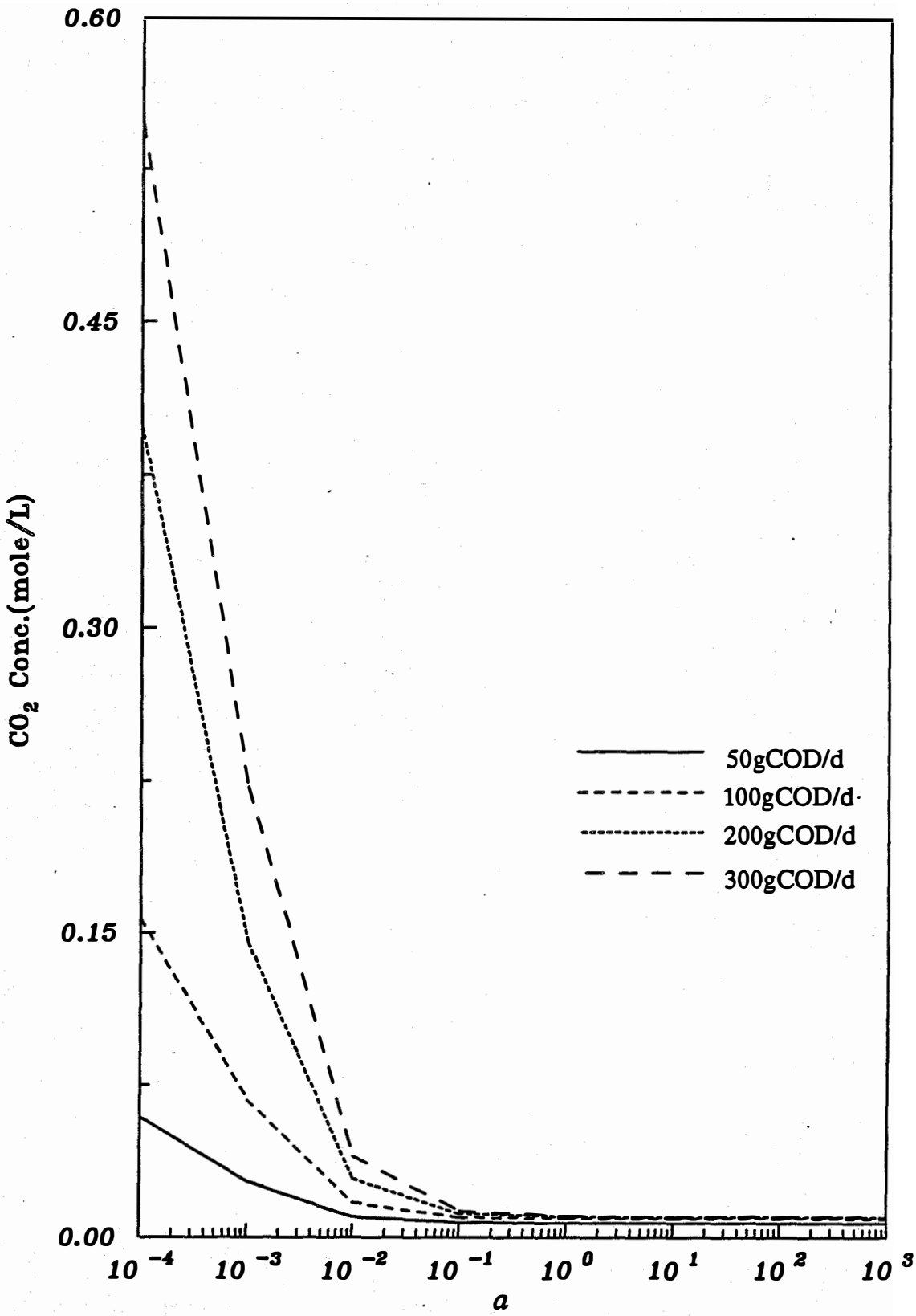

Figure 6-21 The Effects of Organic Flux and a on CO_2 Concentration.

the biogas produced cannot transfer into the gas phase and has to remain in the liquid phase. The increased CO_2 concentration decreases pH and CH_4 partial pressure, as depicted in Figure 6–19. Figures 6–18 and 6–19 demonstrate the lower limitation of a values for gas transfer, while Figures 6–20 and 6–21 more clearly display the limiting value of a for proper contact. As presented in these two figures, the gas transfer starts showing sign of hindrance when the a value is significantly smaller than that of Berl saddle, 187 m^{-1}. One–tenth of this value still yields acceptable results, but when a becomes smaller the restriction on biogas transfer into gas phase increases significantly. Figure 6–18 to 6–21 also pointed out that contact area, instead of organic loading, is the pivotal factor controlling the equilibrium state.

Several researchers adapted the concept of mass transfer in their research, but were unable to accurately determine the K_La values. Andrews and Graef (1970) selected K_La of 100 day^{-1} as being required to model the dissolved CO_2 concentration close to the equilibrium value. Lindgren (1983) used a K_La value of 120 day^{-1} to obtain near equilibrium conditions. These two values, compared to results in Figure 6–17, are in the range that the reactor is nearly at equilibrium and are satisfactory for model simulation. In conclusion, a wide range of K_La values can be used for equilibrium simulation as long as they are above a certain minimum value.

6.4 Diffusional Model

The major advantage of the diffusional model is its ability to simulate the out–diffusion of fermentation end products. The concentration profile of CH_4 in an anaerobic biofilm is useful in determining the behavior of biogas in the biofilm and whether biogas bubbles form in the biofilm and increase the sloughing of the biomass. This simulation may provide important information for the design of a sound biofilm reactor. The required inputs of the diffusional model were the outputs of the equilibrium model. Other parameters used in this model are listed in Table 6–21.

Figures 6–22 and 6–23 are the predictions of the equilibrium model under different levels of acetic acid concentration in the bulk solution. The predictions are based on a substrate flux of 49.59g COD/d and influent inorganic carbon of 1.75×10^{-2} mole/L. Acetate was chosen to represent the rate–limiting substrate in the system. The different pH and CH_4 partial pressure exemplify the buffering effect of acetate which causes a higher total alkalinity when the acetate concentration is higher. The outputs from the equilibrium model, P_{CO_2} and P_{CH_4}, were used to calculate the concentrations of individual inorganic carbon species and CH_4. The pH profiles of anaerobic biofilms under different acetate concentrations were calculated from Eq. 4–33. Figure 6–24 shows the pH profiles of dimensionless anaerobic biofilms at different bulk acetate concentrations and bulk pH of 7. An acetate concentration of 3000mg/L demonstrated the most increase in biofilm pH, while the 100mg/L showed the least. The pH increase is sufficiently small to be almost negligible from a practical viewpoint. It can, therefore, be concluded that the bicarbonate generated in the anaerobic fermentation does not have a significant impact on the pH inside the biofilm.

On the other hand, the CH_4 profile inside the biofilm might be more important. Figure 6–25 shows the dimensionless CH_4 concentration profiles, predicted by Eq. 4–14, which illustrate the significance of the substrate concentrations on the CH_4 concentration inside the biofilm. Figure 6–25 displays that the ratio of the biofilm CH_4 concentration at the rear of the biofilm to the bulk CH_4 concentration ranges from 2.44 at C_A = 100 mg/L to 7.20 at C_A = 3000 mg/L. Since the predicted bulk CH_4

Table 6–21 Parameters Used in Diffusional Model

Parameter	Value	References
D_f	1.37 cm^2/day *	Treybal, 1980
D_{CH_4}	2.29 cm^2/day *	Treybal, 1980
D_{CO_2}	1.14 cm^2/day	Liehr *et al.*, 1988
$D_{HCO_3^-}$	0.6 cm^2/day	Liehr *et al.*, 1988

* Calculated from Wilke and Chang's correlation.

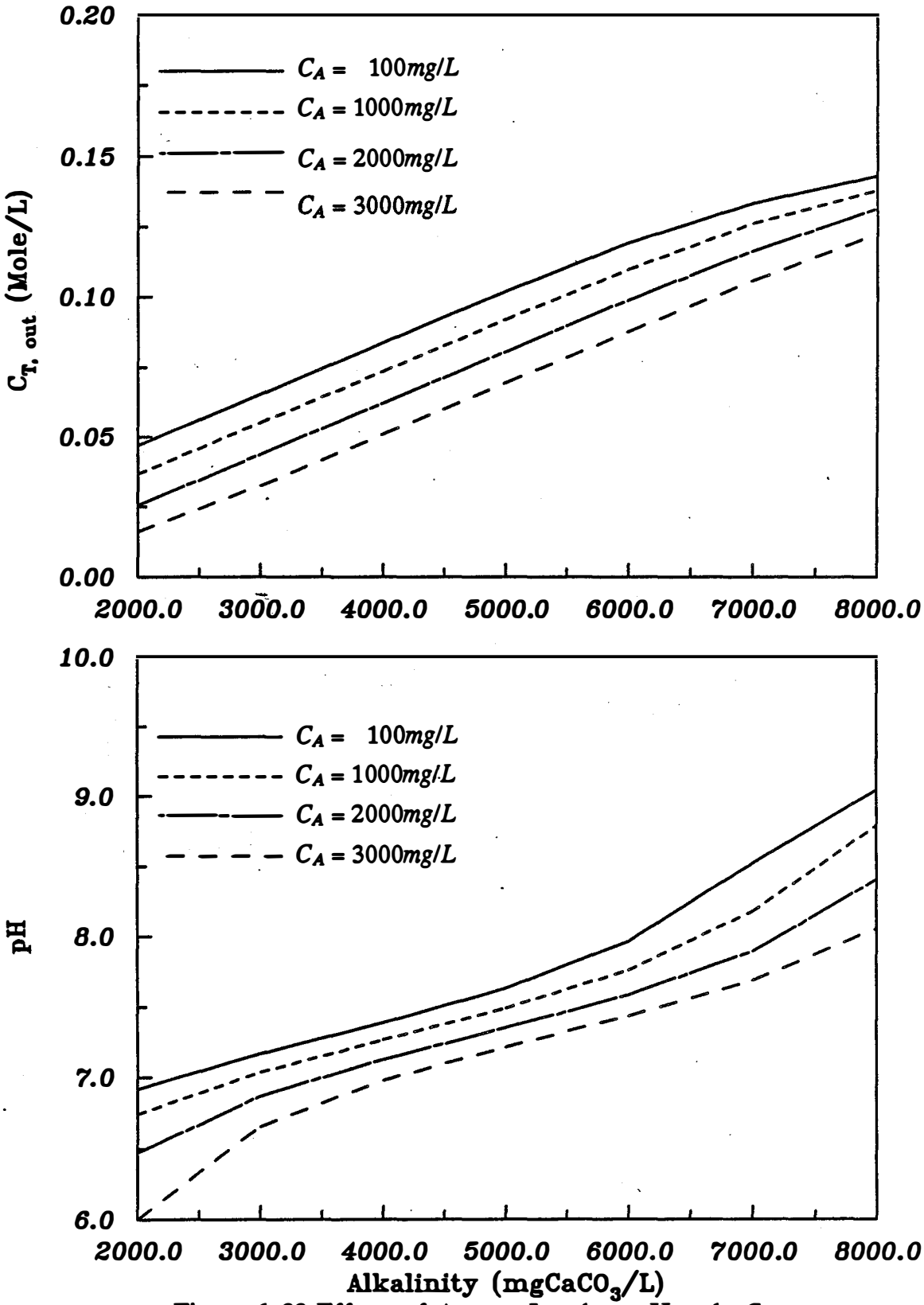

Figure 6–22 Effects of Acetate Level on pH and $C_{T,out}$

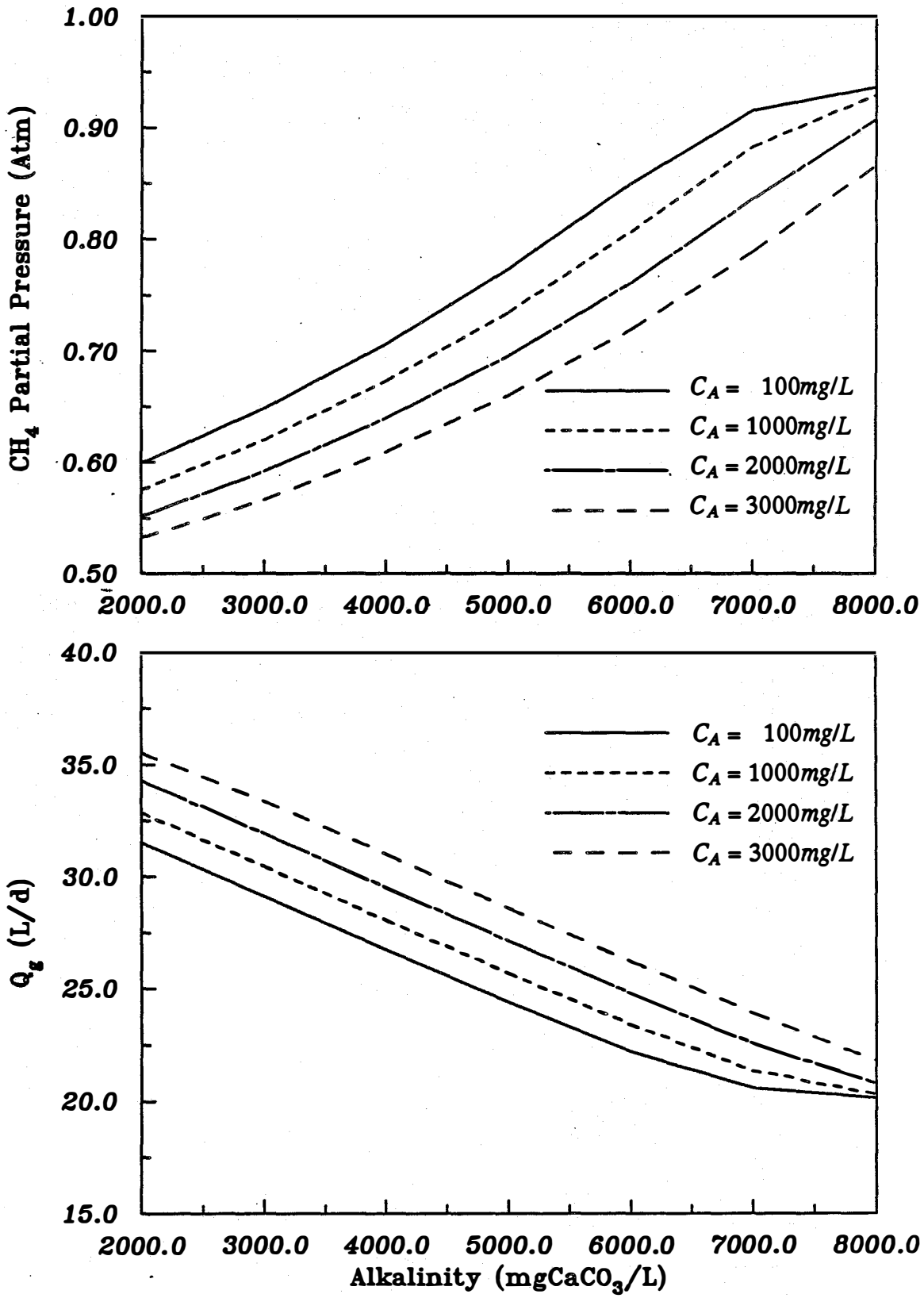

Figure 6–23 Effects of Acetate Level on CH_4% and Q_g

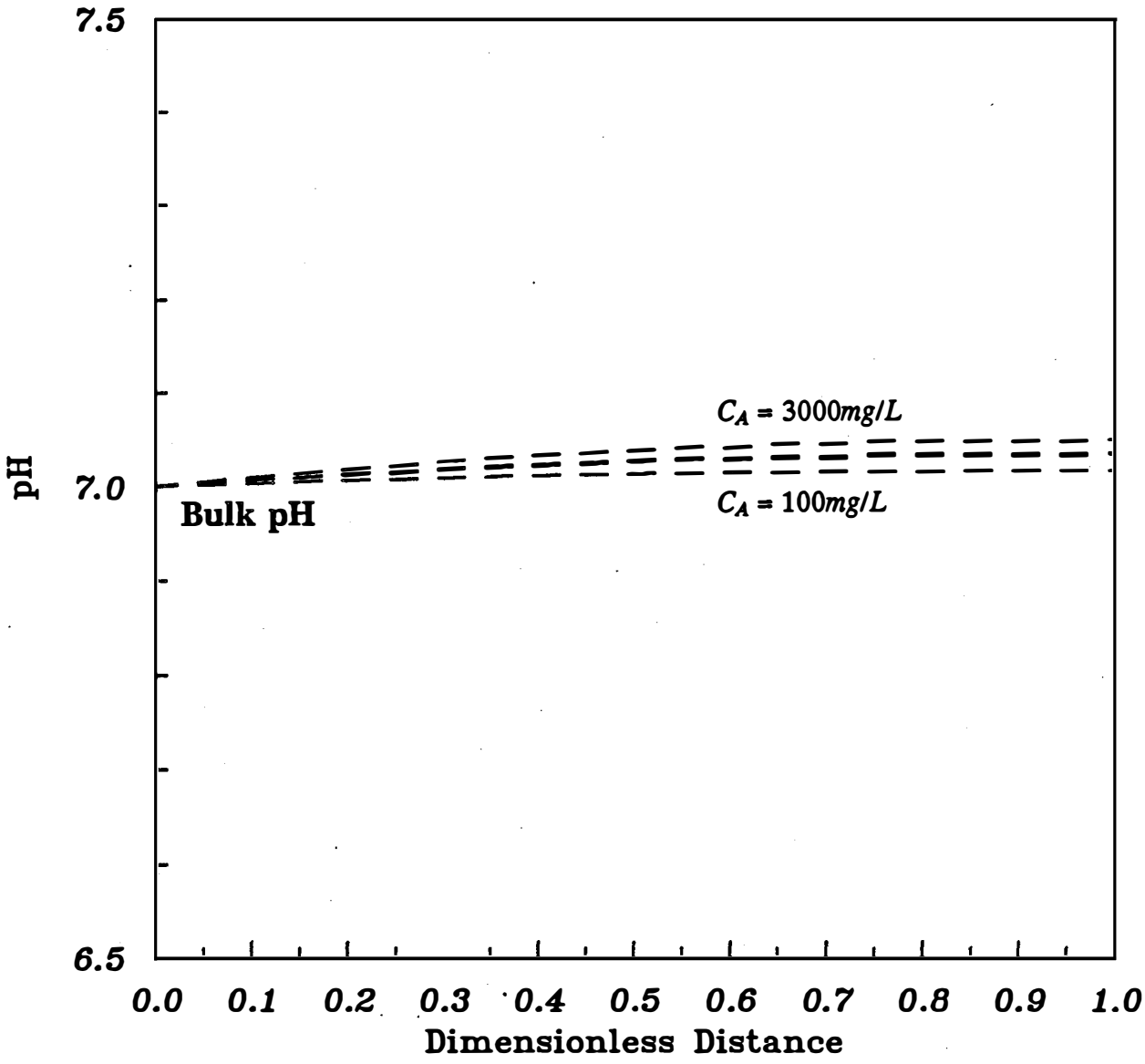

Figure 6–24 pH Profile in Dimensionless Anaerobic Biofilm

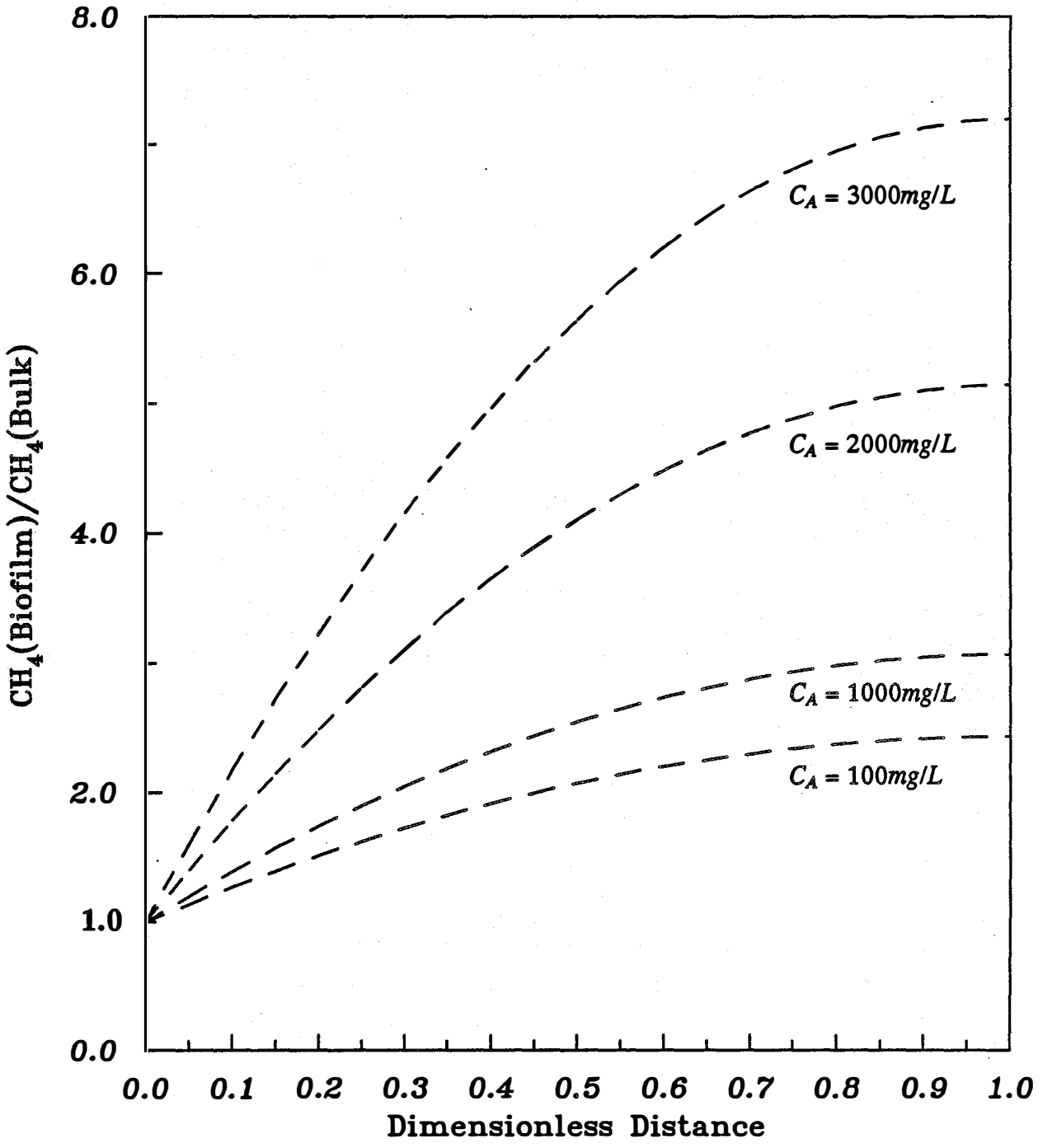

Figure 6–25 Methane Profile in Dimensionless Anaerobic Biofilm

concentration is in equilibrium with a CH_4 partial pressure of about 0.6 atm, the CH_4 partial pressure at the back of the biofilm is higher than 1 *atm*. The biofilm is supersaturated with gas and the CH_4 would be expected to be transported out the biofilm by forming bubbles (Henze and Harremoës, 1983). These bubbles probably will dislodge the biomass from the surface of the support media or cause channels and holes to develop in the biofilm (Switzenbaum and Eimstad, 1987). Harremoës *et al.* (1980) identified the nitrogen saturation at the rear of denitrification biofilms, which is directly related to the substrate and product concentrations in the bulk solution. The nitrogen profile in the denitrifying biofilms is similar to the CH_4 profile in anaerobic biofilm.

Therefore, it is important not only to maintain an acceptable pH inside an anaerobic biofilm reactor, but also to maintain a low substrate level in the bulk solution. The accumulated acid level in an anaerobic biofilm reactor may increase the biofilm sloughing, thus decreasing the total biomass retained in the reactor and cause further deterioration in the operation until the system fails. Consequently, the control of an unbalanced attached–growth reactor requires a strategy different from that of a suspended–growth reactor. In a suspended–growth system, the unbalance can be corrected by maintaining pH near neutrality through adding neutralizing materials (McCarty, 1964c). By contrast, this will be detrimental for an attached–growth reactor because the increased acid concentration in the bulk liquid will increase the partial pressure of biogas and increase bubble formation in the biofilm even though the pH is maintained at neutrality. Therefore, the appropriate technique for restoring an unbalanced biofilm reactor is to reduce the organic loading until the substrate level has reached an acceptable level.

The results of the diffusional model also provide an insight into the limitation of organic loading in a fixed–film reactor. At a low organic loading, the substrate only supports a fully penetrated biofilm because the thickness is sufficiently thin that the diffusion of substrate into the biofilm will not be limited. By contrast, a deep biofilm requires a higher substrate level and the thickness is restricted by the depth of substrate diffusion. The biofilm becomes thicker as the organic loading increases, thus escalating the diffusional resistance. In order to overcome this resistance and generate a higher gradient, the bulk substrate concentration has to increase to a correspondingly higher level. Ideally, when the substrate can not reach the rear of the biofilm thereby depriving the necessary nutrients for microbial growth and attachment, the biomass starts sloughing. However, Figure 6–25 indicates that the maximum possible organic loading is also restricted by the build–up of gaseous products in the biofilm. Consequently, when a biofilm is not yet thick enough to restrict substrate diffusion to the rear, the formation of biogas bubbles in the biofilm might keep the biofilm mass from increasing due to increased sloughing of the biofilm. This biomass loss will decrease the SRT of the system and the associated treatment efficiency. The higher bulk substrate concentration, due to the shorter SRT, will then further elevate the CH_4 concentration inside the biofilm. The maximum possible organic loading of a biofilm reactor is therefore reduced by the biogas bubble build–up.

Experimental verification of the diffusional model may be infeasible because of the difficulties involved in biofilm measurements and bulk concentration control. Arvin and Kristensen and other researchers have measured the pH profile inside the denitrifying However, the measurement of the CH_4 concentration inside the biofilms will be difficult. An experimental design to substantiate the diffusional model, therefore, will provide a better understanding of the biofilm kinetics and can be applied to the design of biofilms reactors.

In spite of the difficulties which might be encountered in verifying the diffusional model microscopically, results of this research can prove it macroscopically. Figures 6–2 to 6–4 of the Haydite reactor substantiate the biofilm kinetics inside anaerobic filters. As shown in Figure 6–2, the biofilm thickness increased steadily with the organic loading until the loading of 13.32 Kg COD / $m^3 \cdot d$ had been reached. The slightly increased bulk COD also suggests that the diffusional resistance is directly proportional to the thickness of biofilms, and consequently elevated substrate concentrations can overcome the additional resistance by building up higher substrate fluxes. Additionally, Suidan *et al. (1987)* pointed out that the biofilm becomes more fully penetrated with higher S_b^* at a given value of L_f^*. Moreover, once the biofilms reach their maximum thickness, the increase of suspended–growth biomass is the only means to cope with higher organic loadings. Since L_f^* remains constant, extra biomass produced from high organic loadings will increase the total decay coefficient. The increased suspended–growth biomass will further deteriorate the reactor performance because the SRT is shortened through biomass loss. Furthermore, the high substrate concentration in the bulk will boost the biogas concentration in the biofilms and increase sloughing. These combined effects, as demonstrated in Figures 6–3 and 6–4, result in a short SRT and higher effluent COD. This cycled sequel will, eventually, cause the system failure.

The biofilms are all very close to fully penetrated, as shown in Table 6–5, denoting that the maximum possible depth has been reduced by external physical constraints of the reactor as well as the internal biogas build–up. Because the flow regime only supports a biofilm that can utilize the loading of 13.32 Kg COD / $m^3 \cdot d$, additional loading just increased the substrate concentration and started the process of sloughing due to biogas bubble formation. Since the biofilm started sloughing prematurely, it would be interesting to operate the reactor under different recycle ratios to examine the corresponding maximum possible thicknesses of the biofilm. If the maximum possible loading and biofilm thickness increases as flow velocity decreases, the hypothesis of reduced biofilm depth by shearing stress will be proved.

CONCLUSIONS

Several conclusions can be drawn from this study, among which the following are felt to be of special significance :

1. The biomass-holding capacity of a packed-bed biofilm reactor is not only decided by the specific surface area of the packing media, but also by other characteristics of the media, such as porosity, density and size. This research has shown that granular activated carbon, despite its tremendous surface area, fails to provide adequate support for biofilm growth in a packed-bed reactor because the shear loss of biofilm due to the abrasion between carbon particles caused by the low porosity and biogas bubbles. Also, flow distribution in the bed is a significant problem due to the channels created by the large gas bubbles that formed in the bed. In order to ensure a better treatment efficiency, ideal packing media should possess a higher porosity for biogas escape and should be heavy enough to withstand the lifting motion from gas movement.

2. The biofilm model can accurately describe the behavior of an anaerobic packed-bed reactor as long as the system parameters are adequately determined. This model also demonstrates the fully penetrated nature of biofilms under these loading rates, thus simplifying the model into a Monod-type expression disregarding mass transport resistances.

3. Experimental results show that the biofilm depth in anaerobic packed-bed biofilm reactors is governed by the organic loading until the maximum depth is achieved. Once the biofilm depth reaches this value, controlled by shear stress, additional loading will increase the concentration of suspended-growth biomass, thus causing a reduction in the SRT due to the loss of biomass in the effluent.

4. The equilibrium and non-equilibrium models successfully describe the behavior of anaerobic packed-bed reactors. Under the conditions investigated, there is no significant difference between these models, which leads to the conclusion that the state of equilibrium prevailed.

5. The specific surface area between gas and liquid, a, is the major factor controlling the state of equilibrium in an anaerobic reactor. Sufficient contact area between phases is required to assure proper mass transfer and to reach an equilibrium state. The organic loading does not have direct impact on the equilibrium as long as the contact area between the liquid and gas phase is unlimited. Numerical results show that an a value larger than 18.7 m^{-1} is accurate enough for computational purpose.

6. The equilibrium model satisfactorily describes the mechanism of methane enrichment and can be applied to industrial-scale reactor designs for methane recovery in anaerobic reactors. Total reactor pressure, pH, alkalinity and influent inorganic carbon concentration are the main factors dictating the methane content of the gas produced by an anaerobic reactor. This model also corroborated the conclusions of Hayes *et al.* (1989) that methane gas of 93% purity can be obtained through proper combination of elevated total pressure, pH, alkalinity and influent inorganic carbon removal.

7. The diffusional model demonstrates that the biogas build-up within anaerobic biofilms is a function of the bulk substrate concentration. The maximum possible

organic loading of an anaerobic biofilm reactor may be significantly reduced because of the sloughing effects caused by methane bubble formation inside the biofilms. This model also suggests an acceptable procedure for restoring unbalanced biofilm reactors is to reduce the organic loading until the biogas bubble formation inside the biofilms is eliminated by substrate depletion. According to the model, the pH change in anaerobic biofilms is sufficiently small that it can be ignored.

8. The selection of packing material is critical in reactor design – the characteristics of the material are as important as the specific surface area. In order to eliminate erroneous conclusions by making comparisons with different materials, packing media made of same material but different specific surface area should be used to study their biomass-holding capacity. Moreover, the media configuration should be identical in order to maintain comparable flow pattern. Therefore, when evaluating biofilm performance, it would be ideal to have packing media which would differ only in size, but would be similar in all other properties.

VIII. ENGINEERING SIGNIFICANCE

Some findings of this study can be applied directly into the design and development of anaerobic fixed-bed reactors.

Many models have been developed to describe the anaerobic reactors of dynamic or steady-state conditions. However, most of these models require complicated numerical solutions and are not practical to engineering practice. The close correlation between the simulated values and the experimental data substantiates the effectiveness of the equilibrium model. The model is especially useful in determining the influence of each parameter in reactor operation, such as alkalinity, pH, biogas productions and methane content. Another important aspect is to apply this model to methane enrichment, which enables the engineers to select the optimal conditions for reactor operation. In addition, all these models were solved by a personal computer which is readily available in every engineering office. This accessibility makes the models more appealing in identifying the behavior of the anaerobic fixed-bed reactors.

The major result of engineering significance is that the nature of biofilms in anaerobic packed-bed reactors has been better identified, thereby providing information for improving reactor design. Experimental results have found that the anaerobic biofilm reactors actually behave more like CSTRs. The simplified Monod-type expression accurately models the biological aspect of the reactor and is numerically simple, whereas the equilibrium model simulates the physical and chemical aspects of the reactor. The diffusional model recognizes the possibility of biofilm sloughing at high bulk substrate concentrations. The addition of a base to raise the pH in a poorly operating biofilm reactor may have a negative effect on the system performance. The elevated bulk substrate concentration will increase the sloughing of the biofilm due to biogas bubble formation within the biofilm. This loss of biomass will decrease the SRT, causing additional loss in efficiency. The remedy for restoring an "acid" biofilm reactor is to reduce the load on the reactor until the substrate is reduced to a low level.

IX. LIST OF REFERENCES

Abramson, S.D., "A Predictive Model for Anaerobic Filters Treating Low Strength Domestic Wastewaters", *Journal of Environmental Systems*, Vol. **16**, No. **3**, 1986–1987, p201–232.

American Public Health Association, *Standard Methods for the Examination of Water and Wastewater*, 15th ed., American Public Health Association, Washington D.C., 1981.

Anderson, G.K. and Duarte, A.C., "Research and Application of Anaerobic Processes", *Environmental Technology Letters*, Vol. **1**, 1980, p484–493.

Andrews, J.F. and Pearson, E.A., "Kinetics and Characteristics of Volatile Acid Production in Anaerobic Fermentation Processes", *Int J. Air Wat. Poll.*, Vol. **9**, 1965, p439–461.

Andrews J.F., "Dynamic Model of the Anaerobic Digestion Process", *Journal of the Sanitary Engineering Division – ASCE*, Vol. **95**, No. **SA1**, Feb. 1969, p95–116.

Andrews J.F. and Graef, S.P., "Dynamic Modeling and Simulation of the Anaerobic Digestion Process", *Anaerobic Biological Treatment Process : Proceedings of the 159th Meeting of the American Chemical Society, Houston, Tex., Feb. 26, 1970*, Advances in Chemistry Series 105, , p126–162.

Arvin, E. and Kristensen, G.H., "Effect of Denitrification of the pH in Biofilms:, *Water Science and Technology*, Vol. **14**, No. **8**, 1982, p833–848.

Atkinson, B. and Davies, I.J., "The Overall Rate of Substrate Uptake (Reaction) by Microbial Film, Part I – A Biological Rate Equation", *TRANS INSTN CHEM ENGRS*, Vol. **52**, 1974, p248–259.

Audic, J.M., Faup, G.M. and NaVarro, J.M., "Specific Activity of *Nitrobacter* Through Attachment of Granular Media", *Water Research*, Vol. **18**, No. **6**, 1984, p745–750.

Babbitt, H.E. and Baumann, E.R., *Sewerage and Sewage Treatment*, 8th ed., John Wiley & Sons, New York, 1958.

Bhadra, A., Scharer, J.M. and Moo–Young, M., "Methanogenesis from Volatile Fatty Acids in Downflow Stationary Fixed–Film Reactor", *Biotechnology and Bioengineering*, Vol. **30**, No. **2**, Aug. 1987, p314–319.

Binot, R.A., Bol, T., Naveau, H.–P. and Nyns, E.–J., "Biomethanation by Immobilized Fluidised Cells", *Water Science and Technology*, Vol. **15**, Nos. **8/9**, 1983, p103–115.

Bird, R.B., Stewart, W.E. and Lightfoot, E.N., *Transport Phenomena*, John Wiley & Sons, New York, 1960.

Borchardt, J.A., "Anaerobic Phase Separation by Dialysis Technique", *Anaerobic Biological Treatment Process : Proceedings of the 159th Meeting of the American Chemical Society, Houston, Tex., Feb. 26, 1970*, Advances in Chemistry Series 105, , p108–125.

Bryant, M.P. *et al.*, "Growth of *Desulfovibrio* in Lactate of Ethanol Media Low in Sulfate in Association with H_2-Utilizing Methanogenic Bacteria", *Applied and Environmental Microbiology*, Vol. **33**, No. **5**, May 1977, p1162–1169.

Bryant, M.P. "Microbial Methane Production – Theoretical Aspects", *Journal of Animal Science*, Vol. **48**, No. **1**, 1979, p193–210.

Bryers, J.D., "Structured Modeling of the Anaerobic Digestion of Biomass Particulates", *Biotechnology and Bioengineering*, Vol. **27**, No. **5**, May 1985, p638–649.

Buswell, A.M. and Mueller, H.F., "Mechanisms of Methane Fermentation", *Industrial and Engineering Chemistry*, Vol. **44**, 1952, p550–552.

Characklis, W.G., "Attached Microbial Growths – I. Attachment and Growth", *Water Research*, Vol. **7**, 1973, p1113–1127.

Chen, S.J., Li, C.T. and Shieh, W.K., "Anaerobic Fluidized Bed Treatment of an Industrial Wastewater", *Journal WPCF*, Vol. **60**, No. **10**, Oct. 1988, p1826–1832.

Chian, E.S.K. and DeWalle, F.B., "Treatment of High Strength Acidic Wastewater with a completely Mixed Anaerobic Filter", *Water Research*, Vol. **11**, No. **3**, 1977, p295–304.

Chin, K.K., "Anaerobic Treatment Kinetics of Palm Oil Sludge", *Water Research*, Vol. **15**, 1981, p199–202.

Chung, K.T., "Inhibitory Effects of H_2 on Growth of *Clostridium cellobioparum*", *Applied and Environmental Microbioligy*, Vol. **31**, No. **3**, March 1976, p342–348.

Chynoweth, D.P. and Mah, R.A., "Volatile Acid Formation in Sludge Digestion", *Anaerobic Biological Treatment Process : Proceedings of the 159th Meeting of the American Chemical Society, Houston, Tex., Feb. 26, 1970*, Advances in Chemistry Series 105, p41–54.

Cohen, A., Zoetemeyer, R.J., van Deursen, A. and van Andel, J.G., "Anaerobic Digestion of Glucose with Separated Acid Production and Methane Formation", *Water Research*, Vol. **3**, 1979, p571–580.

Cohen, A., *Optimization of Anaerobic Digestion of Soluble Carbohydrate Containing Wastewaters by Phase Separation*, Ph.D. Thesis, University of Amsterdam, 1982.

Cohen, A., "Two–Phase Digestion of Liquid and Solid Wastes", *Third International Symposium on Anaerobic Digestion*, 1983, p123–138.

Coulter, J.B., Soneda, A. and Ettinger, M.B., "Anaerobic Contact Process for Sewage Disposal", *Sewage and Industrial Wastes*, Vol. **29**, 1957, p468–477.

Daniels, S.L, "The Adsorption of Microorganisms onto Solid Surfaces : A Review", *Developments in Industrial Microbiology*, Vol. **13**, 1972, p211–253.

Daniels, L., Sparling, R. and Sprott, G.D., "The Bioenergetics of Methanogenesis", *Biochimica et Biophysica Acta*, Vol. **768**, No. **2**, Sept. 1984, p113–163.

DeWalle, F.B. and Chian, E.S.K., "Kinetics of Substrate Removal in a Completely Mixed Anaerobic Filter", *Biotechnology and Bioengineering*, Vol. **XVIII**, No. **9**, Sept. 1976, p1257–1295.

Dolfing, J., "Kinetics of Methane Formation by Granular Sludge at low Substrate Concentration – the Influence of Mass Transfer Limitation", *Applied Microbiology and Biotechnology*, Vol. **22**, 1985, p77–81.

Duarte, A.C., "Studies on Inhibition Modelling in Anaerobic Digestion", *Asian Environment*, Vol. **4**, 1983, p23–33.

Ehlinger, F., Audic, J.M. and Faup, G.M., "Relationship Between the Concentration of Acetate in the Feed and the Composition of a Biofilm in an Anaerobic Filter", *Environmental Technology Letters*, Vol. **8**, 1987, p197–207.

Ehlinger, F., Audic, J.M., Verrier, D. and Faup, G.M., "The Influence of the Carbon Source on Microbiological Clogging in an Anaerobic Filter", *Water Science and Technology*, Vol. **19**, Nos. **1/2**, 1987, p261–273.

Fair, G.M., Geyer, J.C. and Okun, D.A., *Elements of Water Supply and Wastewater Disposal*, John Wiley & Sons, New York, 1973.

Ferguson, J.F., Eis, B.J. and Benjamin, M.N., "Neutralization in Anaerobic Treatment of an Acidic Waste", *Water Research*, Vol. **18**, No. **5**, 1984, p573–580.

Ghosh, S. and Pohland, F.G., "Kinetics of Substrate Assimilation and Product Formation in Anaerobic Digestion", *Journal WPCF*, Vol. **46**, No. **4**, April 1974, p748–759.

Ghosh, S., Conrad, J.R. and Klass, K.L., "Anaerobic Acidogenesis of Wastewater Sludge", *Journal WPCF*, Vol. **47**, No. **1**, Jan. 1975, p30–45.

Ghosh, S. and Klass, D.L., *Two Phase Anaerobic Digestion*, U.S. Patent No. 4,022,665, May 10, 1977.

Ghosh, S. and Klass, D.L., "Tow Phase Anaerobic Digestion", *Process Biochemistry*, Vol. **13**, April 1978, p15–20.

Ghosh, S. and Henry, M.P., "Application of Packed-Bed Upflow Towers in Two-Phase Anaerobic Digestion", *Proceedings : First International Conference on fixed-Film Biological Processes*, Corps of Engineers – U.S. Department of the Army, 1982, p1392–1413.

Gottschalk, G., "Bacterial Fermentation", *Bacterial Metabolism*, 2nd ed., Springer-Verlay, New York, 1985.

Graef, S.P. and Andrews, J.F., "Mathematical Modeling and Control of Anaerobic Digestion", *AIChE SYMPOSIUM SERIES*, Vol. **70**, No. **136**, 1973, p101–131.

Guiot, S.R. and van den Berg, L., "Performance of an Upflow Anaerobic Reactor Combining a Sludge Blanket and a Filter Treating Sugar Waste", *Biotechnology and Bioengineering*, Vol. **27**, No. **6**, June 1985, p800–806.

Harper, S.R. and Pohland, F.G., "Enhancement of Anaerobic Treatment Efficiency through Process Modification", *Journal WPCF*, Vol. **59**, No. **3**, March 1987, p152–161.

Harremoës, P., "The Significance of Pore Diffusion to Filter Denitrification", *Journal WPCF*, Vol. **48**, No., **2**, Feb. 1976, p377–388.

Harremoës, P., Jansen, J.C. and Kristensen, G.H., "Practical Problems Related to Nitrogen Bubble Formation in Fixed Film Reactors", *Progress in Water Technology*, Vol. **12**, No. **6**, 1980, pTor253–Tor269.

Hayes, T.D., Isaacson, H.R. and Frank, J.R., "A Physical–Chemical Method for the Romoval of Carbon Dioxide from Anaerobic Digester Gas", Patent Disclosure, June 1983.

Hayes, T.D., Isaacson, H.R., Pfeffer, J.T. and Liu, Y.M., "In–Situ Methane Enrichment in Anaerobic Digestion", *Biotechnology & Bioengineering*, 1989 (in press).

Henze, M. and Harremoës, P., "Anaerobic Treatment of Wastewater i Fixed Film Reactors – A Literature Review", *Water Science and Technology*, Vol. **15**, No. **8/9**, 1983, p1–101.

Heyes, R.H. and Hall, R.J., "Anaerobic Digestion Modeling – The Role of H_2 ", *Biotechnology Letters*, Vol. **3**, No. **8**, Aug. 1981, p431–436.

Hill, D.T. and Nordstedt, R.A., "Modeling Techniques and Computer Simulation of Agricultural Waste Treatment Processes", *Paper Presented at the 1977 Annual Meeting AMERICAN SOCIETY OF AGRICULTURAL ENGINEERS*, ASCE 77–4030, June 1977.

Hill, D.T. and Barth, C.L., "A Dynamic Model for Simulation of Animal Waste Digestion", *Journal WPCF*, Vol. **49**, No. **10**, Oct. 1977, p2129–2143.

Hoehn, R. and Ray, A.D., "Effects of Thickness on Bacterial Film", *Journal WPCF*, Vol. **45**, No. **11**, Nov. 1973, p2302–2320.

Hungate, R.E., *The Rumen And Its Microbes*, Academic Press, New York, 1966.

IMSL, Inc., "USER'S MANUAL –MATH/PC–LIBRARY, FORTRAN Subroutines for Mathematical Applications on a Personal Computer", April 1984.

Jeris, J.A., "Industrial Wastewater Treatment Using Anaerobic Fluidized Bed Reactors", *Water Science and Technology*, Vol. **15**, Nos. **8/9**, 1983, p169–176.

Jeris, J.S. and McCarty, P.L., "The Biochemistry of Methane Fermentation Using C^{14} Tracers", *Journal WPCF*, Vol. **37**, No. **2**, Feb. 1965, p178–192.

Jones, G.W. and Isaacson, R.E., "Proteinaceous Bacterial Adhesions and Their Receptors", *CRC Critical Reviews in Microbiology*, Vol. **10**, Issue **3**, 1983, p229–260.

Kaspar, J.F. and Wuhrmann, K., "Kinetic Parameters and Relative Turnovers of Some Important Catabolic Reactions in Digesting Sludge", *Applied and Environmental Microbiology*, Vol. **36**, No. **1**, July 1978, p1–7.

Keenan, J.D., "Multiple Staged Methane Recovery from Solid Wastes", *Journal of Environmental Science and Health*, Vol. **A11**, No. **8&9**, 1976, p525–548.

Kennedy, K.J. and van den Berg, L., "Stability and Performance of Anaerobic Fixed Film Reactors During Hydraulic Overloading at 10–35°*C* ", *Water Research*, Vol. **16**, No. **8**, 1982, p1391–1398.

Khan, K.A., Suidan, M.T. and Cross, W.H., "Anaerobic Activated Carbon Filter for The Treatment of Phenol–Bearing Wastewater", *Journal WPCF*, Vol. **53**, 1981, p15–19.

Kleinstreuer, C. and Poweigha, T., "Dynamic Simulator for Anaerobic Digestion Processes", *Biotechnology and Bioengineering*, Vol. **24**, No. **9**, 1982, p1941–1951.

Lawrence, A.W. and McCarty, P.L., "A Kinetic Approach to Biological Wastewater Treatment Design and Operation ", Technical Report No. 23, Dec. 1969, Cornell University Water Resources and Marine Sciences Center, Ithaca, New York.

Lawrence, A.W., "Application of Process Kinetics to Design of Anaerobic Processes", *Anaerobic Biological Treatment Process : Proceedings of the 159th Meeting of the American Chemical Society, Houston, Tex., Feb. 26, 1970*, Advances in Chemistry Series 105, p163–189.

Lettinga, G., Hulshoff Pol, L.W., Wiegant, W., de Zeeuw, W., Hobma, S.W., Grin, P., Roersma, R., Sayed, S. and van Velsen A.F.M., "Upflow Sludge Blanket Processes", *Proceedings of The Third International Symposium on Anaerobic Digestion, August 14–19, 1983, Boston, Massachusetts, USA*, p139–158.

Levenspiel, O., *Chemical Reaction Engineering*, 2nd ed., Wiley, New York, 1972.

Liehr, S.K., Eheart, J.W. and Suidan, M.T., "A Modeling Study of the Effect of pH on Carbon Limited Algal Biofilms", *Water Research*, Vol. **22**, No. **8**, 1988, p1033–1041.

Lindgren, M., "Mathematical Modeling of the Anaerobic Filter Process", *Water Science And Technology*, Vol. **15**, Nos. **8/9**, 1983, p197–207.

Logan, B.E. Hermanowicz, S.W. and Parker, D.S., "A Fundamental Model for Trickling Filter Process Design", *Journal WPCF*, Vol. **59**, No. **12**, Dec. 1987, p1029–1042.

Marshall, K.C., Stout, R. and Mitchell, R., "Mechanism of the Initial Events in the Sorption of Marine Bacteria to Surface", *Journal of General Microbiology*, Vol. **68**, Part **3**, Nov. 1971, p337–348.

McCarty, P.L. (a), "Anaerobic Waste Treatment Fundaments, Part One – Chemistry and Microbiology ", *Public Works*, Vol. **95**, No. **9**, Sept. 1964, p107–112.

McCarty, P.L. (b), "Anaerobic Waste Treatment Fundaments, Part Two – Environmental Requirements and Control", *Public Works*, Vol. **95**, No. 10, Oct. 1964, p123–126.

McCarty, P.L. (c), "Anaerobic Waste Treatment Fundaments, Part Three – Toxic Materials and Their Control ", *Public Works*, Vol. **95**, No. **11**, Nov. 1964, p91–94.

McCarty, P.L. (d), "Anaerobic Waste Treatment Fundaments, Part Four - Process Design", *Public Works*, Vol. **95**, No. **12**, Dec. 1964, p95-99.

McCarty, P.L., "Kinetics of Waste Assimilation in Anaerobic Treatment", *Developments in Industrial Microbiology*, Vol. **7**, 1966, p144-155.

McCarty, P.L., "Energetics and Kinetics of Anaerobic Treatment", *Anaerobic Biological Treatment Process : Proceedings of the 159th Meeting of the American Chemical Society, Houston, Tex., Feb. 26, 1970*, Advances in Chemistry Series 105, p91-107.

McCarty, P.L., "Anaerobic Processes", Presented at *the Birmingham Short Course on Design Aspects of Biological Treatment*, International Association of Water Pollution Research, Birmingham, England, Sept. 18, 1974.

McCarty, P.L., "Stoichiometry of Biological Reactions", *Progress in Water Technology*, Vol. **7**, No. **1**, 1975, p157-172.

McCarty, P.L., "One Hundred Years of Anaerobic Treatment", *Proceeding of the Second International symposium on Anaerobic Digestion in Travemünde, Federal Republic of Germany, on Sept. 1-11*, Elsevier Biomedical Press, 1981, p3-22.

Metcalf and Eddy, Inc., *Wastewater Engineering : Treatment, Disposal, Reuse*, 2nd ed., McGraw-Hill, New York, 1979.

Murray, W.D. and van den Berg, L., "Effect of Support Material on the Development of Microbial Fixed Films converting Acetic Acid to Methane", *Journal of Applied Bacteriology*, Vol. **51**, No. **2**, Oct. 1981, p257-265.

O'Rourke, J.T., "Kinetics of Anaerobic Treatment at Reduced Temperature", Ph.D. Dissertation, Department of Civil Engineering, Stanford University, March 1968.

Oleszkiewicz, J.A. (a), "Attached Growth Anaerobic Treatment Systems", *Seminar on Anaerobic Wastewater Treatment and Energy Recovery, Pittsburgh, Nov. 3-4, 1981*, Duncan, Lagnese and Associates, Inc., 1981.

Oleszkiewicz, J.A. (a), "Suspended Versus Attached Growth Systems", *Seminar on Anaerobic Wastewater Treatment and Energy Recovery, Pittsburgh, Nov. 3-4, 1981*, Duncan, Lagnese and Associates, Inc., 1981.

Ort, J.E., *High Quality Methane Gas Through Modified Anaerobic Digestion*, U.S. Patent No. 3,981,800, Sept. 21, 1976.

Parker, D.S. and Merrill, D.T., "Effect of Plastic Media Configuration on Trickling Filter Performance", *Journal WPCF*, Vol. **56**, No. **8**, Aug. 1984, p955-961.

Parkin, G.F. and Owen, W.F., "Fundamentals of Anaerobic Digestion of Wastewater Sludges", *Journal of Environmental Engineering*, Vol. **112**, No. **5**, Oct. 1986, p867-920.

Perry, R.H. and Chilton, C.H., *Chemical Engineers' Handbook*, 5th ed., McGraw Hill, New York, 1973.

Perry, R.H. and Green, D., *Perry's Chemical Engineers' Handbook*, 6th ed., McGraw-Hill, New York, 1984.

Pette, K.C. and Versprille, A.I., "Application of The U.A.S.B. - Concept for Wastewater Treatment", *Proceeding of the Second International symposium on Anaerobic Digestion in Travemünde, Federal Republic of Germany, on Sept. 6-11, 1981*, Elsevier Biomedical Press, 1981, p121-133.

Pohland, F.G. and Ghosh, S., "Developments in Anaerobic Stabilization of Organic Wastes - the Two-Phase Concept", *Environmental Letters*, Vol. **1**, No. **4**, 1971, p255-266.

Pohland, F.G. and Massey, M.L., "An Application of Process Kinetics for Phase Separation of the Anaerobic Stabilization Process", *Progress in Water Technology*, Vol. **7**, No. **1**, 1975, p173-189.

Pohland, F.G. and Suidan, M.T., "Prediction of pH Stability in Biological Treatment Systems", *Chemistry of Water Technology*, Rubin A.J. editor, Ann Arbor Science, 1978.

Riemer, M., *Kinetics of Denitrification in Submerged Filters*, Ph.D. Thesis, The Technical University of Denmark, Copenhagen, Denmark 1977.

Riemer, M. and Harremoës, P., "Multi-Component Diffusion in Denitrifying Biofilms", *Progress in Water Technology*, Vol. **10**, No. **5/6**, 1978, p149-165.

Rittmann, B.E. , "The Effect of Shear Stress on Biofilm Loss Rate", *Biotechnology and Bioengineering*, Vol. **XXIV**, No. **2** , Feb. 1982, p501-506.

Rittmann, B.E. and McCarty, P.L., "Model of Steady-State Biofilm Kinetics", *Biotechnology and Bioengineering*, Vol. **XXII**, No. **11** , Nov. 1980, p2343-2357.

Rittmann, B.E. and McCarty, P.L., "Substrate Flux into Biofilms of Any Thickness", *Journal of Environmental Engineering Division - ASCE*, Vol. **107**, No. **EE4**, Aug. 1981, p831-849.

Sanchez, E. and Roque-Malherbe, R., "Zeolite as Support Material in Anaerobic Wastewater Treatment", *Biotechnology Letters*, Vol. **9**, No. **9**, Sept. 1987, p671-672.

Shulman, H.L., Ullrich, C.F., Proulx, A.Z. and Zimmerman, J.O., "Wetted and Effective-Interfacial Areas, Gas- and Liquid- Phase Mass Transfer Rates", *A.I.Ch.E. Journal*, Vol. **1**, No. **2**, June 1955, p253-258.

Sinechal, X.J., Installe, M.J. and Nyns, E.J., "Differentiation Between Acetate and Higher Volatile Acids in the Modeling of the Anaerobic Biomethanation Process", *Biotechnology Letters*, Vol. **1**, No. **8**, Aug. 1979, p309-314.

Skelland, A.H.P., *Diffusional Mass Transfer*, Wiley Interscience, New York, NY, 1974.

Snoeyink, V.L. and Jenkins, D., *Water Chemistry*, John Wiley & Sons, New York, 1980.

Song, K-H and Young, J.C., "Media Design Factors for Fixed-Bed Filters", *Journal WPCF*, Vol. **58**, No. **2**, Feb. 1986, p115-121.

Stryer, L., *Biochemistry*, 2nd ed., Freeman, San Francisco, 1981.

Suidan, M.T., Rittmann, B.E. and Traegner, U.K., "Criteria Establishing Biofilm – Kinetic Types", *Water Research*, Vol. **21**, No. **4**, 1987, p491–498.

Suidan, M.T., "Performance of Deep Biofilm Reactors", *Journal of Environmental Engineering*, Vol. **112**, No. **1**, Feb. 1986, p78–93.

Suidan, M.T., Cross, W.H., Fong, M. and Calvert, J.W. Jr., "Anaerobic Carbon Filters for Degradation of Phenols", *Journal of Environmental Engineering Division – ASCE*, Vol. **107**, No. **EE3**, 1981, p563–579.

Suidan, M.T. and Wang, Y.T., "Unified Analysis of Biofilm Kinetics", *Journal of Environmental Engineering*, Vol. **111**, No. **5**, Oct. 1985, p634–646.

Sutherland, I.W., "Microbial Exopolysaccharides – Their Role in Microbial Adhesion in Aqueous Systems", *CRC Critical Reviews in Microbiology*, Vol. **10**, Issue **2**, 1983, p173–201.

Switzenbaum, M.S. and Eimstad, R.B., "Analysis of Anaerobic Biofilms", *Environmental Technology Letters*, Vol. **8**, No. **1**, 1987, p21–32.

Sykes, R.M., "Theoretical Heterotrophic Yields", *Journal WPCF*, Vol. **47**, No. **3**, March 1975, p591–600.

Szwerinski, E., Arvin, E. and Harremoës, P., "pH–Decrease in Nitrifying Biofilms", *Water Research*, Vol. **20**, No. **8**, 1986, p971–976.

Toerien, D.F. and Hattingh, W.H.J., "Anaerobic Digestion – I. The Microbiology of Anaerobic Digestion", *Water Research*, Vol. **3**, 1969, p385–416.

Treybal, R.E., *Mass Transfer Operations*, 3rd ed., McGraw–Hill, New York, 1980.

Trulear, M.G. and Characklis, W.G., "Dynamics of Biofilm Processes", *Journal WPCF*, Vol. **54**, No. **9**, September 1982, p1288–1301.

van den Berg, L. and Lentz, C.P., "Comparison Between Up– and Downflow Anaerobic Fixed Film Reactors of Varying Surface–To–Volume Ratios for the Treatment of Bean Blanching Waste", *Proceedings of the 34th INDUSTRIAL WASTE CONFERENCE*, May 8, 9, and 10, 1979, Purdue University, 1980, p319–325.

van den Berg, L. and Lentz, C.P., "Effects of Film Area–to Volume Ratio, Film Support, Height and Direction of Flow on Performance of Methanogenic Fixed Film Reactors", *Anaerobic Filters : An Energy Plus for Wastewater Treatment, Proceedings of the Seminar/Workshop, January 9–10, 1980, Howey–In–The–Hills, Florida*, Argonne National Laboratory, Jan. 1981, p1–10.

Verrier, D., Mortier,B. and Albagnac, G., "Initial Adhesion of Methanogenic Bacteria to Polymers", *Biotechnology Letters*, Vol. **9**, No. **10**, Oct. 1987, p735–740.

Wang, Y.T., *Modeling of Biological Activity in Expanded–Bed Anaerobic Activated Carbon Filters*, Ph.D. Thesis, University of Illinois, 1984.

Ward, D.M., Mah, R.A. and Kaplan, I.R., "Methanogenesis from Acetate : A Non–Methanogenic Bacterium from an Anaerobic Acetate Enrichment", *Applied and Environmental Microbiology*, Vol. **35**, No. **6**, June 1978, p1185–1192.

Weast, R.C., *CRC Handbook of Chemistry and Physics,* 66th ed., CRC Press, Boca Raton, Florida, 1985.

Williamson, K. and McCarty, P.L. (a), "A Model of Substrate Utilization by Bacterial Films", *Journal WPCF*, Vol. **48**, No. **1**, Jan. 1976, p9–24.

Williamson, K. and McCarty, P.L. (b), "Verification Studies of the Biofilm Model for Bacterial Substrate Utilization", *Journal WPCF*, Vol. **48**, No. **2**, Feb. 1976, p281–296.

Witt, E.R., Humphrey, W.J. and Roberts, T.E., "Full-Scale Anaerobic Filter Treats High Strength Wastes", *Proceedings of the 34th INDUSTRIAL WASTE CONFERENCE*, May 8, 9, and 10, 1979, Purdue University, 1980, p229–234.

Wolfe, R.S., "Unusual Coenzymes of Methanogenesis", *Trends in Biochemical Sciences*", Vol. **10**, No. **10**, Oct. 1985, p396–399.

Woese, C.R. and Wolfe, R.S., *The Archaebacteria*, Vol. **8**, Academic Press, New York, 1985.

Yoda, M., Kitagawa, M. and Miyaji, Y., "Long Term Competition Between Sulfate-Reducing and Methane -Producing Bacteria for Acetate in Anaerobic Biofilm", *Water Research*, Vol. **12**, No. **12**, Dec. 1987, p1547–1556.

Young, J.C., *The Anaerobic Filter for Waste Treatment*, Doctoral Dissertation, Stanford University, Stanford, California, 1968.

Young, J.C., "The anaerobic Filter – Past, Present and Future", presented at *The Third International Symposium on Anaerobic Digestion*, Aug. 14–19, 1983, Boston, Massachusetts, p91–105.

Young, J.C. and McCarty, P.L., "The Anaerobic Filter for Waste Treatment", *Proceedings of the 22nd INDUSTRIAL WASTE CONFERENCE*, May 2, 3, and 4, 1967, Purdue University, 1968, p559–574.

Young, J.C. and McCarty, P.L., "The Anaerobic Filter for Waste Treatment", *Journal WPCF*, Vol. **41**, No. **2**, Feb. 1969, pR160–R173.

Young, J.C. and Dahab, M.F., "Effect of Media Design on the Performance of Fixed-Bed Anaerobic Reactors", *Water Science and Technology*, Vol. **15**, Nos. **8/9**, 1983, p369–383.

ZoBell, E.E., "The Effect of Solid Surface upon Bacterial Activity", *Journal of Bacteriology*, Vol. **46**, 1943, p39–56.

Zoetemeyer, R.J., *Acidogenesis of Soluble Carbohydrate-Containing Wastewaters*, Ph.D. Thesis, University of Amsterdam, 1982.